# DYE SENSITIZATION OF NANOCRYSTALLINE TITANIUM DIOXIDE WITH OSMIUM AND RUTHENIUM POLYPYRIDINE COMPLEXES

Thesis by

Geneviève Sauvé

In Partial Fulfillment of the Requirements

for the Degree of

Doctor of Philosophy

California Institute of Technology

Pasadena, California

1999

(Submitted February 24, 1999)

# Acknowledgments

I would never have been able to do this work without the help of many people. Here, I will mention those who come to my mind as key people, but there are many more and forgive me if I don't mention your name. First, I would like to thank my advisor, Prof. Nathan S. Lewis, who let me join his group in the first place. Overall, Nate was a good advisor who was there when needed, and who taught me to be a better independent researcher. I appreciate all his help and understanding.

I thank all Lewis group members who overlapped with me. I am indebted to Dr. Marion E. Cass and Dr. Stephen J. Doig, who got me started on this project. Marion was especially patient and taught me synthesis. Steve designed the photoelectrochemical cell utilized in this work. I am most obliged to Dr. George M. Coia for making and purifying $K_4[RuL'_3]$ and for making the other emission measurements possible. I also appreciate all his help with other parts of the project and for numerous discussions. I am thankful to Dr. Olaf Krüger for measuring the complexes' lifetimes by photon counting and Katherine Pomykal for helping with the photoelectrochemistry. Thank you Robert C. Rossi and Dr. Glen W. Walker for your help. I am also grateful to our administrative assistants, Pam, Kathleen and Michelle, for there help and for being there. The Lewis group would not have functioned well without you.

I appreciate all the help of other members of the Caltech community. In particular, I am grateful to Dr. Iqbal Bhugun for his help with spectroelectrochemistry, Erik Holmin for showing me how to use the Barton's group fluorescence spectrophotometer, Prof. M. R. Hoffmann's group for letting me use their furnace, Prof. F. C. Anson's Group for letting me use their profilometer and BAS 100B electrochemical analyzer, Dr. Jay Winkler and Yvan Dmochowski for their help with nanosecond lasers.

I am grateful to Dr. Iver Lauermann for helping me obtain $TiO_2$ electrodes, Libbey Owens Ford Co. for giving us conducting glass, Dr. Andy Maverick of Louisiana State University for measuring the emission spectrum of $OsL'_2(NCS)_2$ at low temperature, and Dr. Gerald J. Meyer of Johns Hopkins University for fruitful discussions.

I am indebted to the U.S. Department of Energy for supporting this project, FCAR (Fonds pour la Formation de Chercheurs et l'Aide à la Recherche, Québec, Canada) for a Ph.D. scholarship, and Kodak for additional funding.

Finally, I would like to acknowledge my Fiancee, Michael S. Lewicki, for his constant support, patience and love throughout most of my graduate career. Mike fostered positive change, bringing out the best in me and encouraging me to continue improving various skills. Thank you.

# Abstract

The goal of this work is to explore the idea of replacing the ruthenium metal center of polypyridine complexes with osmium to increase the overlap between the spectral response of the "Grätzel cell" and the solar spectrum. A series of osmium polypyridine dyes with various ground state reduction potentials has been synthesized, purified, characterized and utilized to sensitize nanoporous titanium dioxide electrodes to solar radiation. The dyes are $ML'_2(NCS)_2$, $ML'_2(CN)_2$, $ML'_3^{2+}$ and $ML_2L'^{2+}$ where M is Os(II) or Ru(II), L is bipyridine and L' is 4,4'-dicarboxy-2,2'-bipyridine. The visible absorption spectra of the Os complexes showed an additional absorption band at longer wavelengths than the Ru complexes. The spectral response and current-voltage properties of electrodes modified with the Os dyes have been compared with their Ru analogs. In general, the Os dye showed a similar maximum external quantum yield, an enhanced response at longer wavelengths, a higher photocurrent density and a similar open-circuit voltage than the Ru analog. The Os complexes thus appear to be promising sensitizers for energy conversion applications. The only discrepancy in this trend was observed for the $OsL'_2(NCS)_2$ complex, which showed a much lower maximum external quantum yield, lower photocurrent and lower open-circuit voltage than the Ru analog. Experiments suggest that the regeneration rate of $Os(II)L'_2(NCS)_2$ by iodide does not compete effectively with the regeneration rate of the dye by the electron in the $TiO_2$. The ground-state redox potential of $Os(II/III)L'_2(NCS)_2$ (+0.42 V vs aq SCE in methanol) may represent a limit on how negative the redox potential of the dye can be to obtain efficient regeneration of the sensitizer by $I^-/I_3^-$. For electrodes with very low dye coverage, the open-circuit voltage was mainly determined by the reduction of $I_3^-$, whereas for high dye coverage, the open-circuit voltage also depended on the nature of the complex and on the dye loading level.

# Table of Contents

# List of Illustrations

# List of Tables

# Chapter 1:

# Introduction

Conventional sources of energy, such as oil, coal, natural gas, and nuclear, have negative side-effects. These side-effects include global warming, air and water pollution, resource depletion, and risk of nuclear accidents.[2] As the population of the energy-intense society increases, these side-effects will become more problematic than ever.[2] Already, the greenhouse effect caused by $CO_2$ emissions has become a global problem. And some geologists believe that we will run short of oil in the next 10 to 20 years.[3] As Harry B. Gray also points out, it is crazy to burn fossil fuel when we need them for raw materials for making dyes, drugs, tee-shirts, chairs and automobiles.[4] There is therefore a great need for a clean, inexhaustible energy source. One such energy source is the sun. The amount of solar energy that strikes the earth's surface in only one hour approximately equals the amount of fossil fuels consumed globally in one year.[4] The prospect of harnessing this infinite source of energy with minimal environmental pollution is the driving force of this thesis' work. In this chapter, I will first introduce a way to harness solar energy: photoelectrochemical cells. In section B, I will then focus on dye sensitization of nanocrystalline $TiO_2$ and the "Grätzel cell."

## A. Harnessing Solar Energy: Photoelectrochemical Cells

There are three methods for converting sunlight into energy. These methods are depicted in Figure 1. First, photosynthesis is the way plants transform light into chemical fuels (carbohydrates). During optimal growing season, plants can transform 3-5% of the incident sunlight power into fuels.[5] Many researchers are interested in understanding photosynthesis and in mimicking it using supramolecular systems.[4] The third method shown in Figure 1 is photovoltaics. Photovoltaics are solid state devices that convert sunlight into electricity. They consist of two types of solids connected at a junction. The

solids are typically semiconductors which can absorb light, and the junction provides a means to separate the charges by forming an electric field.[5] Photovoltaics are reliable, light and durable and are used in satellites and space shuttles by NASA.[2] They can transform incident light into electricity at efficiencies of 23-30%, though cheaper commercial photovoltaics have efficiencies of 15% or less.[2] Unfortunately, photovoltaics are still too expensive to compete with conventional sources of energy,[2] and they cannot convert incident light energy into chemical fuels.[5]

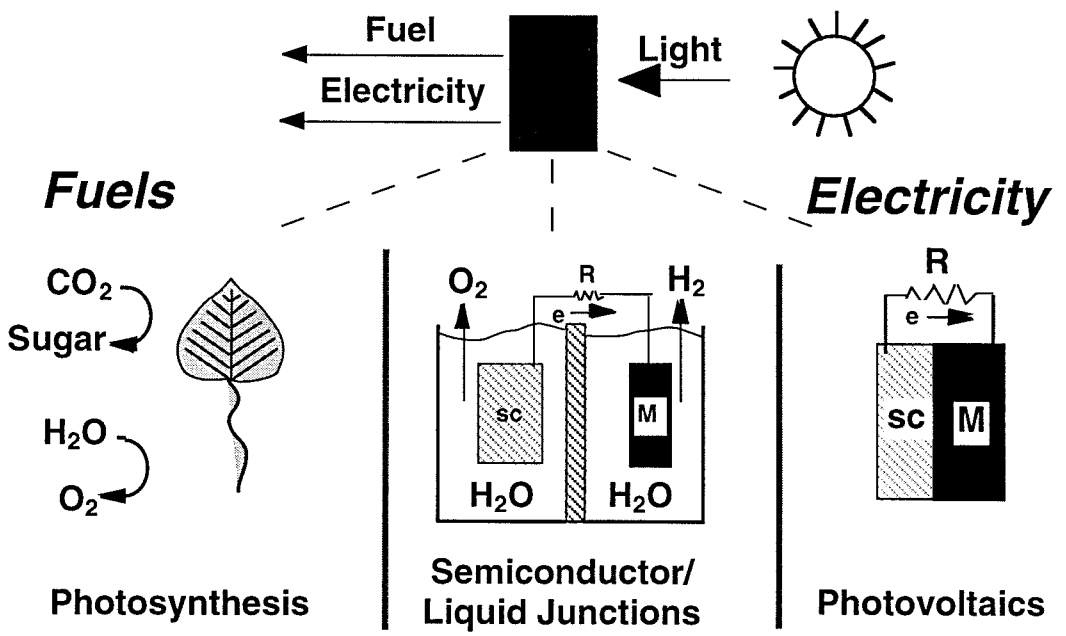


Figure 1: Methods of solar energy conversion.

An intermediate between photosynthesis and photovoltaics is photoelectrochemical cells, or semiconductor-liquid junctions. Photoelectrochemical cells (see Fig. 1) can convert light into either electricity, chemical fuels, or both with efficiencies intermediate between photosynthesis and photovoltaics,[5] and efficiencies as high as 17% have been reported.[6]

Semiconductors are solids whose conductivity increases with temperature. The collection of filled molecular orbitals is called the valence band and the collection of unfilled molecular orbitals is the conduction band. The HOMO and LUMO are usually referred to the valence and conduction band edge, respectively. The energy between those two band edges is the band gap energy. When semiconductors absorb light of equal or greater energy than the band gap, an electron is promoted to the conduction band. Upon immersion into a liquid containing a redox couple, charge flows between the semiconductor and the redox couple in solution, and the electrochemical potential of the two phases equilibrate. This process creates an electric field in the semiconductor, which is the basis for charge separation. Without this electric field, an electron promoted to the conduction band would just recombine with the hole in the valence band, with heat generation and no electricity produced.

A photoelectrochemical cell consists of two electrodes: a semiconductor working electrode and a metal counter electrode in a solution containing a redox couple $A/A^-$. The counter electrode performs the reverse reaction of the semiconductor electrode and electricity is produced with no net chemical changes.

The performance of photoelectrochemical cells is characterized by three quantities, illustrated in Figure 2.[5] The short-circuit current density ($J_{sc}$) is the maximum current density that can flow between the two electrodes. The open-circuit voltage ($V_{oc}$) is a measure of the maximum Gibbs free energy that can be obtained in the cell. The fill factor (ff) characterizes the rate at which the current approaches its limiting short circuit value, and is an indication of how close to ideal the system is. A typical value for ff is 0.7 - 0.8.[5] The total maximum power obtainable is: $J_{sc} \times V_{oc} \times ff$. The conversion efficiency is simply obtained by dividing the maximum power by the incident solar power and multiplying by 100.

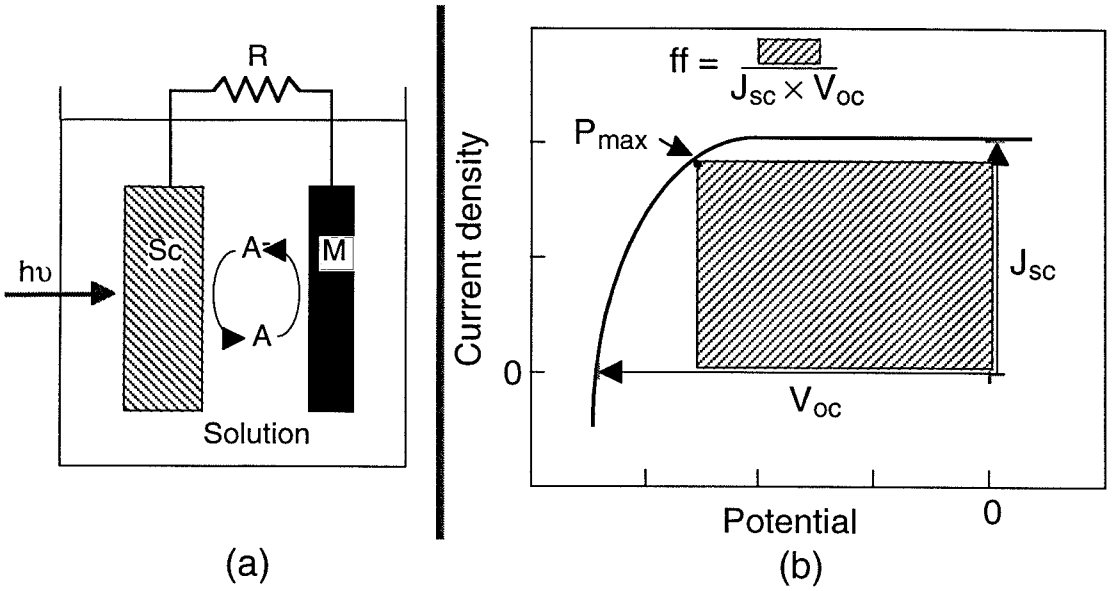


Figure 2: (a) Photoelectrochemical cell. (b) Current density - Potential (J-*E*) curve, generated by varying the magnitude of a resistance R between the two electrodes.

The basic equation describing current-voltage characteristics of a semiconductor-liquid junction is the diode equation:[5]

$$I = I_{ph} - I_0\left[\exp\left(\frac{qV}{kT}\right) - 1\right] \qquad (1)$$

where I is the current, $I_{ph}$ is the photocurrent, $I_o$ is the dark current, q is the charge on an electrode, V is the applied voltage, k is the Boltzmann constant and T is the temperature. At open circuit, the current is zero and for $I_{ph} > I_o$:[5]

$$V_{oc} = \frac{kT}{q}\ln\left(\frac{I_{ph}}{I_0}\right) \qquad (2)$$

If $I_o$ is an indication of the dark current, then $V_{oc}$ can be used as an indirect way to monitor the back current. The more back current for the same $I_{ph}$, the smaller the $V_{oc}$.

Semiconductors with band gap energies between 1.1 - 1.7 eV are ideally suited for efficient conversion of solar energy. Figure 3 compares the spectral response silicon (small band gap of 1.1 eV) with the solar spectrum. A spectral response is a plot of the external quantum yield versus wavelength, where the external quantum yield is the number of

collected charges divided by the number of photons incident onto the cell. Unfortunately, semiconductors with small band gaps are easily corroded and passivated in aqueous solution. Hence, stable photoelectrochemical cells based on small band gap semiconductors can only be obtained in non-aqueous solutions. An alternative is to utilize wide band gap semiconductors, such as $TiO_2$ (band gap of 3 eV), which are stable in water. However, such materials only absorb UV light and have a poor overlap with the solar spectrum. A strategy to circumvent this problem is to use a dye that can absorb visible light and inject an excited electron into the conduction band of $TiO_2$. This strategy is called dye sensitization and is the subject of the next section.

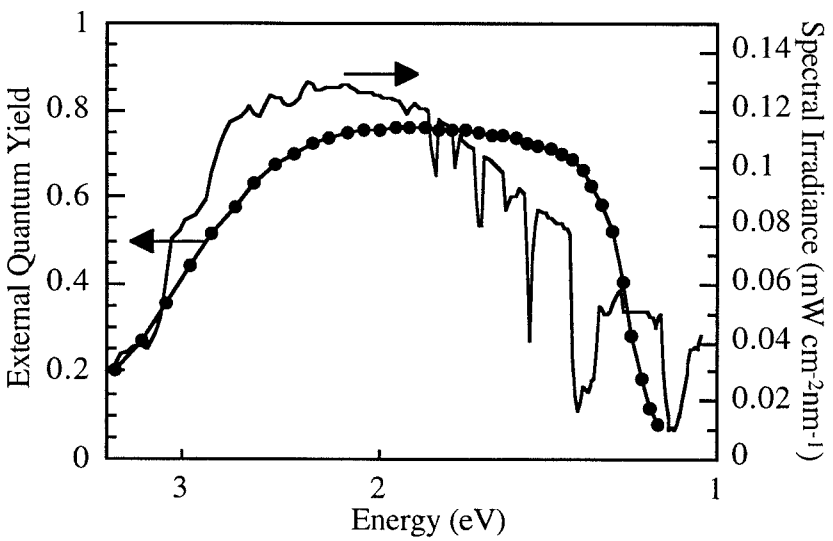


Figure 3: Comparison of the spectral response of silicon (●) with the spectral distribution of sunlight under Air Mass 1.5 conditions (solid line). Air Mass 1.5 (AM 1.5)[7] refers to a standard measurement condition when the sun is 48° above the horizon. Most of the solar irradiation is between 1 and 3 eV.[5]

## B. Dye Sensitization of $TiO_2$ and the "Grätzel Cell"

One approach to the useful conversion of sunlight into electrical energy employs wide band gap semiconductors. These compounds tend to be more stable to oxidation by air and water than small band gap semiconductors such as Si, InP, and GaAs.[5] However, photoelectrodes made from wide band gap materials must be sensitized with dyes or with high concentrations of dopants in order to extend their wavelength responses into the visible region of the solar spectrum.

In the dye sensitization strategy, a molecule (dye or sensitizer) is adsorbed onto the large band gap semiconductor (e.g., $TiO_2$) with the function of absorbing visible light. The excited state of the dye must have enough energy to inject an electron into the conduction band of $TiO_2$. Once in the semiconductor, the electron experiences an electric field and is driven away from the surface. A donor in solution reduces the oxidized dye back to its original state (regenerate the dye) and the oxidized donor is reduced at the counter electrode to complete the circuit. The problem with this system is its poor light harvesting. Because only dyes adsorbed directly at the surface of $TiO_2$ can inject electrons, only one monolayer of dye can effectively be used. One monolayer of dye on a smooth surface absorbs less than 1% of the incident monochromatic light,[8] which results in very low overall device efficiencies.

### *1. Description of the Grätzel Cell*

Recently, Grätzel and co-workers solved this light harvesting problem by using a very high surface area.[9-14] They developed an efficient photoelectrochemical cell which uses sensitizers based on transition metal complexes deposited on nanocrystalline titanium dioxide electrodes.[8,14-16] This cell is commonly known as the Grätzel cell and is depicted in Figure 4. The $TiO_2$ electrode consists of a thin layer (10 μm) of mesoporous nanocrystalline $TiO_2$ deposited onto a transparent conducting glass. The average size of the nanoparticles is 10 nm and the roughness factor is about 1000.[13,16] The most successful

sensitizers employed are polypyridine complexes of ruthenium. In particular, a solar-to-electric energy conversion efficiency as high as 10% was attained using [Ru(II)(4,4'-$(CO_2H)_2$-2,2'-bipyridine)$_2$$(NCS)_2$], abbreviated herein as $RuL'_2(NCS)_2$, as the sensitizer.[16] The carboxylic acid groups are necessary for the attachment of the dye onto $TiO_2$. They form ester bonds at the surface of $TiO_2$.[17-22] The electrolyte consisted of 0.3 M LiI, 0.03 M $I_2$ in acetonitrile. The dye-coated electrode was pretreated by dipping it in 4-tert-butylpyridine for 15 min. This pretreatment was shown to increase $V_{oc}$.[16] The counter electrode consists of Pt deposited electrochemically or by sputtering onto conducting glass. The two electrodes were assembled in a thin-layer sandwich-type of cell by simply clamping the two electrodes together. A thin layer of electrolyte was attracted into the interelectrode space by capillary forces.[14]

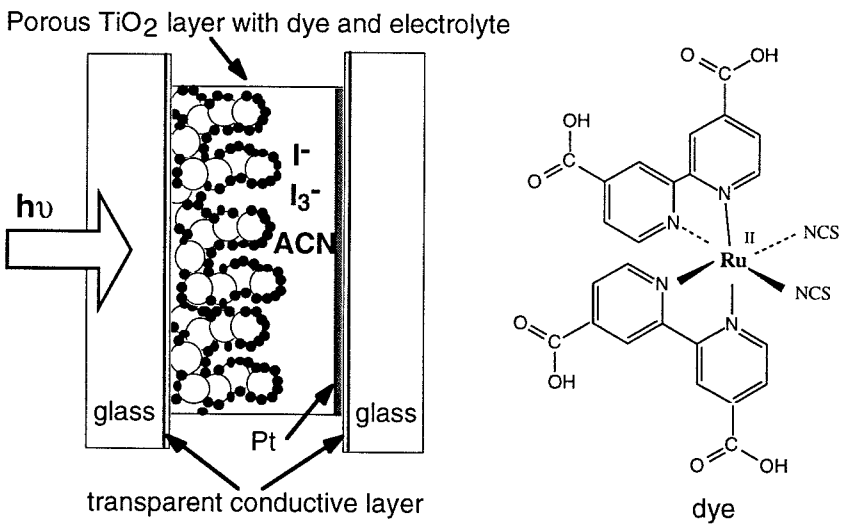


Figure 4: Schematic of the Grätzel cell (not drawn to scale).

This type of cell was initially unstable mainly because the electrolyte evaporated. In future developments, solvents with high boiling points such as propylene glycol or N-methyl-oxazolidine-2-one (NMO), were added to greatly increase the stability.[16] However, such solvents are viscous and cannot transport ions well, limiting the current. Moreover, the iodine/triiodide reduction reaction is most facile in water and acetonitrile, but

becomes increasingly sluggish in propylene carbonate and NMO, again limiting the current.[23] Grätzel and co-workers developed a platinization procedure which increased the counter electrode's electrocatalytic activity and stability to anodic corrosion.[23,24] Using organic solvents with dissolved salts presents other problems besides volatility issues. Salts could precipitate when the cell is used at a very low temperature, and solvents are often incompatible with glues used to seal the cell.[25] Grätzel and co-workers developed molten salts based on alkyl imidazolium iodide to solve these problems.[25] Molten salts are ionic liquids that have high conductivity and ionic mobility, as well as large electrochemical windows and excellent thermal stability.[25,26] INAP (Institut für Angewandte Photovoltaik) use molten salts in their electrolyte. High boiling point electrolytes that contain these molten salts and triiodide can be purchased from Solaronix Inc. For practical purposes and best long-term stabilities, an all solid-state solar cell is desirable.[27,28] Efforts have been made to develop solar cells where the $TiO_2$ is sensitized by polymers,[29,30] where the electrolyte is a polymer gel,[28] and where the electrolyte is an all solid amorphous organic hole-transport material.[27]

To obtain stable sandwich-type solar cells with minimal solvent evaporation, the two electrodes can also be sealed using Surlyn (a PE-Zn-carboxylate-copolymer) (50 μm thick). In a long term stability test, the performance of a $RuL'_2(NCS)_2$-sensitized solar cell was practically unchanged for 7000 h of continuous light exposure, which is equivalent to 6 years of use in Europe.[31] In this test, the electrolyte was glutaronitrile with 0.5 M KI and 50 mM iodine. The two electrodes were sealed using Surlyn 1702 and an epoxy glue.[31] The turnover number for the dye was greater than $10^7$.[31] Stable solar cells are therefore obtainable in such cases. The short-circuit photocurrent densities achieved were in the range of 7 - 8 mA $cm^{-2}$, which is about half of what is expected for this sensitizer under the illumination used. This lower photocurrent, as well as low ff and $V_{oc}$, was attributed to the high viscosity of the solvent.

In this work, we have decided to use a simple electrolyte based on acetonitrile. We have also utilized a three-electrode cell built in-house. Prior to this work, attempts to use a three-electrode cell yielded much lower external quantum yields than with the sandwich-type cell, which was explained by considering the geometry of the cells and the diffusion of iodide and triiodide.[32] In this work, high external quantum yields were achieved.

*2. Energetic and Interfacial Electron Transfer Kinetics of the Grätzel Cell*

Figure 5 shows the energetics of the Grätzel cell. First, the dye absorbs light and becomes excited. The excited state must have sufficient energy to inject an electron into the conduction band of $TiO_2$, yielding Ru(III). The electron in $TiO_2$ diffuses towards the back of the electrode and produces current. It then reduces triiodide to iodide at the Pt counter electrode and iodide regenerates Ru(II) by reducing Ru(III). The cell is regenerative. It is possible that the electron in $TiO_2$ transfers back to Ru(III) or to triiodide. These back reactions (or recombination losses) are illustrated in Figure 5 as $k_{bd}$ and $k_{bi}$, respectively. To avoid the back electron transfer to the dye, the rate of regeneration must be faster than the rate of back electron transfer. The back electron transfer to triiodide must also be relatively slow. Further details on the recombination kinetics will be given below.

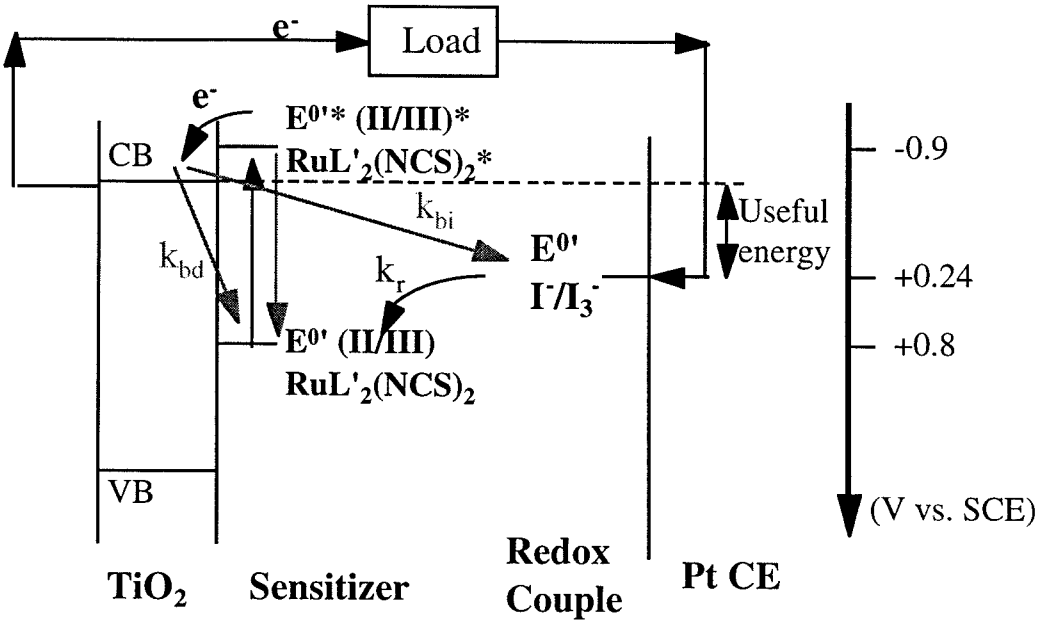


Figure 5: Energetic for the dye sensitization of nanocrystalline $TiO_2$ with [Ru(II)(4,4'-$(CO_2H)_2$bipyridine)$_2$$(NCS)_2$] abbreviated as $RuL'_2(NCS)_2$.

The maximum useful output energy is the difference between the Fermi level of $TiO_2$ and the redox potential of iodide/triiodide. As can be seen in Figure 5, the redox potential of $(RuL'_2(NCS)_2)^{3+/2+}$ is ~ 0.5 V more positive than the redox potential of the $I^-/I_3^-$ system that is used to carry the faradaic charge in the electrolyte. Energy is therefore wasted. To increase $V_{oc}$, one possibility is to use a redox couple in solution that has a more positive redox potential. The only redox couple with a more positive redox potential that works is bromide/bromine, which resulted in larger $V_{oc}$ values but smaller photocurrents.[33] We have attempted to use a faster one electron redox couple (dimethylferrocene/ferrocenium). However, the electrons (at the conducting glass and/or $TiO_2$ surface) back transferred quickly to the acceptor in solution and very little net photocurrent was observed. Iodide/triiodide seems to be the only couple that works well in this system.

The very fact that the Grätzel cell works as a solar cell is interesting in itself. Nanoparticles of $TiO_2$ are too small to support an electric field like the one formed in larger crystalline semiconductors in contact with a solution.[5,34,35] The charges are therefore separated by other means. Various studies have shown that the electron transport of electrons in the $TiO_2$ film occurs via diffusion rather than drift.[36-39] In particular, B. Gregg and co-workers showed that the potential in the $TiO_2$ film does not necessarily correspond to the potential applied to the electrode, that charge transport occurs by diffusion, that the transient electric field between the injected electron and M(III) is quickly neutralized by intercalated $Li^+$, and that a high electrolyte concentration is therefore required to efficiently neutralize the field and allow for the electron to move away.[39] Therefore, ions in solution can screen transient electric fields, such that once in $TiO_2$, the electron does not feel the positive charge of the Ru(III). This partly explains why the electron does not quickly back react and why charge separation can take place.

The success of charge separation in this type of solar cell also relies on kinetics. First, the injection rate has to compete effectively with the excited state relaxation. Initially, injection rates of the order of $10^7$ - $10^9$ $s^{-1}$ were measured.[18,21,40-42] However, such slow injection rates could not account for the success of $RuL'_2(NCS)_2$, which has a lifetime less than 50 ns.[16] More sophisticated ways to measure injection rates have been developed and many workers now report injection rates occurring in subpicosecond time scales.[20,43-49] The lifetime of a dye is therefore unlikely to limit its injection efficiency and other factors are more important (see below).

As mentioned earlier, the regeneration rate of the dye has to compete effectively with the back electron transfer to the dye. In this system, the regeneration rate is believed to be on a time scale of $10^{-8}$ s whereas the back-reaction to the dye is slower, in the $10^{-3}$ - $10^{-7}$ s range.[13,16] The decay kinetics of Ru(III) are usually faster in the presence of iodide.[50-52] The slow back reaction is believed to be due to poor electronic coupling.[53]

The recombination kinetics between electrons in $TiO_2$ and the oxidized dye are not well understood and cannot originate solely from electrons in the conduction band of $TiO_2$. Surface traps of various depths are usually required to explain experimental data. The importance of surface traps on electron transport and interfacial charge transfer processes has been explored by many workers.[54-58] Applying an external potential influences the occupancy of both trap and conduction band states.[50] Several workers have studied the effect of applied bias on recombination rates but with different conclusions.[13,59,60] Recently, Durrant and co-workers showed that charge recombination kinetics depend strongly upon bias voltage.[50] Their results were consistent with recombination kinetics strongly dependent upon the accumulation of electrons in intraband/conduction band states of the $TiO_2$ film.[50] As a side note, Skinner *et al.* measured the electron trapping time to be 180 fs.[61]

The effect of the dye's ground state redox potential on the kinetics of charge recombination is controversial and not well understood. If the electron transfer was simply from the conduction band states of $TiO_2$ to the oxidized dye, then the Marcus theory of electron transfer would apply. However, this is not the case. Not surprisingly, strong evidence for the normal or inverted Marcus region has not been found.[52,53]

The dominant back-reaction in the specific case of $RuL'_2(NCS)_2$ has been proposed to be the reduction of triiodide by electrons in $TiO_2$.[16,32] There have been efforts to lower this back-reaction by pretreating the electrode with 4-*tert*-butylpyridine,[16] pyridine,[32] or with coadsorbates.[62] Pretreatment with 4-*tert*-butylpyridine and pyridine were found to increase $V_{oc}$ without decreases in photocurrent. With pyridine pretreatment, an increase in photocurrent was actually observed, which is the opposite of what would be expected for pH effects on the conduction band edges of $TiO_2$. These results are interpreted solely in terms of blocking the back reaction. Cholonic acid coadsorbates were found to both increase photocurrent and open-circuit voltages. These effects were explained by combining of the blocking effect of the back reaction and the band edge shift of $TiO_2$ with

pH.[62] The probability of back reaction to triiodide increases with triiodide concentration[32] and with the distance between the photoexcited particle and the conducting glass back contact.[32,34] The back electron transfer to triiodide most likely also depend on the film's porosity. Papageorgiou *et al.* modeled the steady-state mass transport of a sandwich-type cell and were able to predict limiting currents of iodine containing electrolytes as a function of the film porosity.[63] The model was used to determine the effective diffusion coefficient of triiodide in porous $TiO_2$ films.[63]

If the dominant back reaction is the reduction of $I_2$ (or triiodide), then we expect that the photovoltage would remain relatively constant at a constant carrier injection level, regardless of which dye is used to generate the injected electrons into the $TiO_2$ support. Use of a series of dyes (Table 9) has allowed us to probe the generality of this hypothesis in order to better understand the factors that control the photovoltage of dye-sensitized nanocrystalline $TiO_2/CH_3CN$ contacts.

*3. Extending the Spectral Response of the Grätzel Cell to Longer Wavelengths*

In order to improve the efficiency of the Grätzel solar cell, it is important to design dyes which show enhanced spectral response at longer wavelengths. As shown in Figure 6, light at wavelengths above 700 nm is not utilized for energy conversion. For this type of complex, the visible absorption band is due to a MLCT from the $t_{2g}$ metal orbital to the empty $\pi^*$ orbital of the bipyridyl ligand.[64] The energy of the absorption band can therefore be related to the energy gap between the ground state and the excited state redox potentials. Lowering that gap will red shift the MLCT band and should consequently enhance the spectral response at longer wavelengths, providing that the energetics are still adequate. We will now discuss the approach of lowering that gap by either making the excited state redox potential more positive or the ground state redox potential more negative.

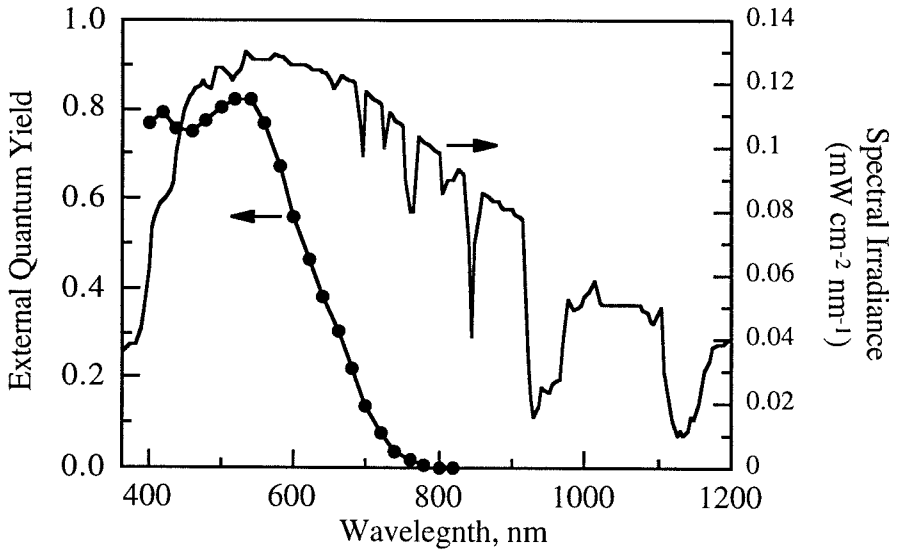


Figure 6: Comparison of the spectral response of $RuL'_2(NCS)_2$ (●) with the spectral distribution of sunlight under Air Mass 1.5 conditions (solid line).

The energy of the excited state can be made more positive by lowering the energy of the $\pi^*$ accepting orbitals. This strategy has been explored by some workers.[18,65,66] In general, lower maximum external quantum yields were obtained when using lower energy $\pi^*$ accepting orbitals. Nazeeruddin *et al.* concluded that the excited state redox potential plays a more important role in the electron injection process than the lifetime of the sensitizer.[65] They also identified the lowest-energy MLCT transitions by resonance-Raman spectroscopy and the excited electrons were localized on the acceptor ligands which contained carboxylate groups. Recently, Jing *et al.* demonstrated that it is important that the excited electron be localized on the ligand with the anchoring groups.[67] Note that Jing *et al.* utilized a phosphonate anchoring group.[67] Some workers now use phosphonate

groups instead of carboxyl groups because carboxyl groups slowly desorb from the $TiO_2$ surface in the presence of water.[68]

The ground state redox potential can be made more negative by destabilizing the $t_{2g}$ orbitals of the metal. This can be done by using better electron donor ligands on the metal, or by replacing the ruthenium metal center with osmium. Grätzel and co-workers have compared a series of $RuL'_2X_2$ where X=$Cl^-$, $NCS^-$ and $CN^-$.[16] As expected, the ground state redox potential was increased from 0.57 V vs SCE for the dichloro complex to 1.16 V vs SCE for the dicyano complex. This concept was also shown for other mixed ligand complexes of ruthenium.[15,65,69]

The strategy of replacing the ruthenium metal center with osmium has been explored by G. Meyer and co-workers with limited success.[1,51] They compared the spectral response of $OsL'_2(CN)_2$ with that of $RuL'_2(CN)_2$ and found that the maximum external quantum yield of the osmium complex were much lower than that of the ruthenium analog.[1] The only key difference they found between the two complexes is their ground-state oxidation potentials, with the Os(III/II) being 340 mV more positive than the Ru(III/II).[51] This difference could result in slower regeneration rates, which would decrease the efficiency of the cell. Meyer and co-workers published time-resolved measurements which support this hypothesis.[51] However, we realized that the ground state oxidation potential of this osmium dye is similar to that of the $RuL'_2(NCS)_2$ and actually more positive than that of another good sensitizer (the black dye, discussed below). There must therefore be some other reason why the $OsL'_2(CN)_2$ sensitizer did not perform well.

There have been other efforts in designing dyes with better absorption at longer wavelengths.[68,70-76] One success worth mentioning is the "black dye," or tris(isothiocyanato)(4,4',4"-tricarboxy-2,2':6',2"-terpyridine)ruthenium(II).[70] The absorption spectra of this sensitizer has a maxima at 620 nm and extends up about 900 nm.

The external quantum yield was 0.8 from 400 to 700 nm (the electrolyte was 0.9 M LiI, 0.1 M $LiI_3$ in propylene carbonate).

Changes in the sensitizer that extend its light absorption to lower energies while maintaining the excited state redox potential at the same energy level relative to the $TiO_2$ can therefore yield improved efficiencies, provided that such changes do not produce concomitant decreases in the open-circuit voltage and/or the fill factor of the resulting photoelectrochemical device.

In this work, we explore the approach of replacing ruthenium with osmium in the transition metal complexes that are used to sensitize the $TiO_2$. The osmium complexes are expected to have an additional absorption band at longer wavelengths compared to a ruthenium complex with the same ligands, because direct excitation to the triplet state in Os(II) $(bipyridine)_xL_y$ systems is not as forbidden as in the Ru(II) $(bipyridine)_xL_y$ systems.[64] Higher photocurrents are therefore expected for $TiO_2$ electrodes coated with the osmium complexes, provided that the excited state in the Os complex effectively injects electrons into the $TiO_2$ support.

The Os complexes have other potential advantages relative to their Ru analogs. Although the excited-state lifetimes for Os complexes are typically shorter than those for the analogous Ru complexes, the Os(II) excited state should be as effective in sensitizing $TiO_2$ because electron injection into nanocrystalline $TiO_2$ is thought to occur on a sub-picosecond timescale.[43,45,48,49,77] Perhaps more importantly, the ground-state potential of the Os complexes can be readily tuned to less positive potentials by using stronger $\sigma$-donor ligands.[69] By using a sensitizer with a less positive ground state redox potential and a constant excited state redox potential, less energy will be wasted in the reduction of Os(III) to Os(II) by iodide, possibly yielding even further improvements in the efficiency of the overall system. However, it is not clear whether the ground states of the Os(III) dyes will have sufficient driving force to oxidize iodide at a rate rapid enough to support the required current density between the electrodes in the cell under typical solar illumination conditions.

We have therefore performed electrochemical experiments to determine both the ground and excited state redox potentials of the Os and Ru complexes in order to probe the device performance as a function of the position of these energetic parameters.

The structure of this thesis is relatively simple. Chapter 2 presents the experimental details. Chapters 3 and 4 present the results and discussions part 1 and 2, respectively. Chapter 3 focuses on the characterization of the complexes in solution, and Chapter 4 focuses on the photoelectrochemistry. Chapter 5 is the conclusion and references are listed at the end.

# Chapter 2:

# Experimental Section

In this chapter I will first enumerate the materials, in section A. Section B describes the synthesis of all the complexes made for this study. Section C describes the methods used, which include the characterization of the complexes, preparation of $TiO_2$ electrodes, and the spectroelectrochemistry. I sometimes refer to my laboratory books, where the first number is the book number and the second number is the page number. For example, gs3p55 corresponds to Geneviève Sauvé's lab book # 3, page 55.

## A. Materials

$(NH_4)_2[OsCl_6]$ (Alfa, 99.99%), 2,2'-bipyridine-4,4'-dicarboxylic acid (Alfa), 2,2'-bipyridine (Aldrich, 99%+), $HPF_6$ (Aldrich), NaCN (EM Science), NaSCN (Alfa), $Na_2S_2O_4$ (Alfa), $KS^{13}C^{15}N$ (Isotech), $K^{15}NO_3$ (Isotech), $CF_3SO_3H$ (Aldrich), $D_2O$ with 1% w/w 3-(trimethylsilyl)-1-propanesulfonic acid, sodium salt (DSS) (Aldrich), $d^6$-DMSO (CIL), ethylene glycol (EM Science), concentrated nitric acid (EM Science), titanium isopropoxide (Aldrich, 99.999%), titanium tetrachloride (Aldrich, 99.9%), Polyethylene glycol M. W. 20 000 (Serva), Sephadex LH-20 (Fluka), and Sephadex DEAE A-25 (Aldrich) were used without further purification. Lithium iodide (Alfa, 99%, anhydrous) was used as received but was stored in a dry box until use. Iodine (Aldrich, 99.99%+) was sublimed under vacuum before use. Pyridinium triflate was purified by dissolving the material (97%, Aldrich) into a minimum amount of warm acetonitrile, and the salt was then precipitated by addition of ethyl ether. The precipitate was filtered through a medium-porosity glass frit and was washed with ether and then dried overnight under vacuum. Pyridine (J.T. Baker) was distilled before use. Lithium perchlorate anhydrous (J.T. Baker) was dried at 180 °C for 48 h under active vacuum. All solvents used were reagent grade (EM Science) except for absolute ethanol, which was purchased from Quantum

Chemicals. Acetonitrile was pre-dried over $CaH_2$ and distilled over $P_2O_5$. 17.8 MΩ cm resistivity water was obtained from a Barnstead NANOpure Inc. filtration system.

## B. Synthesis of Complexes

***cis*-[$OsL_2Cl_2$]: *cis*-bis(2,2'-bipyridyl)dichloroosmium(II).** $OsL_2Cl_2$ (L=2,2'-bipyridyl) was synthesized following the procedure of Kober *et al.*[78] $[OsCl_6](NH_4)_2$ (0.384 g, 8.7 x $10^{-4}$ moles) and 2,2'-bipyridine (0.277 g, 1.77 x $10^{-3}$ moles) were first dissolved in 20 mL of ethylene glycol in a 100 mL round bottom Schlenk flask. The mixture was then heated to 170 °C for 2 h with stirring, under nitrogen. After this time, sodium dithionite (0.4 g, 2.2 x $10^{-3}$ moles) was dissolved in 20 mL of water and added dropwise to the cooled mixture while stirring, in order to convert excess Os(III) to Os(II). The dark purple precipitate was filtered, washed with water to remove ionic products and $[OsL_3]^{2+}$, and washed with ether to remove unreacted ligand. The final product was dried under vacuum overnight. Yield: 0.43g.

**[$OsL_2L'](PF_6)_2$: bis(2,2'-bipyridyl)(4,4'-dicarboxy-2,2'-bipyridyl)-osmium(II) hexafluorophosphate.** $[OsL_2L'](PF_6)_2$ (L'=4,4'-dicarboxy-2,2'-bipyridyl) was prepared as follows: $NaHCO_3$ (0.222 g, 2.65 x $10^{-3}$ moles) and 2,2'-bipyridine-4,4'-dicarboxylic acid (0.213 g, 8.72 x $10^{-4}$ moles) were dissolved in 15 mL of water. This mixture was added to 0.427 g (7.4 x $10^{-4}$ moles) of $OsL_2Cl_2$ dissolved in 15 mL of ethanol, and the solution was refluxed with stirring for 6 h under nitrogen. $NH_4PF_6$ (0.3 g, 1.8 x $10^{-3}$ moles) dissolved in 5 mL of water was then added to the cooled reaction mixture. The ethanol was evaporated using a rotary evaporator and 10 drops of 0.25 M $HPF_6$ were added to precipitate $[OsL_2L'](PF_6)_2$. The resulting mixture was left in the refrigerator overnight. The black precipitate was filtered, washed with pH 1.5 water (acidified with $HPF_6$) and with ether, and dried overnight under vacuum. A parent ion was observed at 748 a.m.u. in the fast atom bombardment mass spectrum (FAB/MS) (mass expected for $[OsL_2L'](PF_6)^+$ is 748 a.m.u), and another peak, ascribed to $[OsL_2L'](PF_6)_3^+$, was observed at 893 a.m.u. The product was dissolved in a minimum

amount of 0.1 M $NaHCO_3$ (aq) and loaded onto a chromatography column (2.5 cm dia.) that had been packed with approximately 30 cm of anion exchange resin (Sephadex DEAE A-25 in water). The eluent was pure water, and the first band (green) was discarded. The second band (brown, major band) was collected and the volume reduced to 5 to 10 mL by rotary evaporation. The product was precipitated upon addition of 1.0 M $HPF_6$ (aq), filtered with a fine-porosity glass frit and washed with 0.1 M $HPF_6$ (aq) and diethyl ether. It was then dried under vacuum overnight. Elemental analysis for $C_{32}H_{24}N_6O_4P_2F_{12}Os \cdot 6H_2O$ gave (calculated values in parentheses) C, 33.46 (33.57); H, 2.80 (3.17); N, 7.22 (7.34). The chloride salt was isolated by taking the eluted band from the ion exchange column, adding a minimum amount of 1.0 M HCl and evaporating to dryness using a rotary evaporator. Elemental analysis for $C_{32}H_{24}N_6O_4Cl_2Os \cdot 6H_2O$ gave (calculated values in parentheses) C, 41.44 (41.52); H, 4.26 (3.92); N, 9.18 (9.08).

**$K_4[OsL'_3]$: potassium tris(4,4'-dicarboxy-2,2'-bipyridyl)osmiate(II).** $[OsCl_6](NH_4)_2$ (0.171 g, $3.90 \times 10^{-4}$ moles), L' (0.2942 g, $1.20 \times 10^{-3}$ moles) and a few drops of 1.0 M NaOH (aq) were mixed in 25 mL of ethylene glycol and heated to 190 °C for 2 h with stirring under nitrogen. The mixture was transferred to a large beaker and 125 mL of water was added. 0.25 M $HPF_6$ (aq) was added dropwise until the pH was 1.5 to 2 and a large excess of $KPF_6$ (1 g, $5 \times 10^{-3}$ moles) was then added in order to precipitate the product. The dark green precipitate was filtered with a fine-porosity glass frit and washed with 0.1 M $HPF_6$ and ether. The FAB/MS parent ion was observed at 924.1 (expected at 924.1 for $[OsL'_3(PF_6)_2]^+$). $[OsL'_3](PF_6)_2$ was then dissolved in 0.2 M KOH (aq) and purified by ion exchange column chromatography using Sephadex DEAE A-25 as the column support. Impurities were eluted with water and 0.2 M KI. The major green-brown band was eluted with 0.4 M KI (aq), collected and evaporated to dryness using a rotary evaporator. The KI was removed by extraction with absolute ethanol until some of the product dissolved. The remaining KI was removed by extraction with acetone, and $K_4[OsL'_3]$ was isolated by filtration.

$K_4[OsL'_3]$ was dissolved in methanol, precipitated upon addition of acetone, filtered, and washed with acetone and ether. It was dried under vacuum overnight. Elemental analysis for $C_{36}H_{18}N_6O_{12}K_4Os \cdot 6H_2O$ gave (calculated values in parentheses) C, 36.70 (36.54); H, 2.60 (2.73); N, 6.97 (7.10). The chloride salt of the fully protonated complex was obtained by dissolving $K_4[OsL'_3]$ in a few mL of water, adding 1 M HCl to precipitate the chloride salt, and filtering with a fine-porosity glass frit. Elemental analysis for $C_{36}H_{24}N_6O_{12}Cl_2Os \cdot 6H_2O$ gave (calculated values in parentheses) C, 39.49 (39.24); H, 3.37 (3.29); N, 7.54 (7.63).

***cis*-[OsL'$_2$Cl$_2$]: *cis*-dichlorobis(4,4'-dicarboxy-2,2'-bipyridine)osmium(II).** The synthesis of $OsL'_2Cl_2$ was adapted from the procedure of Heimer *et al.*[1] $[OsCl_6](NH_4)_2$ (0.1950 g, 4.44 x $10^{-4}$ moles) and L' (0.190 g, 7.78 x $10^{-4}$ moles) were heated at 170 °C for 2 h in 30 mL of ethylene glycol under nitrogen. The mixture was then transferred into a large beaker and diluted with 150 mL of water. $Na_2S_2O_4$ (0.1 g, 6 x $10^{-4}$ moles) was added to reduce any Os(III) to Os(II). The dark purple precipitate was isolated by centrifugation. Purification consisted of dissolving the product in water with a minimum amount of NaOH (aq), precipitating the solid with 2M HCl (aq), and isolating the solid by centrifugation. The product was dissolved in acetone and filtered to remove unreacted ligand (L') (which is insoluble in acetone). Approximately 20 mL of pH 2 water (acidified with HCl) were added to the solution and the product was precipitated by evaporation of the acetone under vacuum. The precipitate was isolated by centrifugation, washed twice with pH 2 water (acidified with HCl), and then dried overnight under vacuum. The yield was 55%. This complex is readily oxidized in air and was therefore kept under an inert atmosphere. A FAB/MS parent ion $(M-H)^+$ peak was observed at 749 (expected at 750 for $[OsL'_2Cl_2]^+$).

***cis* - K[OsL'(L'-H$^+$)(CN)$_2$]: potassium *cis*-dicyanobis(4,4'-dicarboxy-2,2'-bipyridyl)osmiate(II).** This synthesis is adapted from the procedure reported by Heimer and al.[1] $OsL'_2Cl_2$ (0.084 g, 1.1 x $10^{-4}$ moles) was dissolved with

KCN (0.27 g, 4.1 x $10^{-3}$ moles) in 7 mL of water and the solution was refluxed for 12 h with stirring under nitrogen atmosphere. The cooled reaction mixture was poured into 100 mL of DMF to precipitate $K_4[Os(L'\text{-}H^+)_2(CN)_2]$. The brown precipitate was isolated by filtration, washed with DMF and acetone, and dried under vacuum overnight. The crude product was dissolved in water and purified by column chromatography using Sephadex DEAE A-25 as the column support and 0.5 M $KNO_3$ (aq) as the eluent. The major band (green-brown) was collected. The mixture was evaporated to about 100 mL and filtered to remove excess $KNO_3$. The filtrate was further evaporated to 20 mL and filtered to remove additional $KNO_3$. 1 mL of 0.26 M $CF_3SO_3H$ (aq) was added to the filtrate to precipitate the $K[OsL'(L'\text{-}H^+)(CN)_2]$, which was isolated by filtration, washed with 0.26 M $CF_3SO_3H$ (aq) and ether, and then dried under vacuum overnight. Elemental analysis for $C_{26}H_{15}N_6O_8OsK\cdot 3H_2O$ gave (calculated values in parentheses) C, 38.10 (37.96); H, 2.71 (2.57); N, 10.14 (10.21).

***cis*-[OsL'$_2$(NCS)$_2$]: *cis*-bis(4,4'-dicarboxy-2,2'-bipyridyl)bis(isothiocyanato)osmium(II).** This preparation was adapted from the published synthesis of $OsL_2(NCS)_2$.[79] $OsL'_2Cl_2$ (0.16 g, 2 x $10^{-4}$ moles), NaSCN (0.8 g, 1 x $10^{-2}$ moles) and 1 mL of 1.0 M NaOH (aq) were mixed with 15 mL of water and refluxed for 5 h under nitrogen. 2.5 mL of 1.0 M HCl (aq) were then added to precipitate the product. The mixture was left overnight in the refrigerator. The product was filtered and washed with 0.1 M HCl (aq). The product was dissolved in a minimum amount of methanol and purified by column chromatography using Sephadex LH-20 as the column support and methanol as the eluent. The first band (brown-green) was likely due to $OsL'_3{}^{2+}$ and was discarded. Other, orange-colored, bands which eluted quickly were also discarded. The main band, which was dark purple and eluted very slowly, eventually becoming very wide, was collected. The methanol was evaporated from the collected fraction using a rotary evaporator, and the final product was dried overnight under vacuum.

Elemental analysis for $C_{26}H_{16}N_6O_8S_2Os \cdot 5H_2O$ gave (calculated values in parentheses) C, 35.23 (35.29); H, 2.63 (2.96); N, 9.37 (9.50).

***cis*-[OsL'$_2$($^{15}$N$^{13}$CS)$_2$]: *cis*-bis(4,4'-dicarboxy-2,2'-bipyridyl)bis($^{15}$N, $^{13}$C-isothiocyanato)osmium(II).** The $^{15}$N, $^{13}$C labelled sample of the isothiocyanato complex was synthesized by a slightly different procedure. $OsL'_2Cl_2$ (0.0660 g, 8.81 x $10^{-5}$ moles) and $KS^{13}C^{15}N$ (0.0776 g, 7.82 x $10^{-4}$ moles) were dissolved in 4 mL $H_2O$ and 352 µL of 1.0 M KOH (aq). The reaction flask was purged with argon and the reaction refluxed under a positive pressure of argon for 8 h. The product was precipitated with 2 mL of 0.267 M $CF_3SO_3H$ (aq), then centrifuged and the filtrate removed. Twice, the product was redissolved in 350 µL of 1.0 M KOH (aq), precipitated with 2 mL of 0.267 M $CF_3SO_3H$ (aq), centrifuged, and the filtrate removed. The product was then dried in a vacuum dessicator. The FAB/MS of the complex made through an analogous synthesis, but using unlabelled KSCN, yielded a parent ion peak $M^+$ at 796 (expected 796) and an infrared peak at 2111 $cm^{-1}$ (ascribed to the C≡N stretch in M-NCS).

***cis*-[RuL'$_2$Cl$_2$]: *cis*-dichlorobis(4,4-dicarboxy-2,2'-bipyridyl)ruthenium(II).** $RuCl_3 \cdot 3H_2O$ (0.13 g, 5.0 × $10^{-4}$ moles) and L' (0.24 g, 1.0 × $10^{-3}$ moles) were dissolved in 15 mL of ethylene glycol and the solution was purged with argon.[80] It was then stirred for 2 h at 150 °C under argon, and the ethylene glycol removed by distillation under vacuum at 80 °C. The product was then dissolved in ~ 100 mL of methanol and 20 drops of 1 M HCl (aq) were added. The mixture was filtered to remove unreacted ligands and the methanol was evaporated from the filtrate using a rotary evaporator. The product was then redissolved in ~ 1 mL of 1 M NaOH (aq) and precipitated by addition of 1 mL of 1 M HCl (aq). The final product was cooled in an ice bath for a few hours, filtered, washed with 100 mL of 0.1 M HCl (aq) followed by 30 mL of ether, and dried overnight under vacuum.

***cis*-[RuL'$_2$(NCS)$_2$]: *cis*-bis(4,4-dicarboxy-2,2'-bipyridyl)bis(isothiocyanato)ruthenium(II).** $RuL'_2Cl_2$ (0.1 g, $1.7 \times 10^{-4}$ moles) and NaSCN (0.35 g, $4.3 \times 10^{-3}$ moles) were dissolved in 5 mL of water and 1 mL of 1.0 M NaOH (aq). The mixture was stirred at reflux under nitrogen for 22 h. After cooling the mixture, ~ 2 mL of 1.0 M HCl (aq) was slowly added to precipitate the product. The mixture was then left overnight in an ice bath. The product was isolated by vacuum filtration, washed with 0.1 M HCl (aq) and with ether, and dried overnight under vacuum. The dried product contained an impurity, likely $RuL'_3$, as seen by emission spectroscopy. This product was therefore further purified by column chromatography using LH-20 as the column support and methanol as the eluent. The first band (orange) was attributed to $RuL'_3{}^{2+}$ and was discarded. The second band (dark red-purple) was collected. The methanol was evaporated using a rotary evaporator and the product dried overnight under vacuum. Because the $RuL'_3{}^{+2}$ and $RuL'_2(NCS)_2$ bands eluting from the column overlapped slightly, the purification by column chromatography was repeated a second time. After the second purification, the emission spectrum showed no evidence of $RuL'_3{}^{2+}$ in the product. Elemental analysis for $C_{26}H_{16}N_6O_8S_2Ru{\cdot}3H_2O$ gave (calculated values in parentheses) C, 41.16 (41.11); H, 2.67 (2.92); N, 10.85 (11.06).

***cis*-[RuL'$_2$($^{15}$N$^{13}$CS)$_2$]: *cis*-bis(4,4'-dicarboxy-2,2'-bipyridyl) bis($^{15}$N, $^{13}$C-isothiocyanato)ruthenium(II).** The $^{15}N$, $^{13}C$ labelled sample of the isothiocyanato complex was synthesized by a slightly different procedure. $RuL'_2(ox)$ (ox=oxalate) was first synthesized by heating in a boiling water bath $K_4[Cl_5Ru\text{-}O\text{-}RuCl_5]{\cdot}H_2O$ (0.545 g, $7.47 \times 10^{-4}$ moles) and $K_2C_2O_4{\cdot}H_2O$ (0.825g, $4.48 \times 10^{-3}$ moles) in 12 mL of water with stirring under argon atmosphere. After 3 h, 20 mL of methanol, and a solution of 2,2'-bipyridine-4,4'-dicarboxylic acid (0.365g, $1.495 \times 10^{-3}$ moles) in 5 mL of water and 5 mL of 1.0 M KOH (aq), were added to the reaction mixture and heated for an additional 8 h. After cooling, the methanol was removed *in vacuo* and $RuL'_2(ox)$ was precipitated upon addition of 0.27 M $CF_3SO_3H$ (aq). The precipitate was isolated by

centrifugation. The precipitate was dissolved in a minimum amount of 1.0 M KOH (aq), the solid was precipitated with $CF_3SO_3H$ (aq), and the product was isolated by centrifugation. This process was repeated 2-3 times to remove some impurities. The product was then dried under vacuum overnight. To make $RuL'_2(^{15}N^{13}CS)_2$, $RuL'_2(ox)$ (0.0590 g, $8.71 \times 10^{-5}$ moles) and $KS^{13}C^{15}N$ (0.0814g, $8.20 \times 10^{-4}$ moles) were dissolved in 4 mL $H_2O$ and 348 µL of 1.0M KOH (aq). The reaction flask was purged with argon and the reaction refluxed under a positive pressure of argon for 9 h. The product was precipitated with 1.5 mL of 0.267 M $CF_3SO_3H$ (aq), then centrifuged and the filtrate removed. The product was redissolved in 500 µL of 1.0 M KOH (aq), precipitated with 1.5 mL of 0.267 M $CF_3SO_3H$ (aq), centrifuged, and the supernatant removed. The product was dried in a vacuum desiccator.

***cis*-[RuL$_2$($^{15}$N$^{13}$CS)$_2$]: *cis*-bis(2,2'-bipyridyl)bis($^{15}$N$^{13}$C-isothiocyanato) ruthenium(II).** $[RuL_2CO_3]$ was synthesized using a previously reported procedure.[78] $[RuL_2CO_3]$ (0.0600g, $1.27 \times 10^{-4}$ moles) and $KS^{13}C^{15}N$ (0.0896g, $9.03 \times 10^{-4}$ moles) were then dissolved in 4 mL of absolute ethanol. The reaction mixture was refluxed for 8 h under a positive pressure of argon. The product precipitated from the reaction mixture and was washed with two portions of ethanol to remove excess starting materials. The product was dried in a vacuum desiccator.

***cis*-[RuL'$_2$(CN)$_2$]: *cis*-dicyanobis(4,4'-dicarboxy-2,2'-bipyridyl) ruthenium(II).** $RuL'_2Cl_2$ (0.13 g, $2.3 \times 10^{-4}$ moles) and NaCN (0.25 g, $5.1 \times 10^{-3}$ moles) were added to 10 mL of water and the mixture refluxed under nitrogen for 5 h. With caution, 1.0 M HCl (aq) was then added to the cooled mixture to precipitate the product. The dark solid was isolated by centrifugation, washed with 1.0 M HCl (aq) and dried overnight under vacuum. The product was then dissolved in 3 mL of methanol and purified by column chromatography using Sephadex LH-20 as the column support and methanol as the eluent. The first band (orange) was attributed to $RuL'_3{}^{2+}$ and was therefore discarded. The second band (dark brown) was collected, the methanol was

evaporated using a rotary evaporator, and the product dried. The solid was then dissolved in 1.5 mL of 0.1 M $NaHCO_3/Na_2CO_3$ (aq) buffer, and addition of 500 μL of 1.0 M HCl (aq) precipitated the product. 1.5 mL of water and a drop of concentrated HCl were added to the mixture and the solution left overnight in the refrigerator to complete the precipitation. The product was filtered with a fine-porosity glass frit, washed with 0.1 M HCl (aq), and dried overnight under vacuum. Elemental analysis for $C_{26}H_{16}N_6O_8Ru \cdot 3H_2O$ gave (calculated values in parentheses) C, 44.07 (43.76); H, 3.09 (3.39); N, 11.59 (11.78).

**$[RuL_2L'](PF_6)_2$: bis(2,2'-bipyridyl)(4,4'-dicarboxy-2,2'-bipyridyl) ruthenium(II) hexafluorophosphate.** $[RuL_2L'](PF_6)_2$ was prepared by the procedure of Sprintschnik *et al.*[81] 2,2'-bipyridine-4,4'-dicarboxylic acid (0.153 g, $6.26 \times 10^{-4}$ moles), $RuL_2Cl_2.2H_2O$ (0.26 g, $5.0 \times 10^{-4}$ moles), and $NaHCO_3$ (0.15 g, $1.8 \times 10^{-3}$ moles) were dissolved in 5 mL of methanol and 7.5 mL of $H_2O$. The reaction was stirred at reflux for 2.5 h under nitrogen. The final reaction mixture was orange-red. After cooling to room temperature, 2 mL of 1.0 M $HPF_6$ (aq) were added to precipitate the product, which was isolated by filtration, washed with 0.1 M $HPF_6$ (aq) and ether, and dried under vacuum overnight. $[RuL_2L'](PF_6)_2$ was further purified by column chromatography using Sephadex DEAE A-25 as the column support and water as the eluent. The major band was collected and the eluent evaporated to a few mL using a rotary evaporator. 0.4 mL of 1 M $HPF_6$ (aq) was then added to precipitate the $[RuL_2L'](PF_6)_2$. $[RuL_2L'](PF_6)_2$ was isolated by filtration, washed with 0.1 M $HPF_6$ (aq) and ether, and dried under vacuum overnight. Elemental analysis for $C_{32}H_{24}N_6O_4P_2F_{12}Ru \cdot 5H_2O$ gave (calculated values in parentheses) C, 37.31 (37.04); H, 3.13 (3.30); N, 8.10 (8.10). The chloride salt was isolated by taking the eluted band from the ion exchange column, adding a minimum amount of 1 M HCl (aq), and evaporating to dryness using a rotary evaporator. Elemental analysis for $C_{32}H_{24}N_6O_4Cl_2Ru \cdot 4H_2O$ gave (calculated values in parentheses) C, 47.77 (48.01); H, 3.92 (4.03); N, 10.41 (10.50).

**$K_4[RuL'_3]$: potassium tris(4,4'-dicarboxy-2,2'-bipyridyl) ruthenium(II).** $RuL'_2Cl_2$ [82] (0.215 g, 2.87 x $10^{-4}$ moles) was combined with L' (0.0795 g, 3.26 x $10^{-4}$ moles), *ca.* 0.5 mL of triethylamine, 25 mL water and 25 mL ethanol. The mixture was heated at reflux for 3.5 h and then cooled to room temperature. The ethanol was removed by rotary evaporation, and ~ 0.5 g of $NH_4PF_6$ added to the solution. The mixture was then cooled to 5 °C. Precipitation of the crude product was induced by dropwise addition of 3 M HCl (aq) while stirring in an ice bath. The solid was collected on a fine-porosity glass frit and rinsed with acetone followed by diethyl ether. The crude product was then redissolved in 0.01 M $NaHCO_3$ (aq) and loaded onto an anion exchange resin column (2.5 cm × 25 cm of Sephadex DEAE-A-25). Some impurities were eluted first using 0.2 M KI (aq) and discarded. The product was eluted using 0.4 M KI (aq), and the eluent was taken to dryness by rotary evaporation. The KI was removed by extraction with ethanol until some of the product dissolved in ethanol. The remaining KI was extracted with acetone, and the product isolated by filtration. Elemental analysis for $C_{36}H_{18}N_6O_{12}K_4Ru \cdot 6H_2O$ gave (calculated values in parentheses) C: 39.72 (39.59), N: 7.65 (7.70), H: 2.65 (2.77).

## C. Methods

### *1. Characterization of the Complexes*

The $^1H$ (500 MHz) NMR spectra were recorded on a Brucker AM 500 FT NMR Spectrometer. Samples were prepared in $D_2O$ with just enough NaOD added to dissolve the metal complex. The $D_2O$ contained 1% DSS (3-(trimethylsilyl)-1-propanesulfonic acid, sodium salt) for reference (δ 0.00 ppm). All $^{15}N$ (50.70 MHz) and $^{13}C$ (125.77 MHz) spectra were recorded on a Brucker AMX-500 FT NMR Spectrometer. These samples were either prepared in $D_2O$ with NaOD added to dissolve the metal complex (with $K^{15}NO_3$ as the $^{15}N$ reference at 0.0 ppm and 1,4 dioxane as the $^{13}C$ reference at 66.5 ppm), or in $d^6$-DMSO (with $K^{15}NO_3$ as the $^{15}N$ reference at 0.0 ppm and $d^6$-DMSO used for the $^{13}C$ reference at 39.51 ppm).

Mass spectra were obtained with a ProSpecE FAB$^+$ Mass Spectrometer in low resolution mode. Elemental analyses were performed by the Analytical Service at Caltech. Infrared spectra of KBr pellets of the sample were recorded on a Perkin-Elmer 1600 Series FTIR, normally with 2 $cm^{-1}$ resolution.

Electronic absorption spectra were recorded on a Hewlett Packard 8452A diode array spectrophotometer. To obtain reproducible spectra, the solvent was buffered with 1.0 mM pyridine and 1.0 mM pyridinium for acidity control. The chloride salts of $OsL'_3^{2+}$, $RuL_2L'^{2+}$ and $OsL_2L'^{2+}$ were used because they are more soluble in methanol and ethanol.

Emission spectra were recorded at room temperature using a PMT R406 (Products for Research, Inc.) photomultiplier tube cooled with dry ice. The solvent was methanol with 1 mM pyridine and 1.0 mM pyridinium triflate. The emission of $OsL'_2(NCS)_2$ was so weak that it could not be detected at room temperature. Instead, spectra for this system were obtained by Prof. A. Maverick at Louisiana State University in an ethanol/methanol (4:1v/v) glass at 77 K.

The excited state lifetimes were obtained by single-photon counting. The complexes used for the measurements were not purified by column chromatography and were therefore not as pure as they can be. Prior to the measurements, the solutions were deaerated by either purging with $N_2$ for at least 40 min or by the freeze-pump-thaw method. The lifetimes were measured at room temperature.

Ground state electrochemical potentials were determined using a standard three-electrode apparatus. The working electrode was a carbon disk electrode, the counter electrode was Pt foil and the reference electrode was a methanolic saturated calomel electrode (MSCE). The MSCE was periodically calibrated against an aqueous SCE (Fischer). Cyclic voltammograms were collected using either a Princeton Applied Research Model 175 universal programmer and a Princeton Applied Research Model 173 potentiostat/galvanostat or a BAS 100B Electrochemical Analyzer from Bioanalytical

Systems. Differential pulse voltammetry (DPV) spectra were collected using a BAS 100B Electrochemical Analyzer. Methanol was used as the solvent because it was the only non-aqueous solvent into which 1 mM of most of the complexes could be dissolved. Except where noted, the supporting electrolyte was 1.00 M $LiClO_4$, and 10 mM pyridine and 10 mM pyridinium triflate were added to control the acidity. For experiments with $OsL'_3^{2+}$ and $Ru(L'\text{-}2H^+)_3^{4-}$, pyridine was omitted because its presence caused precipitation of the dye even at dye concentrations as low as 0.1 mM. Such a low concentration of the dye, coupled with the fact that the cyclic voltammogram occurred at very positive potentials where methanol is also oxidized, rendered the accurate determination of oxidative electrochemical potential of $Ru(L'\text{-}2H^+)_3^{4-}$ by cyclic voltammetry very difficult. The formal potential of this complexe was therefore measured using DPV. In the case of $RuL'_2(NCS)_2$, the cyclic voltammogram was irreversible in methanol. The electrochemical potential was therefore also measured using DPV. The redox behavior of $RuL'_2(NCS)_2$ was more reversible in $CH_3CN$-1.00 M $LiClO_4$, and its cyclic voltammogram was obtained in this electrolyte. The pyridine/pyridinium triflate buffer was omitted in $CH_3CN$ because it caused precipitation of the complex.

The spectroelectrochemistry of $OsL_2L'^{2+}$ was carried out in a thin layer cell consisting of a 1 mm path length quartz cuvette with two side arms attached for inserting Ag/AgCl reference (BAS) and Pt wire counter electrodes. The cell is illustrated in Figure 7. The solution consisted of 10 mM $[OsL_2L'](PF_6)_2$ (not purified by column chromatography) and 1.0 M $LiClO_4$ in dry acetonitrile, and was degassed with argon prior to transferring into the cell. The counter electrode compartment contained a solution of 1.0 M $LiClO_4$ in dry acetonitrile. The potential was applied using a BAS 100 potentiostat and the UV/vis spectra was monitored with a spectrophotometer. (gs2p127-128)

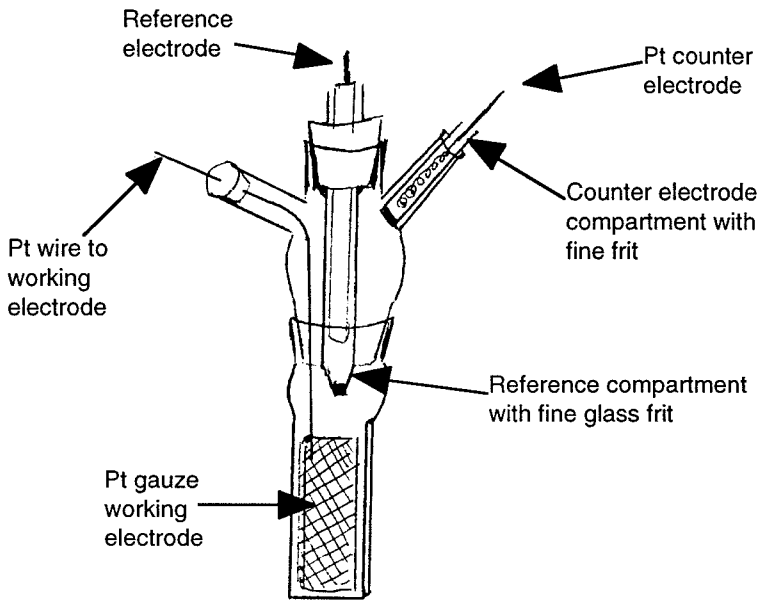


Figure 7: Cell used for the spectroelectrochemical measurements (not drawn to scale).

*2. Preparation of Nanocrystalline $TiO_2$ Electrodes*

The $TiO_2$ colloid was prepared as follows. 1.3 mL of concentrated nitric acid were added to 187.5 mL of water in a 1 L conical flask and the solvent was mixed very vigorously with a large stirring. To minimize flocculation, it is essential to stir vigorously throughout the preparation. 31.25 mL of titanium isopropoxide was added to the solution dropwise from a pressure-equalizing dropping funnel that had a short plastic tube and a pipette tip (for 100 μL pipettes) at the bottom of the funnel to lower the drop rate (see gs2p98). The titanium isopropoxide was added over a one hour period. As the titanium isopropoxide was added, some white precipitate formed, which was unavoidable and went away later during the preparation. The mixture was stirred for 2 h at room temperature and for 8 h at 80 °C to evaporate the propanol. The resulting $TiO_2$ colloid was a pale white color, and can be stored indefinitely. The $TiO_2$ colloid size was measured by TEM (by Carol Garland, Caltech) and the bulk particle size was between 5 and 7 nm in diameter. To

increase the average particle size, 80 mL of the sol was autoclaved at 220 °C for 12 h in a large capacity acid digestion bomb (4748, Parr Instrument Company). The sol can also be autoclaved at 200 °C for more transparent electrodes (which is what Kathy Pomykal did for the experiments shown in her thesis). The autoclaved colloidal solution was white. It was stirred for a few minutes to remove globs formed during autoclaving. If necessary, the sol can be filtered to remove large particles. The bulk particle size was 8 to 10 nm diameter and the $TiO_2$ concentration was determined to be 0.04 g/g (determined as the weight of dried aliquot divided by the weight of aliquot). The sol was concentrated under vacuum at 40 °C to a concentration between 0.11 g/g and 0.15 g/g. Polyethylene glycol was added to the $TiO_2$ paste in the amount of 40% weight equivalent of $TiO_2$. For example, 7.8 g of colloidal $TiO_2$ with a concentration of 0.11 g/g contains 0.89 g of $TiO_2$ and therefore requires 0.35 g of polyethylene glycol. The $TiO_2$ paste was stirred overnight. This $TiO_2$ colloidal solution must be used within a few months.

The electrodes were prepared as follows. Conducting glass (3 mm thick clear glass coated with a conducting layer of F-doped $SnO_2$ (Libbey-Owens-Ford, 8 Ω/sq.)) was cut into 6 × 1 inch strips. The long edges of the glass strip were masked with Scotch tape, leaving a band of 6 × 0.5 inch of uncovered glass. This tape acted as a spacer for making the $TiO_2$ layer. First, the conducting glass was coated with an underlayer of titanium isopropoxide as follow: 66 μL of 10 mM $TiCl_4$ in isopropanol (0.022 mL $TiCl_4$ was added to 200 mL of distilled isopropanol with stirring in a fume-hood, until the fuming subsides) was evenly spread by pulling a glass slide across the surface of the electrode. After the isopropanol had evaporated, about 180 μL of $TiO_2$ colloid solution was spread onto the conducting glass in a similar fashion and allowed to dry (until transparent, about 1 h). Once this layer had dried, the electrodes were fired in a tube furnace under flowing air at 450° C for 30 min. Once the electrodes had cooled, they were cut into 0.5 inch wide electrodes. The $TiO_2$ layers were approximately 5 μm as measured by profilometry. All electrodes made before Sept. 1997 utilized the above procedure.

Interestingly, attempts to reproduce the above procedure (after Sept. 1997) lead to bad $TiO_2$ layers, which were cracked. The $TiO_2$ colloid was prepared as above except that the titanium isopropoxide was added drop-wise from a dropping funnel over a period of about 2 min. The final $TiO_2$ colloid had interesting properties: it became very viscous when stored, but became more liquid by adding a small stir bar, closing the vial and shaking vigorously. To make smooth transparent $TiO_2$ layers, the following changes were made. First, no $TiCl_4$ underlayer was spread. 100 μL of colloid was put at one end of a 6 inch long strip and allowed to stand for 20 min. It was then spread by passing a clean glass rod three times (between 2 pieces of Scotch tapes) and allowed to dry at room temperature for 2 h. The tape was then removed carefully and the electrodes fired for 30 min in a tube furnace under flowing air at 450 °C. The cooled electrodes were transparent (see UV-vis spectra, gs2p103), and were not used for any of the results published in this thesis.

Unless otherwise stated, the $TiO_2$ electrodes used in this work were obtained from the Institut fuer Angewandte Photovoltaik, abbreviated as INAP. These electrodes are screen-printed with a machine. According to Iver Lauermann (who used to work at INAP), they are much more uniform in thickness, porosity and inner surface than the hand-made samples and give more reproducible results. As a future alternative, I would like to point out that the $TiO_2$ colloid can now be purchased from Solaronix Inc. Solaronix Inc. offers three types of colloid for making either opaque, transparent or highly transparent electrodes.

*3. Preparation of Dye-coated Nanocrystalline $TiO_2$ Electrodes*

The $TiO_2$ electrodes (INAP) consisted of conducting glass (3 mm thick) coated with a transparent $TiO_2$ layer of 5 μm to 6 μm thick (measured by profilometry, Dektak 3030). The 90 × 15 mm strips were cut into 0.5 inch wide electrodes, carefully avoiding any contact with the $TiO_2$ surface. The electrodes were first treated by depositing three drops of 0.2 M $TiCl_4$ (aq), covering the electrodes and allowing to sit overnight. It is important

that the 0.2 M $TiCl_4$ (aq) does not evaporate, otherwise the $TiO_2$ layer will peel off. This $TiCl_4$ overlayer improves the photocurrent (gs5p135).[83] The 0.2 M $TiCl_4$ (aq) was unstable ($TiO_2$ precipitated out of solution after 2 days) and was freshly-made from a 2.0 M $TiCl_4$ (aq) stock solution (which was stable). The stock solution was made by adding 22 mL of $TiCl_4$ from a dropping funnel to 100 mL of water in ice, with vigorous stirring and under nitrogen. Once the solution cleared, it was transferred to a bottle and stored. The electrodes were then rinsed with water, rinsed with ethanol, dried with flowing nitrogen, and fired in a tube furnace under flowing air at 450 °C for 30 min. Once the electrodes were cooled to about 120 °C, they were immersed in an ethanolic solution containing $5 \times 10^{-5}$ M to $1 \times 10^{-4}$ M of the desired dye, 1.0 mM pyridine and 1.0 mM pyridinium triflate. Immersion was performed overnight to obtain high loadings, but was limited to only 15 min for experiments at low dye loadings. The absorbances of the ethanolic solutions containing a dye in a 1.0 cm path length were typically 0.7 - 1.3 at the maximum of the metal-ligand charge-transfer band of the complex. In most cases, the dye utilized was isolated as the fully protonated form. $ML_2L'^{2+}$ was isolated as the chloride salt and the $PF_6^-$ salt; in this work, the $PF_6^-$ salts were used because they yielded better open-circuit voltage values than the corresponding chloride salts. In the case of $M(L'-2H^+)_3$, the potassium salts were utilized. In these potassium salts, the carboxylic groups are deprotonated and more pyridinium triflate was necessary to dissolve the dye in ethanol: the ethanolic solution contained 2.0 mM pyridinium triflate and 1.0 mM pyridine. The dye-coated electrodes were stored in an ethanolic solution (may or may not contain dye) and the electrodes were utilized within 3 days. Electrodes coated with $RuL'_2(NCS)_2$ changed color (blue shift of MLCT band) when left in air overnight. Grätzel and co-workers have shown that $RuL'_2(NCS)_2$ coated on $TiO_2$ can be oxidized, and oxidation is accompanied by sulfur loss and formation of the dicyano complex.[31] Oxidation of this complex coated on $TiO_2$. The UV/vis spectra of the electrodes were obtained prior to the photoelectrochemistry. The

blank used was a $TiO_2$ electrode which had been treated nominally identically to the other electrodes but which was immersed instead into an ethanolic solution that contained no dye.

*4. Current Density-Potential Curves*

The current density-potential (J-*E*) curves and spectral response data were both recorded using a three-electrode potentiostatic set-up (shown in Figure 8) with a Pt wire reference and Pt gauze counter electrode. The distance between the working and counter electrodes was approximately 2 mm and the solution was not stirred. The cell was filled with electrolyte by using a syringe, keeping the cell up (vertical) to avoid trapping of air bubbles at the surface of the working electrode. If any air bubbles were present, the cell was tapped against the bench, keeping it vertical, until the bubbles were out of the illuminated working electrode area. In Figure 8a, the two top pieces of the cell are screwed to the base with 8 screws. Between these two pieces, there is a long silicon spacer with an oval whole delimiting the cell's inside volume. The reference and counter electrodes are also connected between those two pieces. For a better seal and long-term stability, vacuum grease was applied on both sides of that spacer before assembly. Unless a leak was observed, these two pieces were never disassembled. The silicon spacer used between the bottom part of the cell (Fig. 8a) and the $TiO_2$ electrode had no vacuum grease. The working electrode was illuminated through the conducting glass and the illuminated surface area was 0.25 $cm^2$.

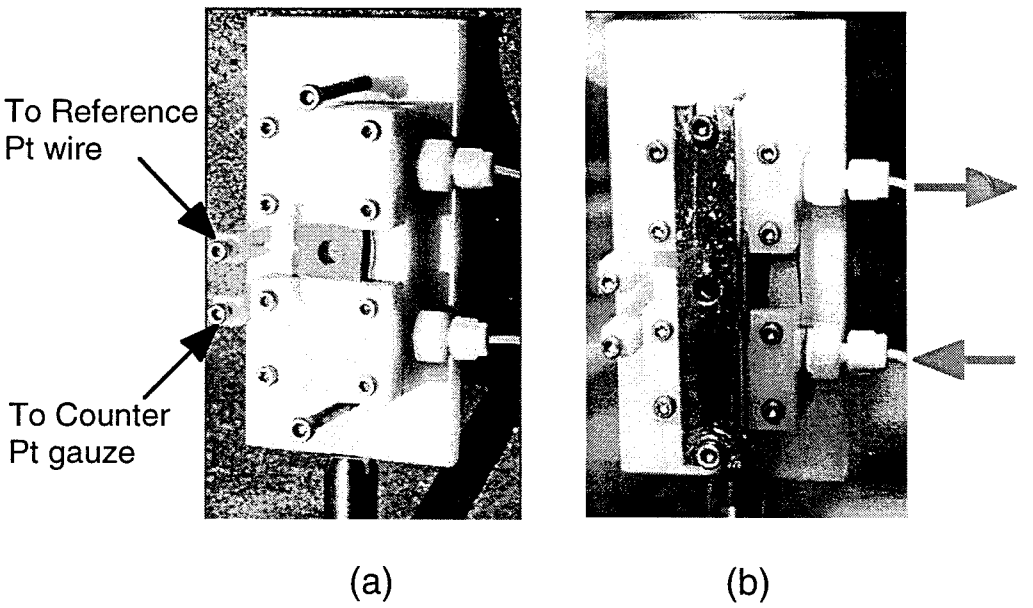


Figure 8: Photoelectrochemical cell. (a) Cell when not in use. (b) Cell when fully assembled with a dye-coated $TiO_2$ working electrode facing towards the solution. The electrolyte is filled through the small tubes on the right.

The choice of electrolyte has a history of its own. Kathy Pomykal found that the presence of water rendered the cell unstable: $V_{oc}$ increased and $J_{ph}$ decreased with time. She added pyridine/pyridinium triflate to the solution to control the acidity of the electrolyte solution, thus stabilizing the conduction band edges of $TiO_2$ and hence the open-circuit photovoltage, $V_{oc}$.[84] The conduction band edge of $TiO_2$ is known to change with pH in aqueous solution. The notion of acidity also applies when using acetonitrile as the solvent, though we cannot quantitate it. In preliminary results, Kathy Pomykal looked at the effect of electrolyte acidity on current-voltage curves of $RuL'_2(NCS)_2$-sensitized $TiO_2$ electrodes.[84] The initial electrolyte consisted of 0.5 M LiI, 0.04 M $I_2$, 1 mM pyridine and 1 mM pyridinium triflate. Upon adding proton sponge to the electrolyte, the $V_{oc}$ increased and the current decreased, in good agreement with the hypothesis that the conduction band

edge of $TiO_2$ becomes more negative with pH. Upon adding the original electrolyte, the original $V_{oc}$ was restored. Though the presence of pyridine/pyridinium triflate in the electrolyte could potentially block the back reaction to triiodide to some extent, we believe that it also stabilizes the electrolyte's and $TiO_2$ surface's acidity and hence stabilizes the conduction band edge. When we omit adding both pyridine and pyridinium triflate to the electrolyte, the $V_{oc}$ is unstable. This particular buffer was chosen because the reagents are soluble in acetonitrile, and because the aqueous $pK_a$ of pyridinium is 5.21 in water, which is near the point of zero charge for $TiO_2$ in aqueous solutions.[85-87]

I first experimented with different electrolytes using 'homemade' transparent $TiO_2$ electrodes (gs3p105-119). When using the electrolyte 0.5 M LiI - 0.04 M $I_2$ and 1 mM pyridine - 1 mM pyridinium triflate, the photocurrent was stable but $V_{oc}$ increased with time: for one experiment, $V_{oc}$ increased by 60 mV in 30 min (gs3p106). When using the electrolyte containing 0.5 M LiI - 0.04 M $I_2$ and 0.2 M 4-tert-butylpyridine, the $V_{oc}$ was very stable but the current slowly decreased with time, irrespective of whether the cell was illuminated or not. I believe the dye was desorbing at such high pH, a problem that might not be an issue when using thin sealed sandwich cells. I then tried the electrolyte containing 0.5 M LiI - 0.04 M $I_2$ and 20 mM pyridine - 20 mM pyridinium triflate. The photocurrent was stable under AM1.0 illumination for 30 min, with fluctuations most likely related to the lamp instability (gs3p113). The $V_{oc}$ was much more stable than using only 1 mM buffer, increasing by only 6 mV in 30 min. Because of a calculation mistake, the electrolyte utilized for all further experiments was: 0.500 M LiI - 0.040 M $I_2$ / 0.050 M pyridine-0.020 M pyridinium triflate in dry $CH_3CN$. Using this electrolyte and electrodes obtained from INAP, I obtained reasonably stable and reproducible photoelectrochemical properties. The $V_{oc}$ stabilized within approximately 5 min at open circuit under the desired illumination. No prior equilibration was found necessary. In a longer term stability experiments with $[OsL_2L']Cl_2$-coated $TiO_2$ electrodes (gs5p13), the current-voltage curves obtained the day of assembly, 1 day later and 4 days later were compared. The cell was left

on the bench at open circuit between the measurements. The photocurrent did not change over the 4 day period, but the open-circuit voltage increased by about 10 mV per day. Therefore, for reproducible $V_{oc}$ values, it is best to record the value the same day the cell is assembled (i.e., same day the dye-coated electrode is exposed to the electrolyte).

The presence of water was found to cause deterioration of the electrodes, so care was taken to reduce water levels as much as conveniently possible.[84] The electrolyte was kept in a dry Schlenk tube under nitrogen, and all cells were purged with nitrogen and then filled with the electrolyte. The cell was cleaned with absolute ethanol between measurements. These precautions led to greatly improved reproducibility. Once the electrodes were removed from the cell, they were observed to be visibly degraded outside the area that had been exposed to the electrolyte. For this reason, fresh electrodes were used in all experiments.

The electrolyte could be changed by refilling the cell with the new electrolyte without disassembling the cell. Refilling the cell by pushing through about 3 times the volume of the cell ( $3 \times 2$ mL) was found to be sufficient to replace the old electrolyte. This feature was utilized for the [LiI] study where electrolytes with different concentrations of LiI, $I_2$, and $LiClO_4$ were tested on the same electrode.

$V_{oc}$ values between the Pt reference and working electrodes were recorded after equilibration at open-circuit under the desired light intensity for 5 min, or once the $V_{oc}$ had reached a stable value. This equilibration time was especially necessary immediately after current had passed through the cell. The $V_{oc}$ measured using this procedure was consistently larger by about 20 mV than the $V_{oc}$ deduced from the x-intercept of a J-*E* scan, regardless of whether the scan rate was 20 mV $s^{-1}$ or 0.5 mV $s^{-1}$. The $V_{oc}$ values reported herein were reproducible and did not change significantly over the course of several hours.

J-*E* data were collected using a Solartron SI 1287 Electrochemical Interface that was controlled with Coreware v. 2.1a software. The scan rate was 20 mV $s^{-1}$. All potentials were recorded vs a Pt wire that was immersed into the solution. The cell potential for the

electrolyte (0.500 M LiI-0.040 M $I_2$/0.050 M pyridine-0.020 M pyridinium triflate in dry $CH_3CN$) was +0.08 V vs aq SCE. The cell was illuminated by an ELH-type W-halogen bulb and light intensities were determined using a calibrated silicon photodiode (Solarex). A 385 nm cut-off filter was used during measurements (but not during the calibration with the photodiode) to avoid direct excitation of electron-hole pairs in the titanium dioxide. Prior to obtaining J-*E* data, the cell was short-circuited under illumination for 30 s because initial J-*E* scans showed higher currents, which dropped down rapidly and then leveled off to a constant, reproducible, value which was the one reported herein. The J-*E* properties of these junctions remained stable for several hours.

Where indicated, J-*E* data were corrected for ohmic resistance and concentration overpotentials in the solution, using procedures that have been described in detail previously.[88,89] A platinum foil working electrode, placed in a nominally identical position as the various $TiO_2$ electrodes, was used to obtain the J-*E* data needed to perform these corrections. The ohmic resistance of the cell was determined to be 56 ohm (gs3p152). The contribution of $\eta_{conc}$ is, in many cases, estimated to be negligible due to the high surface area of $TiO_2$ which yields small current densities. When the contribution of $\eta_{conc}$ was estimated with current densities based on electrode surface area (instead of actual $TiO_2$ surface area), the curves were overcorrected.

*5. Spectral Response*

Spectral response data were obtained by biasing the cell to short-circuit and measuring the current with a Keithley 177 microvolt DMM multimeter. Monochromatic light was obtained from a Spex 1682A tungsten lamp mated to a Spex 1681B monochromator equipped with 2.5 mm slits. The large slits were necessary to obtain sufficient light intensity (see below). The monochromator output beam was split with a glass slide into sample and reference beams. The system calibration was performed by placing a calibrated Si photodiode (obtained from United Detector Technology, Inc.) in the same position as the $TiO_2$ working electrode and measuring the photocurrent at short-circuit

from each system. The calibrated diode had a mask with the same surface area as the $TiO_2$ working electrode, and the ratio of the response of the $TiO_2$ cell to that of the calibration diode gave the quantum yield for the $TiO_2$ cell. Any variation in the light intensity between measurements was accounted for by dividing the current obtained from the sample or calibration device by the current produced by the reference beam, which was directed onto a separate, second silicon photodiode (obtained from United Detector Technology, Inc.). The quantum yields were therefore computed using the following equation:

$$\Phi_{smp} = \Phi_{cal}\left(\frac{I_{smp} / area}{I_{ref,smp}}\right)\left(\frac{I_{ref,cal}}{I_{cal} / area}\right) \qquad (3)$$

where $\Phi_{smp}$ and $\Phi_{cal}$ are the quantum yields for the sample and the calibrated photodiode, respectively, $I_{smp}$ and $I_{cal}$ are the photocurrents obtained at the sample and at the calibrated diode, respectively, and $I_{ref}$ is the photocurrent of the reference diode. The external quantum yields obtained using this measurement procedure were not corrected for optical scattering or reflection losses nor for incomplete absorption by the dye at certain wavelengths.

For the $TiO_2$ electrodes, the dark current was not negligible compared to the light current at the low light levels used in the spectral response experiments, and the dark current value also tended to drift slightly over time. The dark current was therefore measured periodically and the photocurrent was obtained by subtracting the dark current from the measured total current. Light intensities as high as possible were utilized to minimize the contribution of the dark current.

Furthermore, at very low light intensity, i.e., at photocurrents less than approximately 2 $\mu A\ cm^{-2}$, the quantum yield was found to be dependent on the light intensity, so the data reported herein always refer to measurements performed at current densities which are higher than this value. For example, Figure 9 shows a plot of quantum yield vs light intensity for a $RuL'_2(NCS)_2$-coated electrode, using 1.25 mm slits and an old lamp. The light intensity was varied by adding neutral density filters in front of the

monochromator output beam. At 100% light intensity, the external quantum yield just started to plateau and the total light current was 1.1 μA. Ideally, the measured external quantum yield should not depend on light intensity. The external quantum yield of $TiO_2$ electrodes with low dye coverage could not be measured accurately because the quantum yield depended on light intensity (gs4p68). This last experiment suggests that it is not the absolute light intensity value that really matters, but the total photocurrent. An explanation consistent with this observation is that surface states must first be filled before photocurrent can flow.

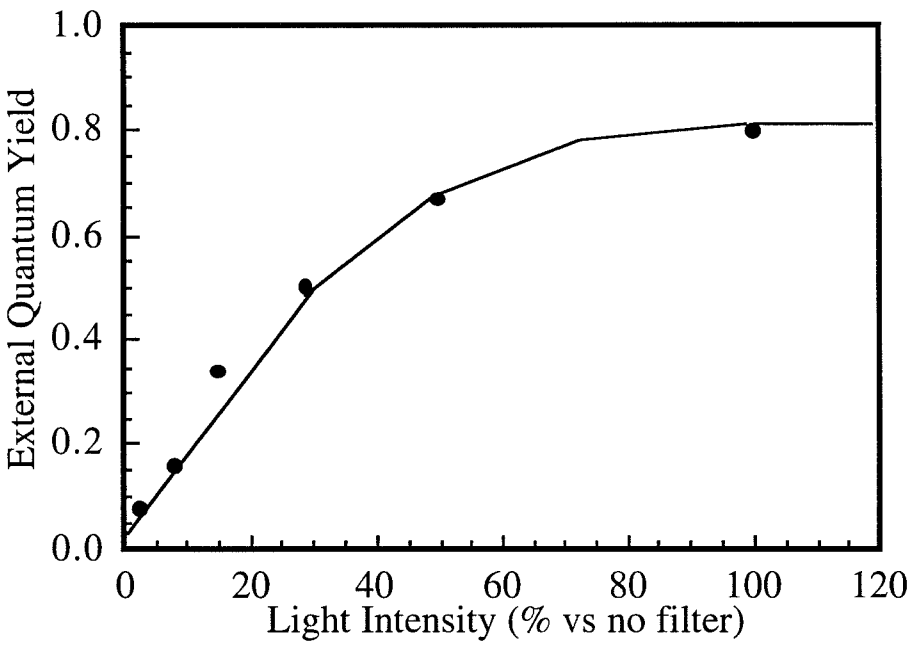


Figure 9: Light intensity dependence of external quantum yields. The measurement was performed with a $RuL'_2(NCS)_2$-coated $TiO_2$ electrode, using 1.25 mm slits and an old lamp. The light intensity was varied by adding neutral density filters in front of the monochromator output beam. The total light current at 100% light intensity was 1.1 μA.

# Chapter 3:

# Results and Discussion, Part 1:

# Characterization of Dye Molecules

## A. NMR Spectra of the Various Complexes

Nitrogen-15 and Carbon-13 NMR studies were carried out on the doubly labelled complexes $K^{15}N^{13}CS$, $RuL_2(^{15}N^{13}CS)_2$, $RuL'_2(^{15}N^{13}CS)_2$ and $OsL'_2(^{15}N^{13}CS)_2$, in order to determine if the $NCS^-$ ligands were N- or S- bound to the ruthenium and osmium metal centers in complexes that contained the 2,2'-bipyridine-4,4'-dicarboxylic acid ligands.

### *1. $^1H$ NMR Characterization*

The $^1H$ NMR spectral data for the complexes in $D_2O$/NaOD are listed in Table 1 and the numbering scheme for the assignment is shown in Figure 10. In this solvent, the carboxylate groups on the ligands were deprotonated. The $^1H$ NMR spectra of $ML'_2X_2$, where X is $Cl^-$, $NCS^-$ or $CN^-$, all showed six signals in the aromatic region, arising from the six inequivalent protons on each of two equivalent 2,2'bipyridine-4,4-dicarboxylic acid ligands. This splitting pattern is indicative of *cis*-$ML'_2X_2$ structures having $C_2$ symmetry. The assignments are based on integration, splitting patterns and chemical shifts. Figures 11 and 12 display the aromatic region for X = $NCS^-$ and $CN^-$. In the case of $RuL'_2(NCS)_2$, the signals were further assigned based on literature values.[17,90] The chemical shifts for $RuL'_2(NCS)_2$ reported here agree with those previously reported.[72,90] The $^1H$ NMR spectra of $RuL'_2(NCS)_2$ and $OsL'_2(NCS)_2$ also showed a series of much smaller signals that we ascribe to the mixed bound $ML'_2(NCS)(SCN)$ complexes. Most of those signals overlapped with the more intense signals arising from the all-nitrogen bound complex, except for the most downfield doublet. This doublet is associated with hydrogen (a) of one of the L' ligands, and appeared at 9.64 ppm for $RuL'_2(NCS)_2$ and 9.54 ppm for

$OsL'_2(NCS)_2$. The ratio of the major product to the mixed-bound product was about 7:1. This ratio could not be increased upon increasing the reaction time. The presence of the mixed-bound complex of ruthenium was also observed by Grätzel and co-workers.[72]

The $^1H$ NMR spectra for the $ML_2(L'\text{-}2H^+)$ complexes (Table 2 and Figure 13) illustrate that these complexes possess $C_2$ symmetry, having two equivalent 2,2-bipyridine ligands (L) each with eight inequivalent protons, and one 2,2'-bipyridine-4,4'-dicarboxylic acid ligand (L') possessing an axis of symmetry that produces three sets of two equivalent protons. Eleven inequivalent protons in each complex give rise to the resonances (with some overlapping of the signals). The aromatic region of the $^1H$ NMR spectra of $M(L'\text{-}2H^+)_3^{4-}$ complexes (Table 2 and Figure 14) show a simple $^1H$ NMR spectrum that consists of one singlet and two doublets, indicative of $D_3$ symmetry.

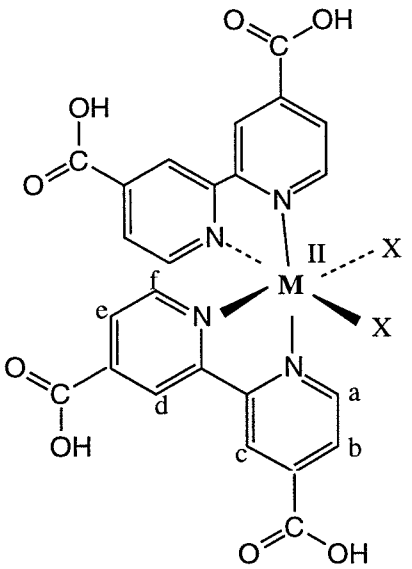


(A)

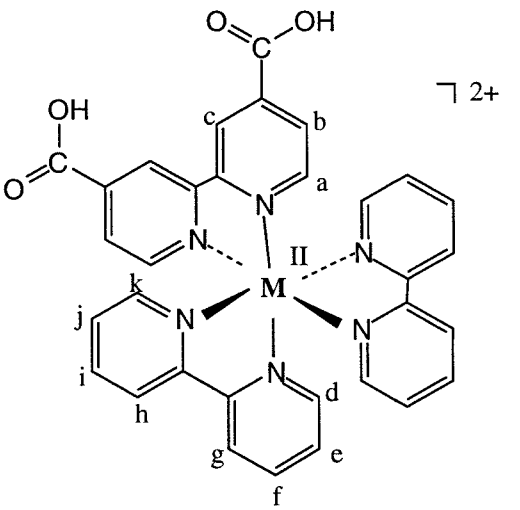


(B)

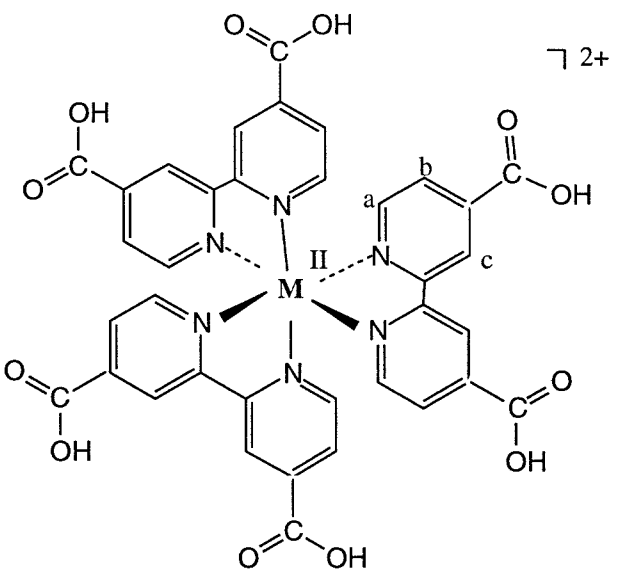


(C)

Figure 10: Hydrogen numbering for the $^1H$ NMR assignment of the complexes. (A) $ML'_2X_2$ where X = $NCS^-$, $CN^-$ or $Cl^-$. M is Os or Ru. L' is 4,4'-$(CO_2H)_2$bpy. (B) $ML_2L'^{2+}$ where L is bipyridine. (C) $ML'_3{}^{2+}$.

Table 1: $^1H$ NMR Data for the Complexes M(II)$L'_2X_2$ in $D_2O$/NaOD

| Complex | Chemical Shift δ (ppm) | | Proton-Proton Coupling Constants | | Assignment |
|---|---|---|---|---|---|
| | | | $^3J$ (Hz) | $^4J$ (Hz) | |
| **$C_2$ Complexes** | | | | | |
| $RuL'_2(NCS)_2$ | 9.46 | d | 6 | | a |
| | 8.84 | s | | | c |
| | 8.68 | s | | | d |
| | 8.12 | dd | 6 | 2 | b |
| | 7.73 | d | 6 | | f |
| | 7.43 | dd | 6 | 2 | e |
| $RuL'_2(CN)_2$ | 9.53 | d | 6 | | a or f |
| | 8.79 | s | 1 | | c or d |
| | 8.70 | s | | | c or d |
| | 7.99 | dd | 6 | 2 | b or e |
| | 7.69 | d | 6 | | a or f |
| | 7.54 | dd | 6 | 2 | b or e |
| $OsL'_2Cl_2$ | 9.59 | d | 6 | | a or f |
| | 8.84 | s | | | c or d |
| | 8.63 | s | | | c or d |
| | 7.94 | dd | 6 | 2 | b or e |
| | 7.61 | d | 6 | | a or f |
| | 7.14 | dd | 6 | 2 | b or e |
| $OsL'_2(NCS)_2$ | 9.34 | d | 6 | | a or f |
| | 8.82 | s | | | c or d |
| | 8.64 | s | | | c or d |
| | 7.98 | dd | 6 | 1 | b or e |
| | 7.63 | d | 6 | | a or f |
| | 7.26 | dd | 6 | 1 | b or e |
| $OsL'(L'-H^+)(CN)_2^{1-}$ | 9.64 | d | 6 | | a or f |
| | 8.79 | s | | | c or d |
| | 8.70 | s | | | c or d |
| | 7.91 | dd | 6 | 2 | b or e |
| | 7.66 | d | 6 | | a or f |
| | 7.49 | dd | 6 | 2 | b or e |

All chemical shifts were reported as referenced to DSS as an internal standard (0.00 ppm). n.a.= not assigned, s = singlet, d = doublet, dd = doublet of doublets, vt = virtual triplet, m = multiplet, rel I = relative integration.

Table 2: $^1H$ NMR Data for the Complexes $M(II)L_2L'^{2+}$ and $M(II)(L'\text{-}2H^+)_3^{4-}$ in $D_2O$/NaOD

| Complex | Chemical Shift δ (ppm) | | Proton-Proton Coupling Constants | | Assignment |
|---|---|---|---|---|---|
| | | | $^3J$ (Hz) | $^4J$ (Hz) | |
| **$C_2$ Complexes** | | | | | |
| $RuL_2L'^{2+}$ | 8.87 (rel I:1) | s | | 1 | c |
| | 8.54 (rel I:2) | two d | 8 | | g and h |
| | 8.05 (rel I:2) | two vt | n.a. | n.a. | f and i |
| | 7.92 (rel I:1) | d | 6 | | a |
| | 7.81 (rel I:1) | d | 5 | | |
| | 7.79 (rel I:1) | d | 6 | | d and k |
| | 7.66 (rel I:1) | dd | 6 | 2 | b |
| | 7.37 (rel I:2) | two vt | n.a. | n.a. | e and j |
| $OsL_2L'^{2+}$ | 8.85 (rel I:1) | s | | | c |
| | 8.51 (rel I:2) | two d | ~ 7 | | g and h |
| | 8.86 (rel I:3) | m | n.a. | n.a. | a , f and i |
| | 7.12 (rel I:1) | d | 5 | | d or k |
| | 7.68 (rel I:1) | d | 6 | | d or k |
| | 7.55 (rel I:1) | dd | 6 | n.a. | b |
| | 7.28 (rel I:2) | two vt | n.a. | n.a. | e and j |
| **$D_3$ Complexes** | | | | | |
| $Ru(L'\text{-}2H^+)_3^{4-}$ | 8.88 | s | | | c |
| | 7.88 | d | 6 | | a |
| | 7.68 | dd | 6 | 2 | b |
| $Os(L'\text{-}2H^+)_3^{4-}$ | 8.86 | s | | | c |
| | 7.78 | d | 6 | | a |
| | 7.58 | dd | 6 | 2 | b |

All chemical shifts were reported as referenced to DSS as an internal standard (0.00 ppm). n.a.= not assigned, s = singlet, d = doublet, dd = doublet of doublets, vt = virtual triplet, m = multiplet, rel I = relative integration.

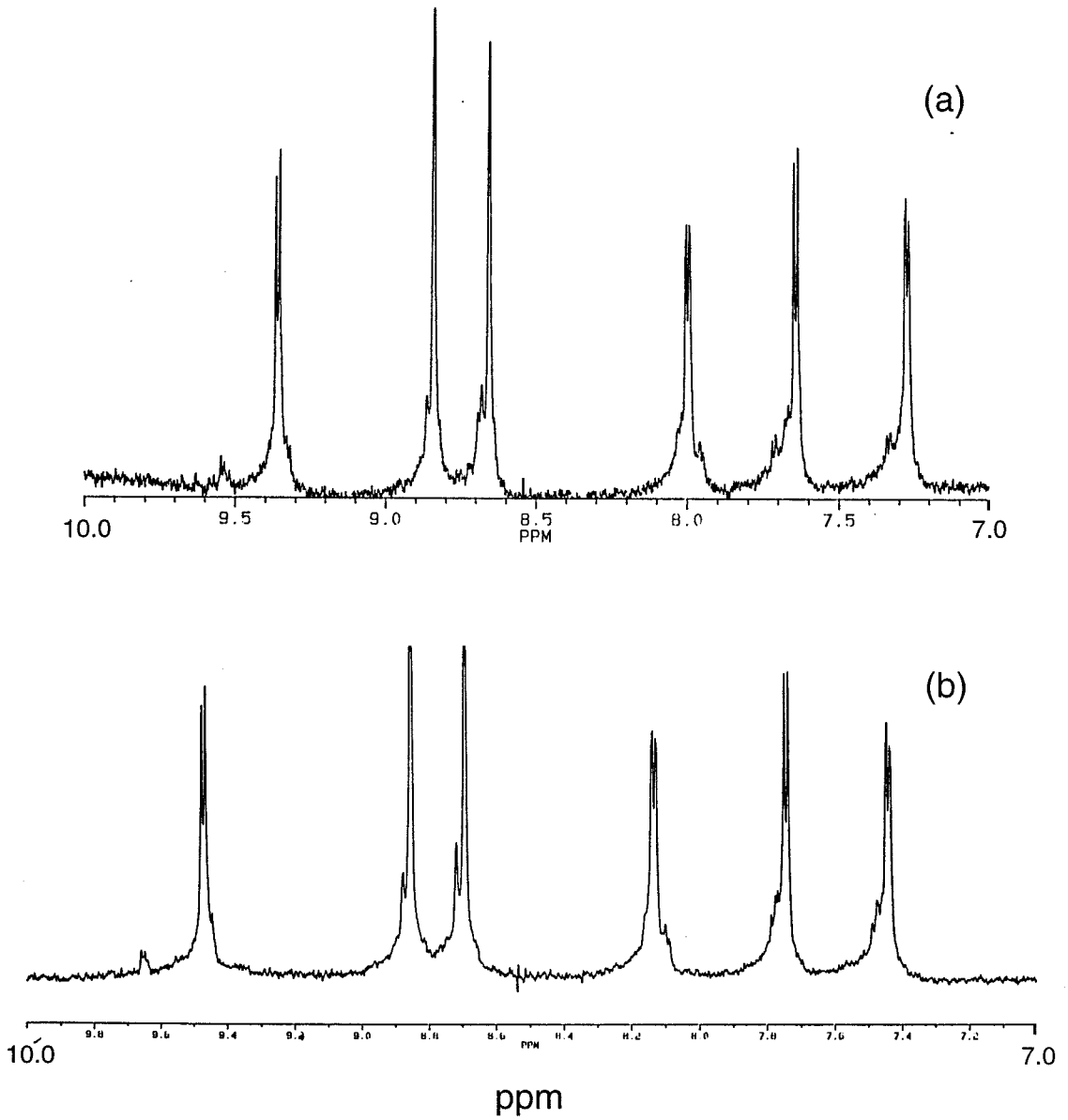


Figure 11: Aromatic region of the $^1H$ NMR spectra of complexes $M(II)L'_2(NCS)_2$ in $D_2O$/NaOD. (a) $OsL'_2(NCS)_2$ (b) $RuL'_2(NCS)_2$.

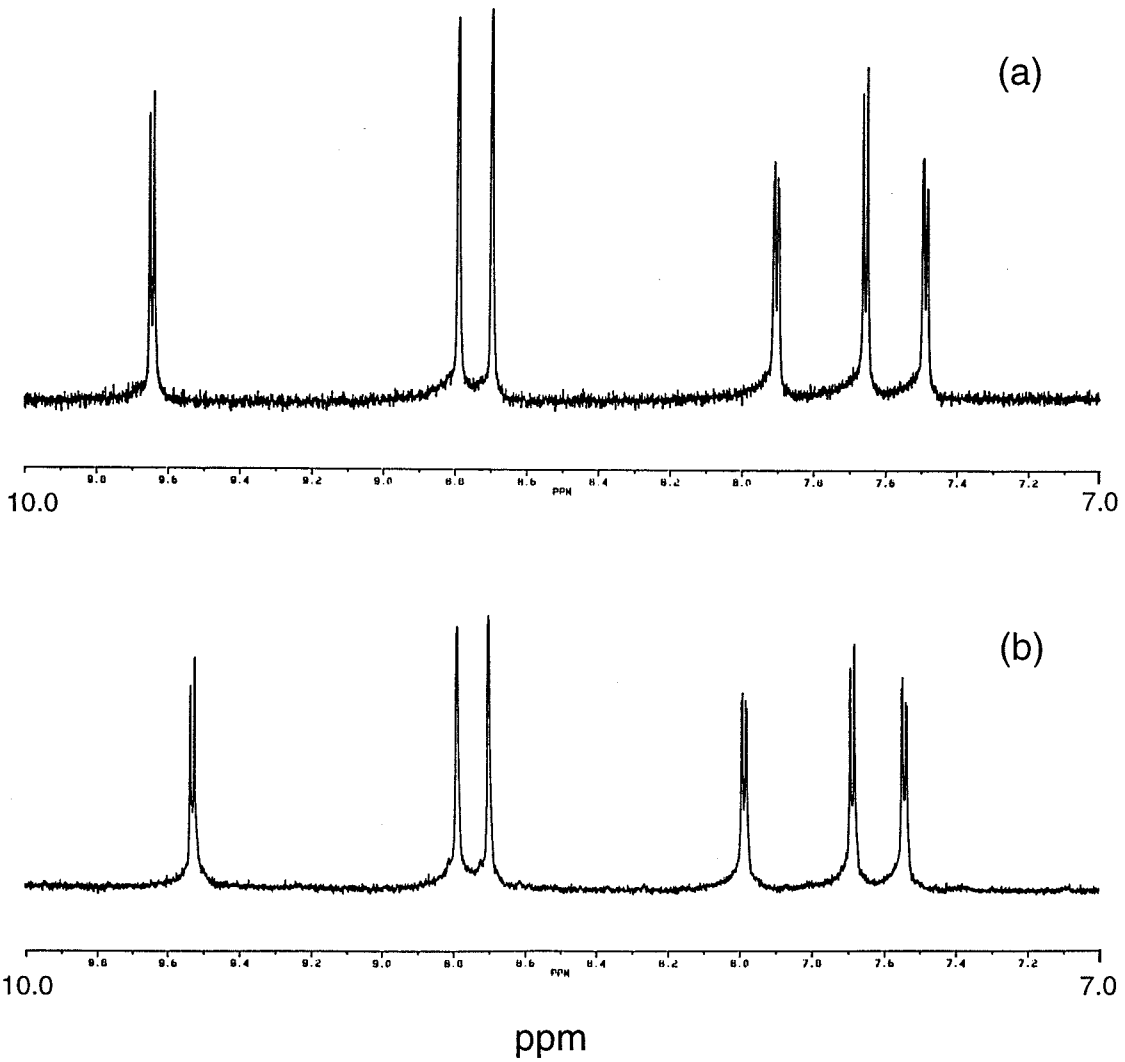


Figure 12: Aromatic region of the $^{1}H$ NMR spectra of complexes $M(II)L'_2(CN)_2$ in $D_2O$/NaOD. (a) $OsL(L'\text{-}H^{+})(CN)_2^{1-}$ (b) $RuL'_2(CN)_2$.

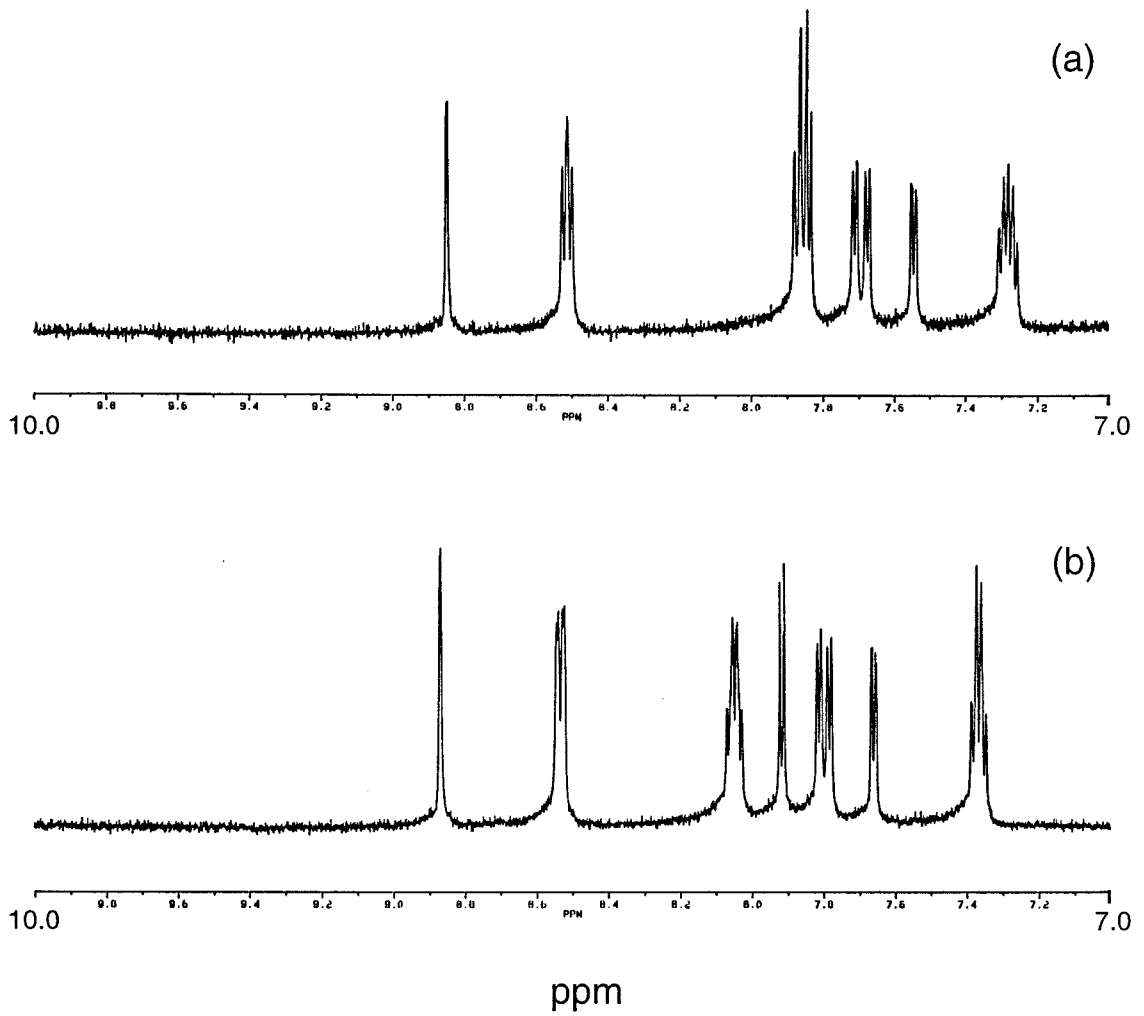


Figure 13: Aromatic region of the $^1H$ NMR spectra of complexes $M(II)L_2L'^{2+}$ in $D_2O$/NaOD. (a) $OsL_2L'^{2+}$ (b) $RuL_2L'^{2+}$.

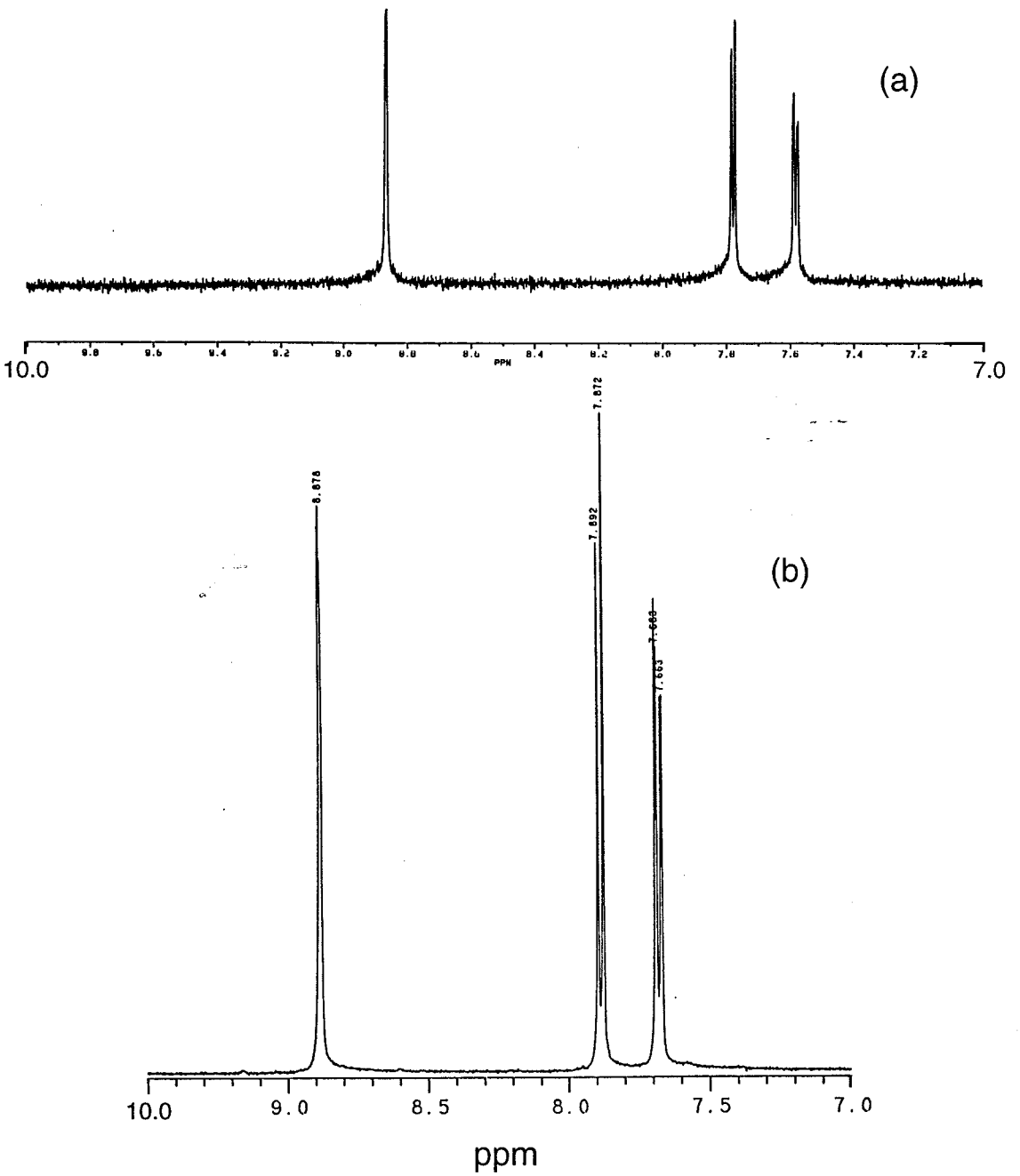


Figure 14: Aromatic region of the $^{1}H$ NMR spectra of complexes $M(II)(L'\text{-}2H^{+})_3^{4-}$ in $D_2O$/NaOD. (a) $Os(L'\text{-}2H^{+})_3^{4-}$ (b) $Ru(L'\text{-}2H^{+})_3^{4-}$.

## 2. *$^{15}N$ and $^{13}C$ NMR Study to Determine Linkage Isomerism in $NCS^-$ Complexes*

Two previous studies (one examining $^{14}N$ and the other utilizing $^{15}N$ NMR) on a variety of metal complexes have shown that S-bound metal thiocyanato complexes (M-S-C≡N) have a nitrogen chemical shift slightly downfield of that observed for the free thiocyanate ion (represented as KSCN or NaSCN dissolved in the NMR solvent of choice) whereas nitrogen-bound metal isothiocyanato complexes (M-N≡C-S) exhibit $^{14}N$ or $^{15}N$ resonances "shifted by a comparatively large amount upfield of the free thiocyanate ion."[91,92] The nitrogen chemical shifts of metal thiocyanato and isothiocyanato complexes reported in these two studies are compiled in Table 3. In this tabulation, all chemical shifts have been either measured or calculated as referenced to the $KNO_3$ standard at 0.0 ppm. Additionally, we have chosen the convention of reporting signals that occur upfield of $KNO_3$ as having negative chemical shifts and those that occur downfield from $KNO_3$ as having positive chemical shifts.

Table 3: A Comparative Study of $\delta$ $^{15}N$ Chemical Shift for M-SCN and M-NCS Complexes

| Compound | Solvent | $\delta$ $^{15}N$ ($NO_3^-$=0.0 ppm) | $\delta$ $^{14}N$ ($NO_3^-$= 0.0 ppm) | Ref. |
|---|---|---|---|---|
| KSCN | $H_2O$ | | -166 | 91 |
| KSCN | $CH_2Cl_2$[a] | -160.2 | | 92 |
| KSCN | $D_2O$ | -170.8 | | This work |
| KSCN | $d^6$-DMSO | -156.0 | | This work |
| $C_2H_5SCN$ | $CHCl_3$ | | -98.5 | 91 |
| $C_2H_5NCS$ | pure | | -268 | 91 |
| **M-SCN Complexes** | | | | |
| $Na_2[Pd(SCN)_4]$ | $H_2O$ | | -148 | 91 |
| $Na_2[Pt(SCN)_4]$ | $H_2O$ | | -166 | 91 |
| $Na_2[Rh(SCN)_6]$ | $H_2O$ | | -158 | 91 |
| $Na_2[Ir(SCN)_6]$ | $H_2O$ | | -163 | 91 |
| $Na_2[Hg(SCN)_4]$ | $H_2O$ | | -157 | 91 |
| $(Bu_4N)_2[Pd(SC^{15}N)_4]$ | $CH_2Cl_2$[a] | -123.9 [b] | | 92 |
| $(Bu_4N)_2[Pd(SC^{15}N)_4]$[c] | $CH_2Cl_2$ | -125.1 [b] | | 92 |
| $(Bu_4N)_2[Hg(SC_{15}N)_4]$ | $CH_2Cl_2$[a] | -134.7 [b] | | 92 |
| **M-NCS Complexes** | | | | |
| *cis*-$[Pt(NCS)_2(Bu_3P)_2]$ | $CHCl_3$ | | -302 | 91 |
| *cis*-$[Pt(NCS)_2(Bu_2PhP)_2]$ | $CHCl_3$ | | -249 | 91 |
| *trans*-$[PtH(NCS)(Et_3P)_2]$ | $CHCl_3$ | | -239 | 91 |
| *cis*-$[Pt(NCS)_2(Bu_3As)_2]$ | $CHCl_3$ | | -303 | 91 |
| *trans*-$[Ni(NCS)_2(Et_3P)_2]$ | $CHCl_3$ | | -293 | 91 |
| *trans*-$[Ni(NCS)_2(Bu_2PhP)_2]$ | $CHCl_3$ | | -291 | 91 |
| $Na_2[Cd(NCS)_4]$ | $H_2O$ | | -178 | 91 |
| $Na_2[Cd(NCS)_4]$ | $CH_3OH$ | | -220 | 91 |
| $Na_2[Zn(NCS)_4]$ | $CH_3CH_2OH$ | | -255.5 | 91 |
| $(Bu_4N)_2[Zn(^{15}NCS)_4]$ | $CH_2Cl_2$[a] | -218.1 [b] | | 92 |
| $(Bu_4N)_2[Cd(^{15}NCS)_4]$ | $CH_2Cl_2$[a] | -200.5 [b] | | 92 |
| *trans*-$[Pt(^{15}NCS)_2(n\text{-}Bu_3P)_2]$[d] | $CH_2Cl_2$[a] | -306.0 [b] | | 92 |
| $Mg(H_2O)_x(NCS)_y(OH)_z$ | $H_2O$ | -193 to -197[e] | | 93 |
| $K_2[Ru(NCS)_5(NO)]$ | $H_2O$ | | -268 | 91 |

a) Solvent may be $CH_2Cl_2$, although the solvent was not explicitly stated for each sample.

b) Value of $\delta$ reported here as referenced to $NO_3^-$ at 0.0 ppm: Values were originally reported with a reference of $NH_4Cl$ = 0 ppm. On a relative scale, $NO_3^-$ appears at 376.53 ppm and $NH_4Cl$ appears at 27.34 ppm.[92,94]

c) Thiocyanate ligand was determined to be bound through sulfur from the analysis of the $^{195}Pt$ chemical shift and the observed $^3J(^{195}Pt\text{-}^{15}N)$ Coupling Constant of 12 Hz.

d) Thiocyanate ligand was determined to be bound through nitrogen from the analysis of the $^{195}Pt$ chemical shift and the observed $^1J(^{195}Pt\text{-}^{15}N)$ Coupling Constant of 589 Hz.

e) In this study, $^{15}N$ chemical shifts were reported as $\Delta\delta$ relative to $KSC^{15}N$. Values reported here have been readjusted relative to $NO_3^-$ at 0.0 ppm.

$^{15}N$ NMR data for doubly-labelled complexes and for free doubly-labelled thiocyanate obtained in this work are reported in Table 4. In all spectra, one principal doublet was observed, representing an $^{15}N$ signal split by a single adjacent $^{13}C$ atom in the nitrogen NMR spectrum. The $^{15}N$ resonances observed for $RuL'_2(^{15}N^{13}CS)_2$ and $OsL'_2(^{15}N^{13}CS)_2$ in $D_2O$/NaOD are shifted by significantly large amounts upfield of the free thiocyanato ion, suggesting that both $RuL'_2(NCS)_2$ and $OsL'_2(NCS)_2$ are isothiocyanato complexes bound to the metal through nitrogen. In support of this assignment, the non carboxylated analog of $RuL'_2(NCS)_2$, $RuL_2(NCS)_2$, which has been established by X-ray crystallography to have nitrogen-bound thiocyanato ligands,[95] has a very similar chemical shift for the labelled $^{15}N^{13}CS^-$ thiocyanato ligand (-241.8 for $RuL_2(^{15}N^{13}CS)_2$ vs -245.2 ppm for $RuL'_2(^{15}N^{13}CS)_2$). A crystallographic structure of the ethyl ester derivative of $RuL'_2(NCS)_2$, Ru(4,4'-$(COOEt)_2$-2,2'-bipyridine)$_2(NCS)_2$, shows that this analog also has N-bound thiocyanato ligands.[90]

Table 4: $^{13}C$ and $^{15}N$ NMR Data

| Compound | NMR Solvent | $\delta$ $^{13}C$ | $^{1}J^{13}C$-$^{15}N$ ($^{13}C$ NMR) | $\delta$ $^{15}N$ | $^{1}J^{13}C$-$^{15}N$ ($^{15}N$ NMR) | Ref. |
|---|---|---|---|---|---|---|
| $KS^{13}C^{15}N$ | $D_2O$/NaOD | 132.9[a] | 13.56 Hz | -170.8[c] | 13.56 Hz | d |
| $RuL'_2(^{15}N^{13}CS)_2$ | $D_2O$/NaOD | 132.0[a] | 28.8 Hz | -234.3[c] | 27.1 Hz | d |
| $OsL'_2(^{15}N^{13}CS)_2$ | $D_2O$/NaOD | 126.4[a] | 32.2 Hz | -258.6[c] | 33.9 Hz | d |
| Ionic $S^{13}CN^-$ | $D_2O$/NaOD | 134.2 | | | | 72 |
| $RuL'_2(N^{13}CS)_2$ | $D_2O$/NaOD | 132.8 | | | | 72 |
| $RuL'_2(N^{13}CS)(S^{13}CN)$ | $D_2O$/NaOD | 132.8, 126.8 | | | | 72 |
| $KS^{13}C^{15}N$ | $d^6$-DMSO | 129.6[b] | 10.17 Hz | -158.6[c] | 13.56 Hz | d |
| $RuL'_2(^{15}N^{13}CS)_2$ | $d^6$-DMSO | 134.6[b] | 28.8 Hz | -245.2[c] | 27.2 Hz | d |
| $RuL_2(^{15}N^{13}CS)_2$ | $d^6$-DMSO | 133.4[b] | 28.8 Hz | -241.8[c] | 27.1 Hz | d |
| Ionic $S^{13}CN^-$ | $d^4$-MeOH | 133.6 | | | | 72 |
| $RuL'_2(N^{13}CS)_2$ | $d^4$-MeOH | 135.4 | | | | 72 |
| $RuL'_2(N^{13}CS)(S^{13}CN)$ | $d^4$-MeOH | 136.0, 124.2 | | | | 72 |
| $RuL'_2(S^{13}CN)X$ ($X= S^{13}CN^-, Cl^-$) | $d^4$-MeOH | 124, 125 | | | | 72 |

a. $\delta$ $^{13}C$ shifts referenced to dioxane at 66.5 ppm

b. $\delta$ $^{13}C$ shifts referenced to DMSO at 39.51 ppm

c. $\delta$ $^{15}N$ shifts referenced to $KNO_3$ at 0.0 ppm

d. This work.

Previously, it was reported that the chemical shift in the $^{13}C$ NMR spectrum of metal thiocyanate complexes could be used as a diagnostic tool to determine the linkage isomerism of the $NCS^-$ ligand.[96] Kargol *et al.* analyzed a series of S- bound and N-bound thiocyanate compounds and observed upfield chemical shift differences ranging from 3 to 20 ppm relative to ionic thiocyanate for the $^{13}C$ shift of S-bound complexes and downfield chemical shift differences of 1 to 16 ppm for the $^{13}C$ signal of N-bound complexes. These data were generalized into the simple rule that S-bound thiocyanate shows chemical shifts upfield relative to the ionic thiocyanate and N-bound $NCS^-$ shows downfield chemical shifts relative to the ionic thiocyanate. There were a few exceptions to this rule, however, in which the $^{13}C$ resonance of N-bound thiocyanato ligands appeared slightly (approximately 1 ppm) upfield of that reported for ionic thiocyanate in the same solvent.

The $^{13}C$ NMR data for our doubly-labeled complexes are reported in Table 4, along with the $^{13}C$ NMR data reported by Grätzel and co-workers on $RuL'_2(N^{13}CS)_2$ and $RuL'_2(N^{13}CS)(S^{13}CN)$ in both $D_2O$/NaOD and in $d^4$-methanol for comparison. In all but one case (for the sample of $RuL'_2(^{15}N^{13}CS)_2$), only one doublet was detected in each spectrum, which indicated that the syntheses produced only one product, to the detection limit of the NMR method. In the $^{13}C$ NMR spectrum of $RuL'_2(^{15}N^{13}CS)_2$, however, another signal was observed at the 10% level, which likely arises from the presence of a mixed-bound ligand species that is similar to the species reported by Grätzel and co-workers.[72]

The $^{13}C$ NMR signals of $RuL'_2(^{15}N^{13}CS)_2$ and $OsL'_2(^{15}N^{13}CS)_2$ measured in $D_2O$/NaOD exhibit $^{13}C$ chemical shifts upfield of free thiocyanate ion by 0.9 and 6.5 ppm respectively (Table 4). Applying the general rule discussed above would suggest that the thiocyanates are bound through the sulfur atom, which is inconsistent with all the other NMR data reported in this work. Grätzel and co-workers also observe the $^{13}C$ chemical shifts for $RuL'_2(N^{13}CS)_2$ in both $D_2O$/NaOD and $d^4$-methanol to appear upfield of the free thiocyanate ion in the same solvent.[72] However, they also observed another lower

intensity peak further upfield, so they assigned the principle product of the cis-$RuL'_2Cl_2$ starting material with thiocyanate to produce an N-bound thiocyanate species. Unless a resonance is observed further upfield that could be attributed to S- bound thiocyanate, we cannot unequivocally assign the isomer linkage of thiocyanate using $^{13}C$ NMR in $D_2O$/NaOD. Two low intensity doublets at 133.75 ppm and 121.55 ppm were observed in the $^{13}C$ NMR spectrum of $RuL'_2(^{15}N^{13}CS)_2$, possibly arising from a species with mixed-linkage $NCS^-$ ligands $RuL'_2(^{15}N^{13}CS)(S^{13}C^{15}N)$ similar to those reported by Grätzel and co-workers.[72]

The $^{13}C$ NMR spectra of the $RuL_2(^{15}N^{13}CS)_2$ and $RuL'_2(^{15}N^{13}CS)_2$ complexes in $d^6$-DMSO showed downfield $^{13}C$ shifts relative to ionic thiocyanate of 3.8 and 5.0 ppm respectively (Table 4), indicative of linkage through the nitrogen. Both $RuL'_2(NCS)_2$ and its non-carboxylated analog showed similar $^{15}N$ and $^{13}C$ chemical shifts, confirming the above assignment that the linkage occurs through the nitrogen.

The linkage isomerism of the $NCS^-$ complexes was assigned based on our $^{15}N$ and $^{13}C$ NMR study. The $RuL'_2(NCS)_2$ complex was assigned to contain predominantly nitrogen-bound thiocyanato ligands. This assignment is in agreement with the prior literature for various ruthenium isothiocyanato complexes.[65,68,72,90,95,97] We believe that $OsL'_2(NCS)_2$ is predominantly an isothiocyanato complex based on the $^{15}N$ NMR data, as opposed to the more questionable interpretation of $^{13}C$ NMR data. Furthermore, these data indicate that $^{15}N$ NMR appears to be a more reliable spectroscopic tool than $^{13}C$ NMR spectroscopy for the assignment of linkage isomerism in metal complexes of the thiocyanate ligand.

## B. Absorption, Emission, and Lifetimes of the Os and Ru Complexes

Figures 15-18 present the electronic absorption and emission spectra of the Os and Ru complexes used in this work, and Table 5 summarizes the spectrochemical properties. For a given ligand environment, the Os complexes all showed an additional absorption band at longer wavelengths than the Ru complexes. This lower energy band had a smaller

extinction coefficient than that of the main metal-to-ligand charge transfer (MLCT) bands. The red shift in the absorption of the Os complexes relative to the analogous Ru complexes is consistent with expectations of an enhanced oscillator strength for an electronic transition between the ground state and the triplet excited state of the Os complexes.[64] In addition, this lowest MLCT band is red-shifted when the ligands are changed from L (or L') to $CN^-$ to $NCS^-$, consistent with the destabilization of the metal $t_{2g}$ orbitals in the presence of stronger $\sigma$ donor ligands.[65] As expected, the emission spectra for the Os complexes were also red-shifted relative to those of the Ru complexes having identical ligands.

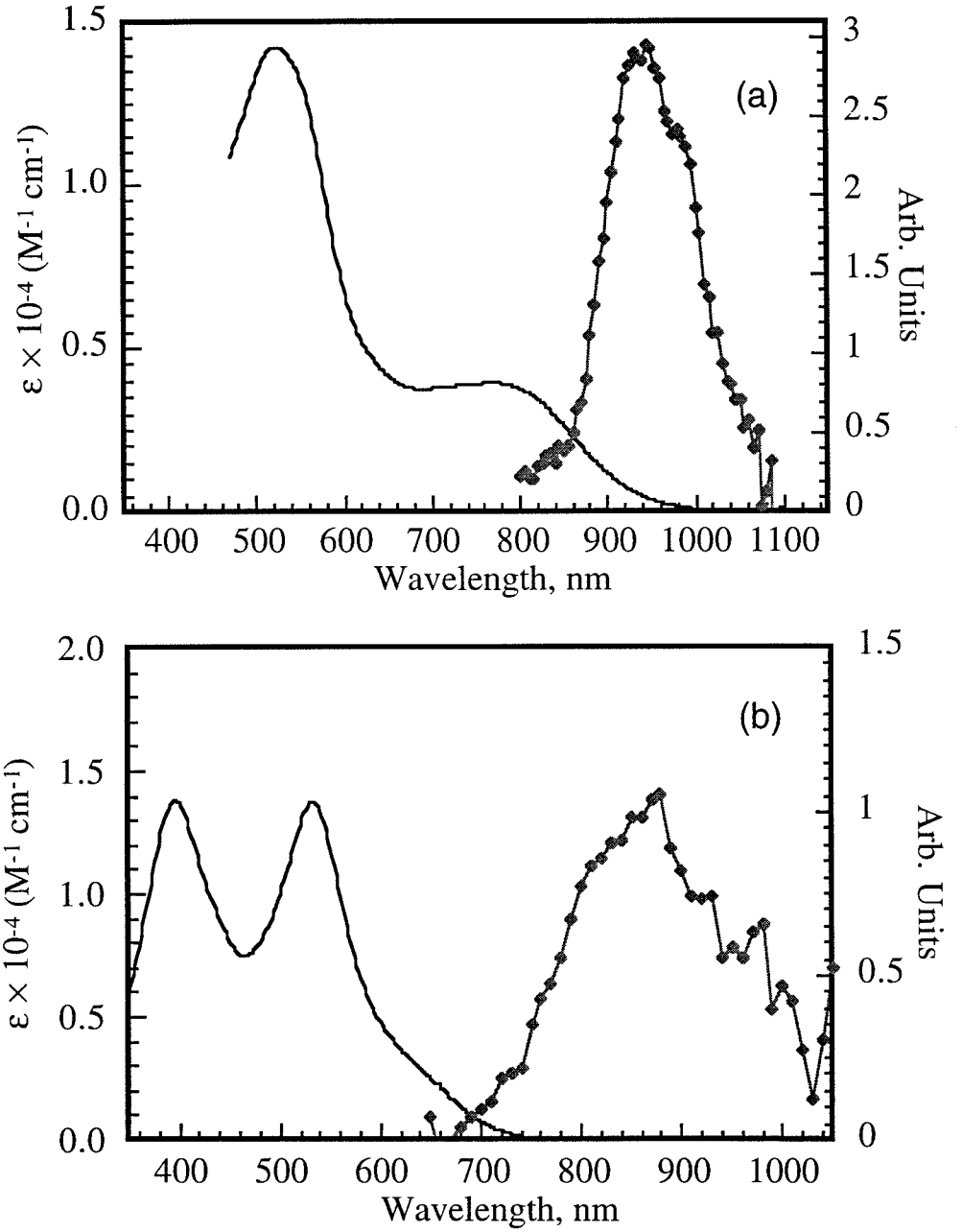


Figure 15: UV/visible absorption spectra (solid line, no circle) and emission spectra (circle) of the complexes $M(II)L'_2(NCS)_2$ in methanol containing 1 mM pyridine and 1 mM pyridinium triflate. (a) $OsL'_2(NCS)_2$ (b) $RuL'_2(NCS)_2$.

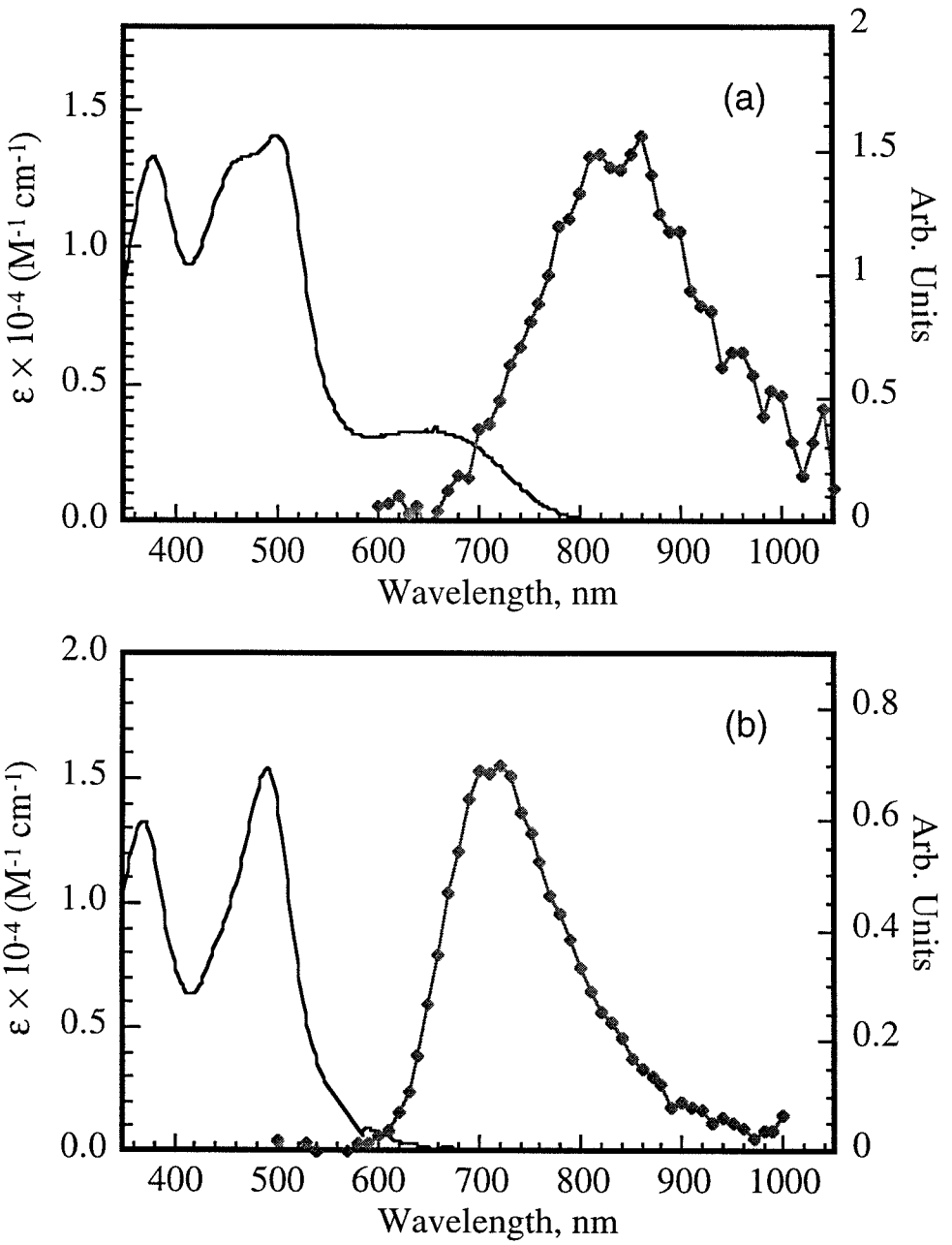


Figure 16: UV/visible absorption spectra (solid line, no circle) and emission spectra (circle) of the complexes M(II)L'$_2$(CN)$_2$ in methanol containing 1 mM pyridine and 1 mM pyridinium triflate. (a) OsL'$_2$(CN)$_2$ (b) RuL'$_2$(CN)$_2$.

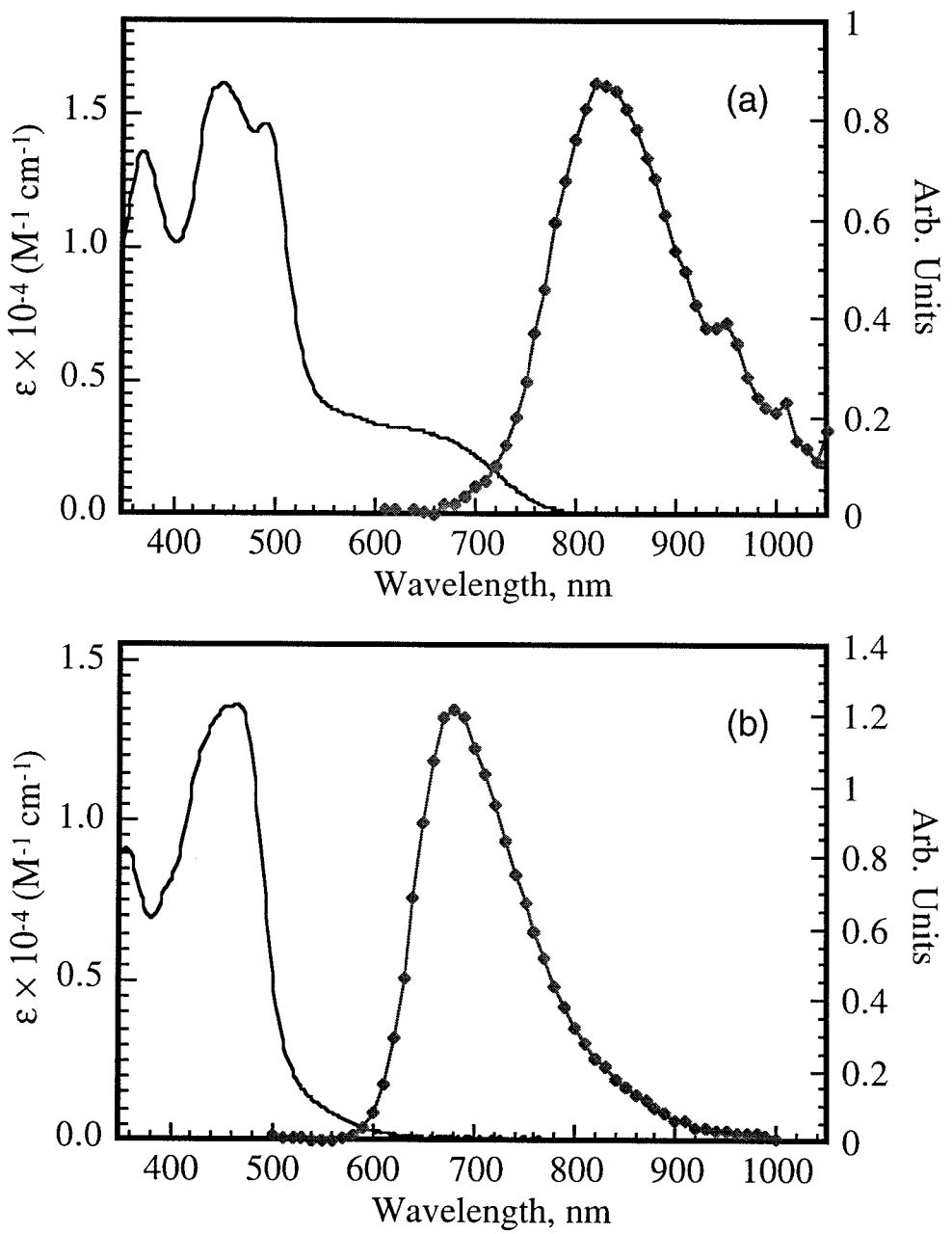


Figure 17: UV/visible absorption spectra (solid line, no circle) and emission spectra (circle) of the complexes $M(II)L_2L'^{2+}$ in methanol containing 1 mM pyridine and 1 mM pyridinium triflate. (a) $OsL_2L'^{2+}$ (b) $RuL_2L'^{2+}$.

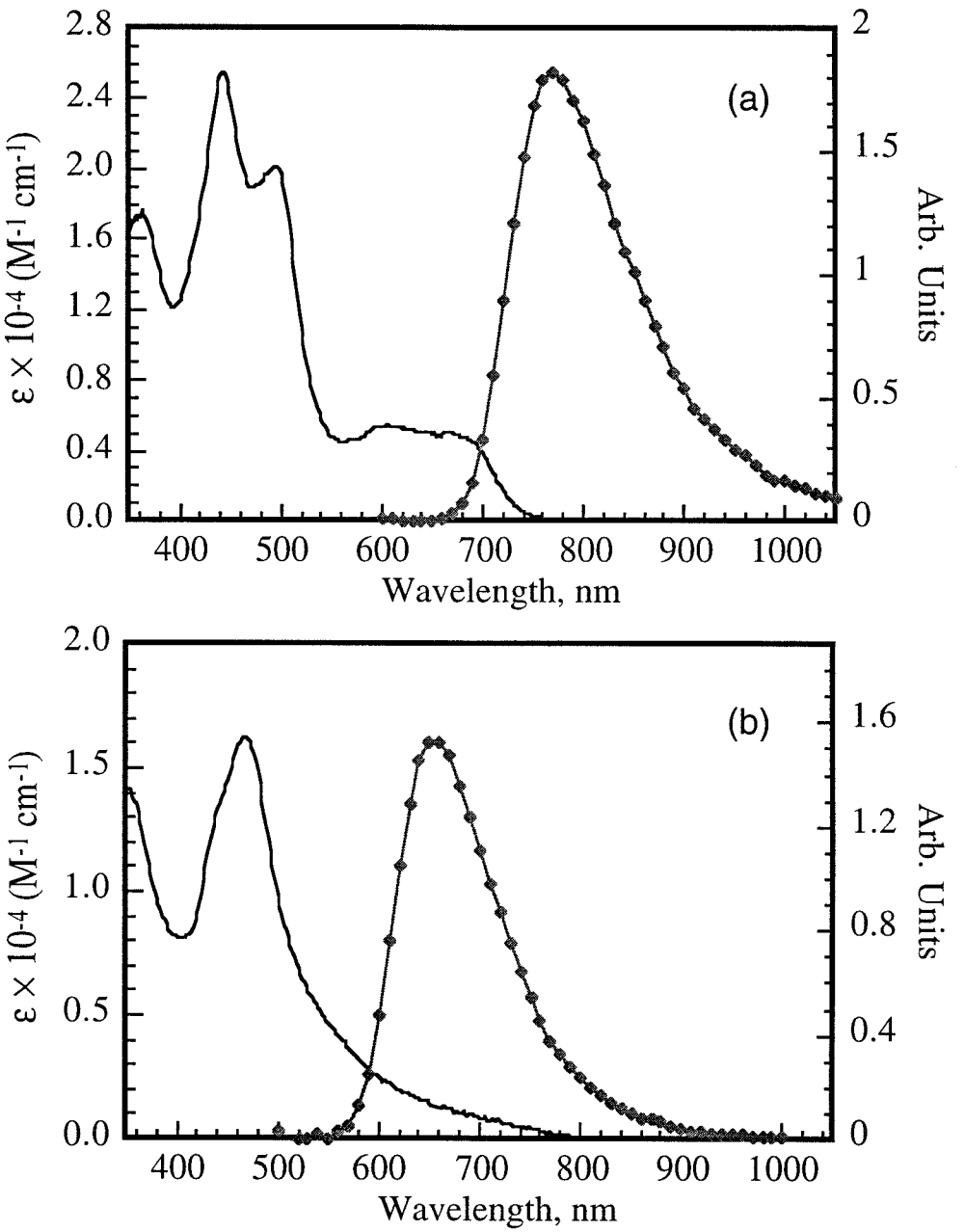


Figure 18: UV/visible absorption spectra (solid line, no circle) and emission spectra (circle) of the complexes $M(II)L'_3^{2+}$ in methanol containing 1 mM pyridine and 1 mM pyridinium triflate. (a) $OsL'_3^{2+}$ (b) $Ru(L'\text{-}2H^+)_3^{4-}$.

Table 5: Spectrochemical Properties of the Complexes

| Complex | Abs max / nm ($\varepsilon/10^4$ $M^{-1}$ $cm^{-1}$) in EtOH[a,b] | | | Emission[c] in MeOH[a] |
|---|---|---|---|---|
| $OsL'_2(NCS)_2$ | 412 (1.43±0.05) | 530 (1.51±0.06) | ~ 780 (0.5) | 940[d] |
| $RuL'_2(NCS)_2$ | 398 (1.24±0.03) | 538 (1.21±0.03) | | 880 |
| $OsL'_2(CN)_2$ | 382 (1.40±0.05) | 508 (1.44±0.05) | ~ 680 (0.368±0.005) | 840 |
| $RuL'_2(CN)_2$ | 376 (1.31±0.01) | 496 (1.49±0.01) | | 720 |
| $OsL_2L'^{2+}$ | 448 (1.68±0.05) | 494 (1.48±0.05) | ~ 640 (0.4) | 820 |
| $RuL_2L'^{2+}$ | 356 (1.01±0.06) | 470 (1.39±0.04) | | 680 |
| $OsL'_3{}^{2+}$ | 442 (2.48±0.02) | 496 (2.02±0.02) | ~ 640 (0.6) | 770 |
| $Ru(L'\text{-}2H^+)_3{}^{4-}$ | | 464 (1.99±0.08) | | 660 |
| | **Abs max / nm in MeOH[a]** | | | |
| $RuL'_2(NCS)_2$ | 396 | 534 | | |
| $OsL'_2(CN)_2$ | 378 | 500 | ~ 660 | |
| $OsL'_3{}^{2+}$ | 442 | 494 | ~ 640 | |

a. Solution contained 1 mM pyridine and 1 mM pyridinium triflate.

b. ε are averages of 3 or more solutions.

c. Measured at room temperature.

d. In EtOH/MeOH 4:1 glass at 77 K.

The lifetimes of the excited states of the complexes in deaerated methanol (and in basic water for the $M(L'\text{-}2H^+)_3{}^{4-}$) at room temperature are summarized in Table 6. The lifetimes of the osmium complexes were consistently much shorter than those of the ruthenium analogs (25-33 times shorter), but the trends were similar within each series:

$$ML'_2(NCS)_2 < ML'_2(CN)_2 < M(L'\text{-}2H^+)_3{}^{4-} < ML_2L'^{2+}$$

Creutz *et al.* studied a series of polypyridine complexes of Ru(II) and Os(II) and also observed that osmium lifetimes were 10-30 times shorter than the ruthenium lifetimes, and that the lifetimes for complexes with the same metal center followed the same rough order.[98] In our work, the excited state lifetime of $OsL'_2(NCS)_2$ at room temperature was not measured because no emission was observed at room temperature. However, based on

the trends in Table 6, one would expect its lifetime to be at least 25 times shorter than the ruthenium analog, i.e., less than 0.3 ns.

Table 6: Excited State Lifetimes of Complexes in Deaerated Methanol
($\lambda_{exc.}$ = 330 nm, measured at room temperature)

| **Complex** | **Concentration of solutions used (μM)** | **Wavelengths of observation (nm)** | **Lifetime (ns)** | **N[b]** |
|---|---|---|---|---|
| $OsL'_2(NCS)_2$ | | | << 8 | |
| $RuL'_2(NCS)_2$ | 85 | 820 | 7.6 | 1 |
| $OsL'_2(CN)_2$ | 20, 100 | 800, 825 | 8.4 ± 0.1 | 5 |
| $RuL'_2(CN)_2$ | 35, 50, 100 | 680, 690, 700, 710 | 205 ± 10 | 11 |
| $[OsL_2L'](PF_6)_2$ | 50 | 740 | 44.9 ± 0.4 | 2 |
| $[RuL_2L'](PF_6)_2$ | 20 | 640 | 1123 ± 1 | 2 |
| $[Os(L'\text{-}2H)_3]^{4-}$ | 140[a] | 760, 770, 825 | 23.86 ± 0.05 | 5 |
| $[Ru(L'\text{-}2H)_3]^{4-}$ | | | 800[c] | |
| $RuL'_3{}^{2+}$ | | | 600[d] | |

a. Measured in water with 2 mM NaOH.

b. Total number of measurements

c. Measured in water at pH 10 by Kalyanasundaram *et al.*[69]

d. Measured in water at pH 2 by Devilvestron *et al.*[40]

The trend in lifetimes among a series with the same metal mostly correlated with the destabilization of the metal $t_{2g}$ orbitals and the ground state redox potentials, except for the $ML'_3{}^{2+}$ complex. This discrepancy could be due to the lower excited state energy of the tris complexes (see Table 7). According to the energy gap law, lowering the excited state energy gap is accompanied by larger non-radiative decays, which in turn yields shorter lifetimes:[64]

$$\frac{1}{\tau} = k_r + k_{nr} \qquad (4)$$

where $\tau$ is lifetime, $k_r$ and $k_{nr}$ are the rate constants for the radiative and nonradiative decays, respectively. For polypyridine complexes of Ru(II), the excited state energy gap is related to the separation between the lowest polypyridine ligand $\pi^*$ and the metal $t_{2g}$ orbitals.[69] Therefore, the excited state energy gap can be lowered by either raising the energy of the $t_{2g}$ or decreasing the energy of the $\pi^*$ orbitals.[69] The validity of the energy gap law was verified for a series of Ru(II) complexes containing 4,4'-dicarboxy-2,2'-bipyridine[69] and two series of Os((II) polypyridine complexes.[99]

Despite its relatively short lifetime, the photoexcited $RuL'_2(NCS)_2$ was shown to effectively inject an electron into the $TiO_2$ conduction band.[16] This is possible because the injection into nanocrystalline $TiO_2$ is thought to occur on a sub-picosecond timescale.[43,45,48,77] Ferrere *et al.* showed that $FeL'_2(CN)_2$ can also photosensitize $TiO_2$.[49] $FeL'_2(CN)_2$ has a 330 ps lifetime, and, based on arguments pertinent to iron polypyridine complexes, argues that the injection must occur in less than 25 ps. Though the lifetime of photoexcited $OsL'_2(NCS)_2$ is not known, it is reasonable to assume that it should be long enough to inject an electron into nanocrystalline $TiO_2$. Furthermore, Nazeeruddin *et al.* concluded (for a series of polypyridine complexes) that the excited state redox potential is actually more important than lifetimes in determining the photosensitizing effectiveness of a dye.[65] The excited state redox potential of $OsL'_2(NCS)_2$ is sufficiently negative (see below) to inject an electron into $TiO_2$.

## C. Electrochemical Properties of the Complexes

Table 7 displays the ground state formal oxidation potentials ($E^{o'}$) of these various complexes. Figure 19 shows the CV and DPV spectra of $OsL'_2(NCS)_2$ in dry methanol containing 1.0 M $LiClO_4$, 10 mM pyridine and 10 mM pyridinium triflate. Both methods yielded the same $E^{o'}$ (0.42 V vs SCE). All the osmium complexes displayed reversible cyclic voltammograms (see Fig. 19 and 21).

Table 7: Electrochemical Properties of the Complexes

| **Complex** | **E°', V vs aq. SCE[a]** | **estimated $E_{0-0}$ (eV)** | **estimated E°'* (V vs. SCE)** |
|---|---|---|---|
| $OsL'_2(NCS)_2$ | 0.42 | 1.4 | -1.0 |
| $RuL'_2(NCS)_2$ | 0.68[b] | 1.8 | -1.1 |
| | 0.80[c] | | |
| $OsL'_2(CN)_2$ | 0.72 | 1.8 | -1.1 |
| $RuL'_2(CN)_2$ | 1.08[d] | 2.0 | -0.9 |
| $OsL_2L'^{2+}$ | 0.81 | 1.7 | -0.9 |
| $RuL_2L'^{2+}$ | 1.23 | 2.1 | -0.9 |
| $OsL'_3{}^{2+}$ | 1.01[e] | 1.8 | -0.8 |
| $Ru(L'-2H^+)_3{}^{4-}$ | 1.40[e,f] | 2.1 | -0.7 |

a. in MeOH with 10 mM pyridine, 10 mM pyridinium triflate and 1.0 M $LiClO_4$; determined by cyclic voltammetry.

b. irreversible; determined by DPV.

c. in acetonitrile with 1.0 M $LiClO_4$; determined by cyclic voltammetry; reversible.

d. quasi-reversible.

e. in MeOH with 10 mM pyridinium triflate and 1.0 M $LiClO_4$.

f. determined by DPV.

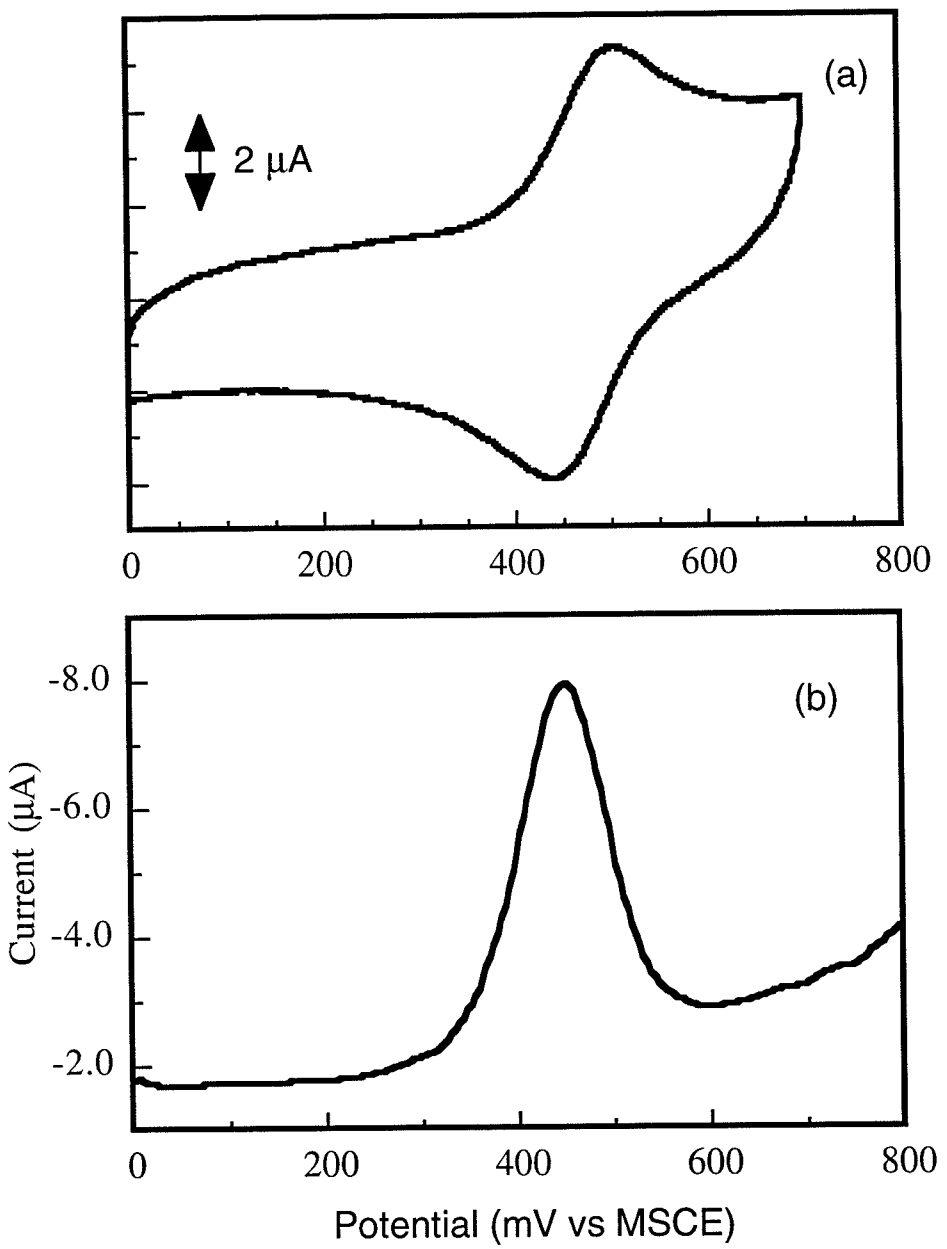


Figure 19: (a) CV and (b) DPV for $OsL'_2(NCS)_2$ in methanol with 10 mM pyridine, 10 mM pyridinium triflate and 1.00 M $LiClO_4$. MSCE was -0.05 V vs aqueous SCE. The CV was obtained at a scan rate of 100 mV $s^{-1}$ and $\Delta E$ was 60 mV. For the DPV, the pulse amplitude was 50 mV.

$RuL'_2(NCS)_2$ displayed irreversible behavior in methanol (Fig. 20a) and its electrochemistry was consequently determined by DPV (Fig. 20b). $RuL'_2(NCS)_2$ displayed more reversible behavior in $CH_3CN$ (Fig. 20c), and its formal potential determined in $CH_3CN$, $E^{\circ'}$=0.80 V vs SCE, is in good agreement with the reported value of $E^{o'}$=0.85 vs SCE,[16] The difference between our measurement and the reported value could be due to a difference in the dye protonation state during the measurements. The formal potential of these dyes was observed in our work to be pH-dependent, as would be expected of acidic redox species.[100] For instance, the formal potential of $K_4[RuL'_3]$ was 1.25 V vs SCE in methanol with no pyridine or pyridinium present, but was 1.4 V vs SCE in the presence of 10 mM pyridinium. Also, the value of the formal potential of $OsL'_2(NCS)_2$ decreased upon addition of higher concentrations of pyridine. These results suggest that deprotonation lowers the value of $E^{\circ'}$, which is consistent with the expectation that more electron-rich ligands will render the metal center easier to oxidize and therefore yield a more negative $E^{\circ'}$ value.

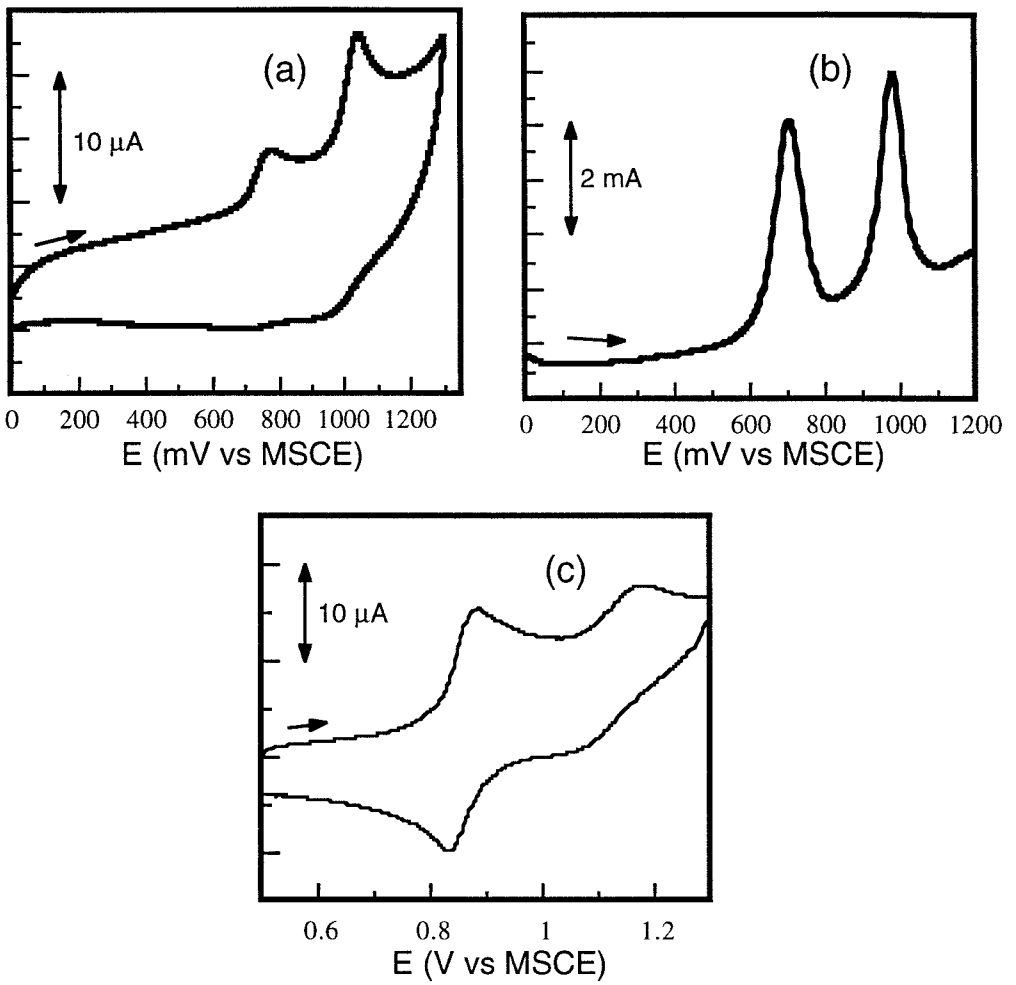


Figure 20: Electrochemistry of $RuL'_2(NCS)_2$. (a) CV and (b) DPV in methanol with 10 mM pyridine, 10 mM pyridinium triflate and 1.00 M $LiClO_4$. (c) CV in acetonitrile with 1.0 M $LiClO_4$. MSCE was -0.05 V vs aqueous SCE. The CV was obtained at a scan rate of (a) 100 mV $s^{-1}$ (b) 50 mV $s^{-1}$. For the DPV, the pulse amplitude was 50 mV.

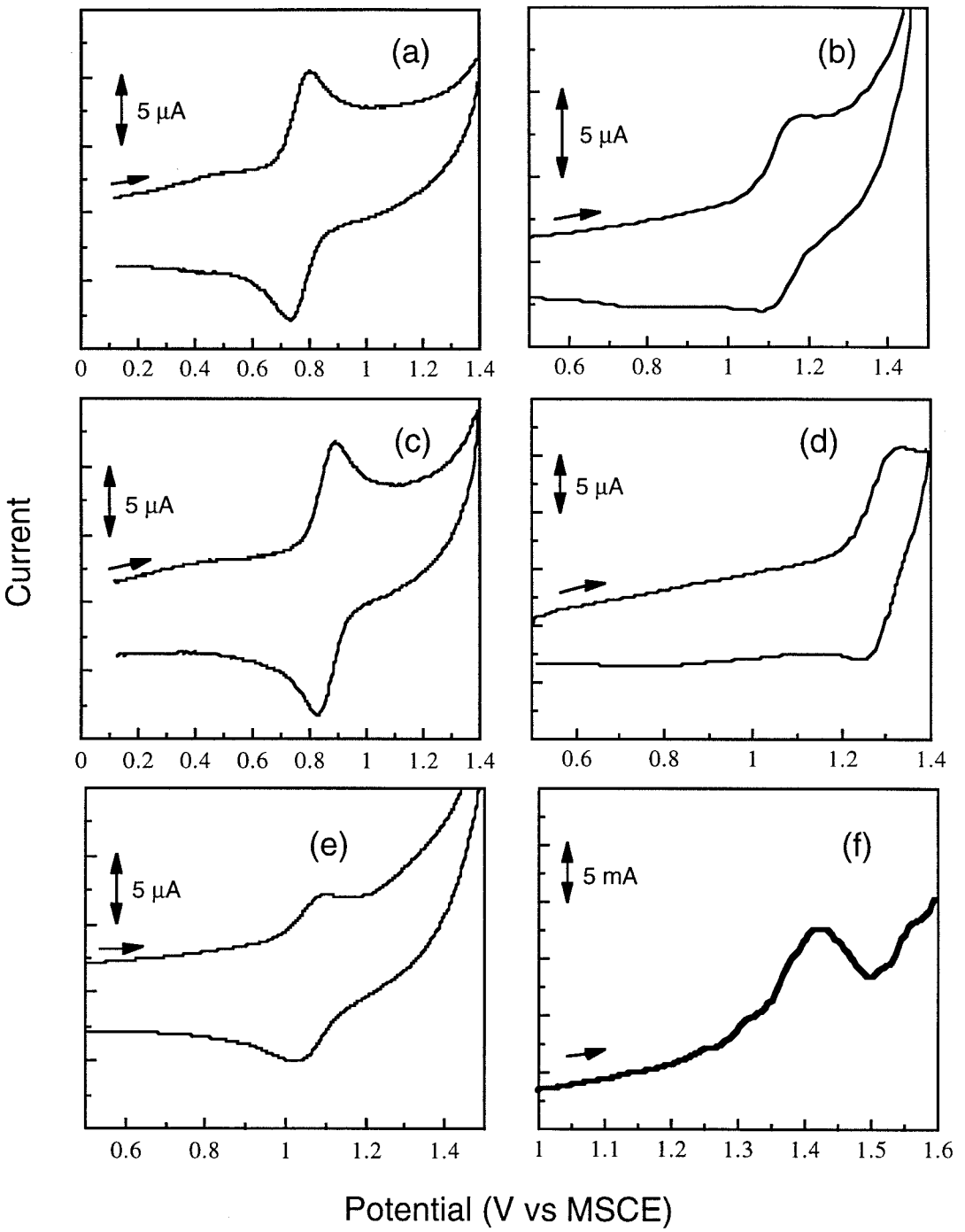


Figure 21: Electrochemistry of complexes. Cyclic voltammetry of (a) $OsL'_2(CN)_2$, (b) $RuL'_2(CN)_2$, (c) $OsL_2L'^{2+}$, (d) $RuL_2L'^{2+}$ in methanol with 10 mM pyridine, 10 mM pyridinium triflate and 1.00 M $LiClO_4$. CV of (e) $OsL'_3{}^{2+}$ and DPV of (f) $Ru(L'\text{-}2H^+)_3{}^{4-}$ in methanol with 10 mM pyridinium triflate and 1.00 M $LiClO_4$. MSCE was -0.05 V vs aqueous SCE. The CVs were obtained at a scan rate of 50 mV $s^{-1}$. For the DPV, the pulse amplitude was 50 mV.

As expected, the redox potentials of the Os complexes were more negative than those of the analogous ruthenium complexes. Also, within a series with the same metal, the trend for the ground state redox potential $E^{\circ\prime}$[M(III)/M(II)] was:

$$ML'_2(NCS)_2 < ML'_2(CN)_2 < ML_2L'^{+2} < ML'_3{}^{+2}$$

where M is Os or Ru. This trend correlates with the electron donating/π-accepting properties of the ligands around the metal center. Ligands with more electron donating properties (such as $NCS^-$) will destabilize the metal $t_{2g}$ orbitals and facilitate oxidation of the metal, which is observed through a more negative ground state redox potential. Increasing the π-acceptor properties of the ligands has the opposite effect. The ground state redox potentials can therefore be readily fine-tuned by varying the metal and the ligands in this series of complexes.

The excited state redox potentials, $E^{\circ\prime}$[M(III)/M(II)]*, were estimated using eq 2:

$$E^{\circ\prime} * = E^{\circ\prime} - \boldsymbol{E}_{0-0} / q \qquad (5)$$

where $E^{\circ\prime}$ is the formal reduction potential of the ground state, $E^{\circ\prime}$* is the formal reduction potential of the excited state (for the half-reaction M(II)* → M(III) + $e^-$), and $\mathbf{E}_{0\text{-}0}$ is the minimum energy between the ground state and excited state. $\mathbf{E}_{0\text{-}0}$ was estimated as the intersection between the absorption and emission spectra of the dye of concern (Fig. 15-18, Table 7). The $E^{\circ\prime}$* values for the osmium complexes were similar to those for the corresponding ruthenium complexes. This is expected because the electron density in the MLCT excited state of these systems is centered primarily on the bipyridyl ligands. The π* orbitals of the carboxylated bipyridine ligand lie at lower energy than those of the non-carboxylated bipyridine. As a result, the excited state potential of the $ML'_3{}^{2+}$ complex is more positive than that of the $ML_2L'^{2+}$ complex. The lower apparent $E^{\circ\prime}$* values for the $ML'_3{}^{2+}$ complexes could also arise because their ground state redox potentials were measured at a different pH than the other complexes. Further trends among the $E^{\circ\prime}$* values are not considered to be significant due to the error associated with the determination of these excited states potentials.

## D. Spectroelectrochemistry of $OsL_2L'^{2+}$

For future measurements of back electron transfer rates, it is important to know the absorbance spectra of the M(III) complex. This can be done by spectroelectrochemistry, assuming the M(III) complex is stable. $[Os(II)L_2L']^{2+}$ was oxidized to $[Os(III)L_2L']^{2+}$ by applying +1.1 V vs Ag/AgCl. Figure 22a shows the evolution of the UV/vis spectra with time. The MLCT band in the visible disappeared upon oxidation, and the oxidation was complete within 20 min. An isobestic point was observed at 354 nm, indicating the presence of only two species, the Os(II) and Os(III) complexes. The UV/vis spectra of Os(II) completely recovered within 8 min by applying +0.5 V vs Ag/AgCl (see Figure 22b), indicating that the Os(III) complex was stable during the time scale of this experiment (1 h).

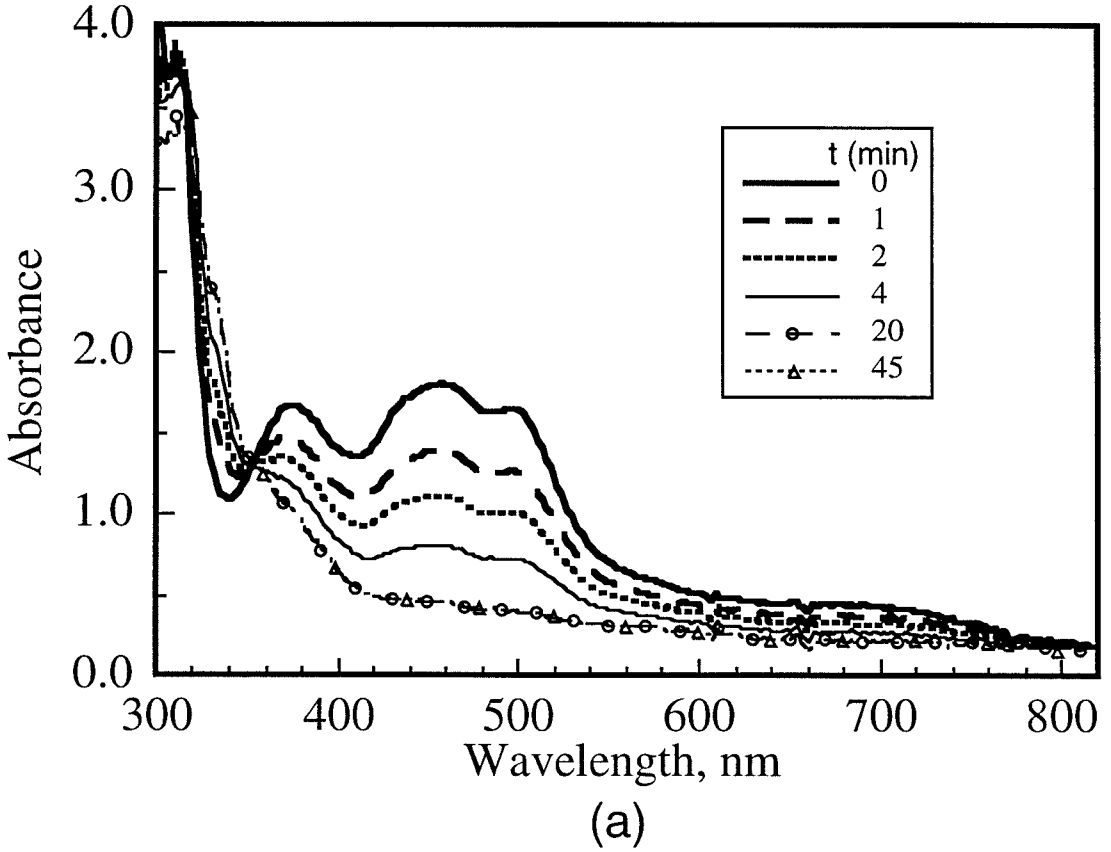


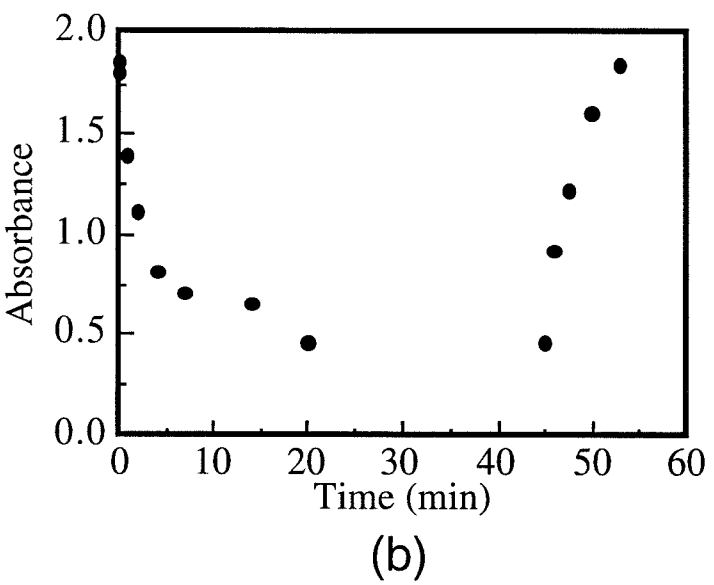


Figure 22: Spectroelectrochemistry of $[Os(II)L_2L'](PF_6)_2$. (a) Oxidation of $[Os(II)L_2L'](PF_6)_2$ obtained by applying 1.1 V vs Ag/AgCl in acetonitrile solution containing 10 mM $[Os(II)L_2L'](PF_6)_2$ and 1.0 M $LiClO_4$. (b) Absorbance monitored at 454 nm. At t = 0 min, 1.1 V vs Ag/AgCl is applied to oxidize Os(II). At t = 45 min, 0.5 V vs Ag/AgCl is applied to reduce Os(III) back to Os(II).

# Chapter 4:

# Results and Discussion, Part 2:

# Photoelectrochemistry

## A. Results

*1. Spectral Response Characteristics of Os- and Ru- Coated $TiO_2$ Electrodes*

Figure 23 and 24 display the spectral response characteristics, collected under short-circuit conditions, of the various dye-coated $TiO_2$ electrode systems studied in this work. As expected, the spectral response of each dye-coated $TiO_2$ electrode shows a strong correlation with the absorption spectrum of the metal complex.

Sensitization with $RuL'_2(CN)_2$ produced very high maximum external quantum yields, with the analogous $OsL'(L'\text{-}H^+)(CN)_2^{1-}$ complex yielding similar maximum quantum yields and even better response in the red region of the spectrum. The $Ru(L'\text{-}2H^+)_3^{4-}$ and $Os(L'\text{-}2H^+)_3^{4-}$ complexes showed quantum yields similar to each other, with the Os complex again showing an improved response in the red relative to the Ru system. Similar enhancements in the red response were also observed in a comparison between the $RuL_2L'^{2+}$ and $OsL_2L'^{2+}$ systems. In contrast, although the red response was improved by changing from $RuL'_2(NCS)_2$ to $OsL'_2(NCS)_2$, the Os complex yielded very low ($\Phi \approx 0.1$) steady-state quantum yields throughout the visible region. This phenomenon was investigated in detail and is discussed below. Even the complexes with the lowest excited state redox potentials, the $OsL_3'$ and $RuL_3'$ systems, produced high maximum quantum yields for injection. On an overall basis, the $OsL'(L'\text{-}H^+)(CN)_2^{1-}$-, $RuL'_2(NCS)_2$- and $Os(L'\text{-}2H^+)_3^{4-}$- coated electrodes had the best-matched spectral response for illumination by sunlight and their spectral response characteristics are compared in Figure 25.

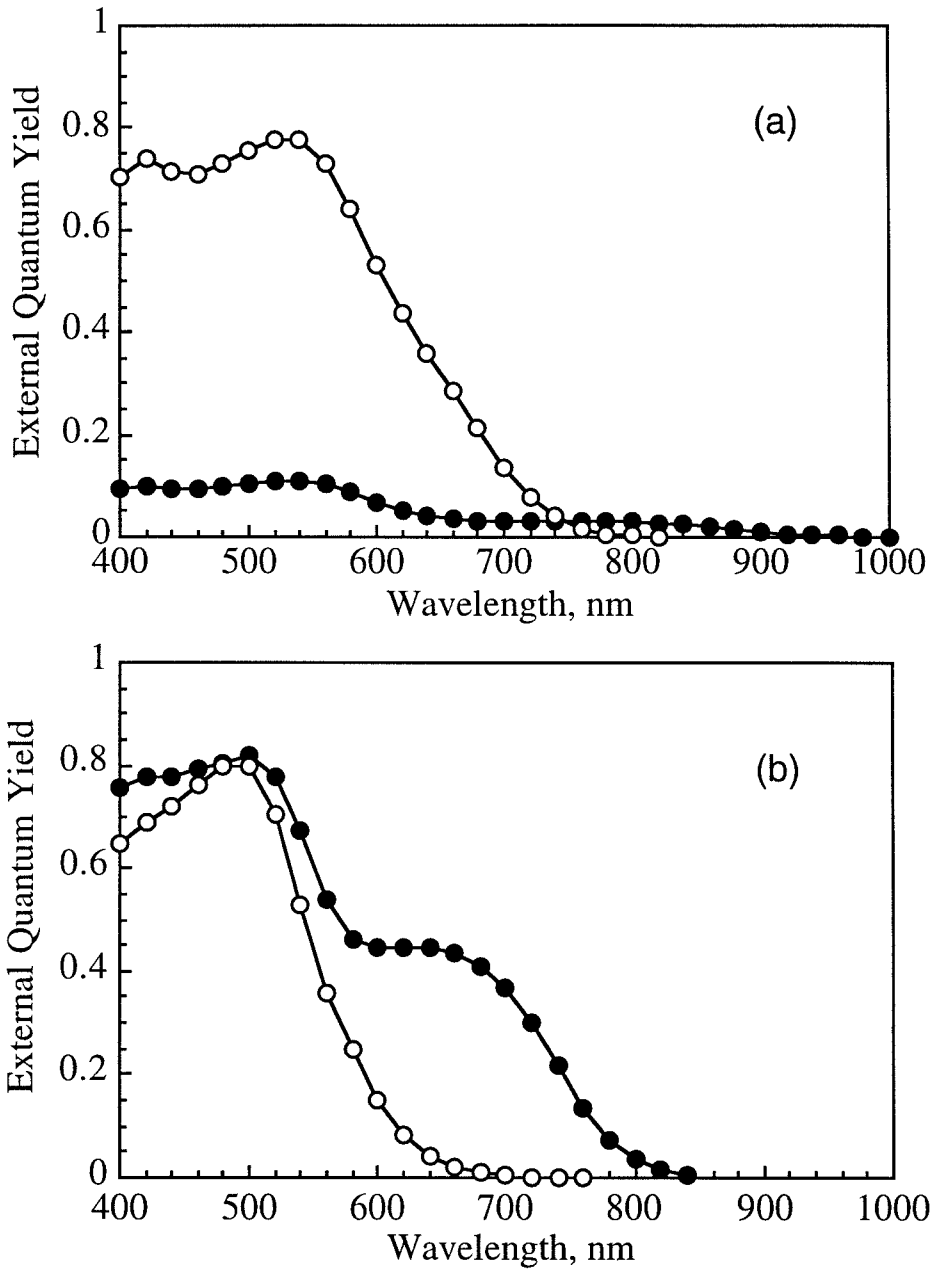


Figure 23: Spectral response data for the (a) $ML'_2(NCS)_2$- and (b) $ML'_2(CN)_2$- coated $TiO_2$ electrodes. (●) M = osmium, (o) M = ruthenium. The spectral responses are the average of three or more measurements and the sample standard deviations for the external quantum yields were less than 0.05.

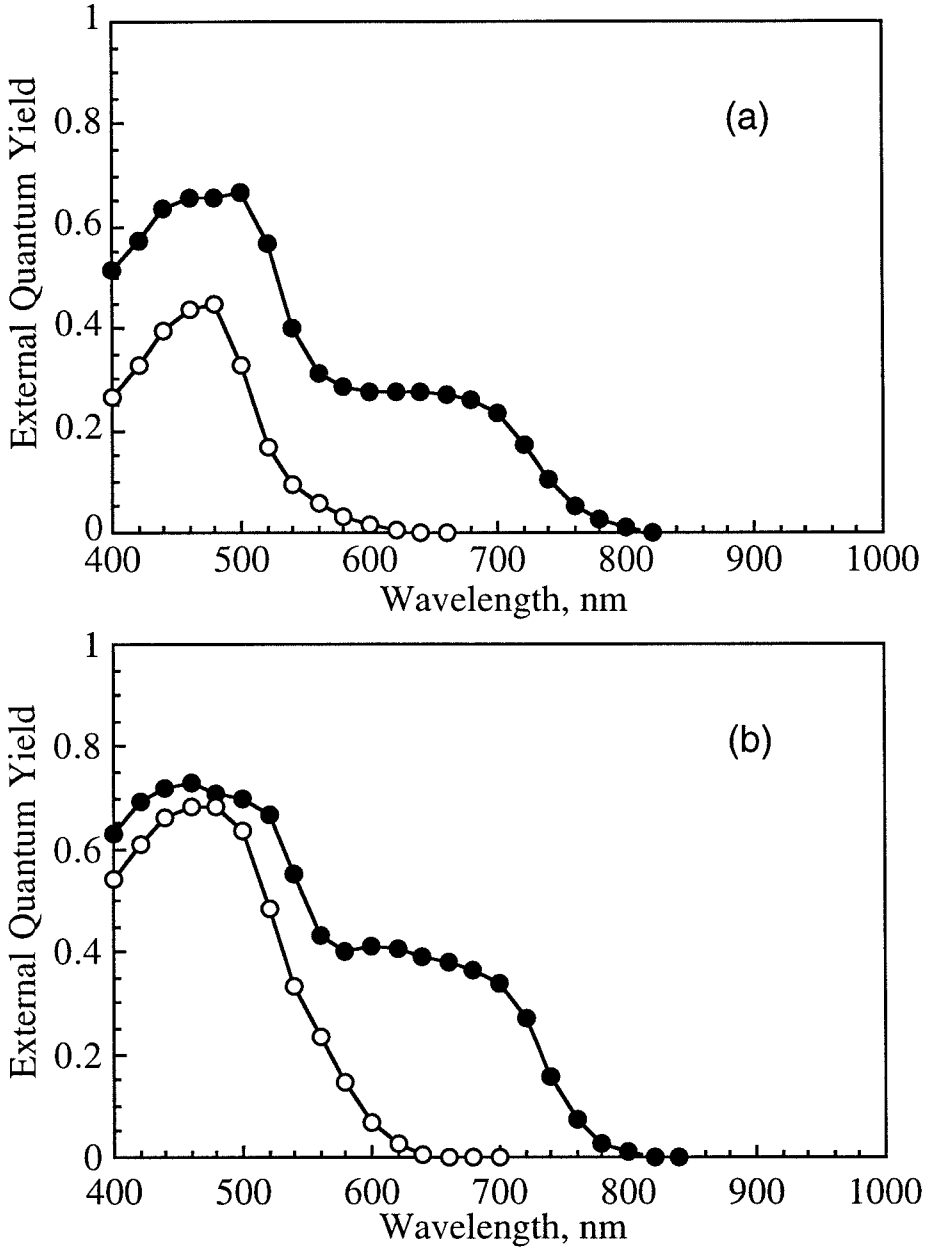


Figure 24: Spectral response data for the (a) $ML_2L'^{2+}$- and (b) $M(L'\text{-}2H^+)_3^{4-}$- coated $TiO_2$ electrodes. (●) M = osmium, (o) M = ruthenium. The spectral responses are the average of three or more measurements and the sample standard deviations for the external quantum yields were less than 0.05.

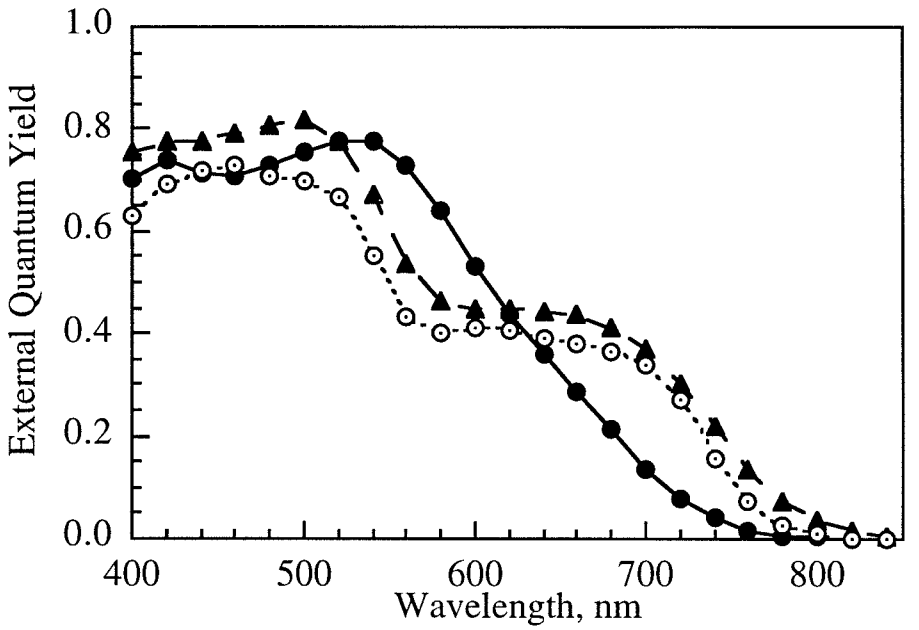


Figure 25: Spectral response data obtained for (●) $RuL'_2(NCS)_2$-, (▲) $OsL'(L'\text{-}H^+)(CN)_2^{1-}$ and (o) $Os(L'\text{-}2H^+)_3^{4-}$ coated electrodes. The spectral responses are the average of three or more measurements and the sample standard deviations for the external quantum yields were less than 0.05.

The maximum external quantum yield for a typical electrode containing each dye was corrected for the absorbance of the dye using eq 3:

$$\Phi_{corrected} = \frac{\Phi_{external}}{\left(\frac{100 - \%T}{100}\right)} \qquad (6)$$

where %T is the percent transmittance of the dye-coated electrode at the wavelength of maximum external quantum yield. The corrected quantum yields are reported in Table 8 and representative absorbance spectra of dye-coated electrodes are shown in Figure 26. Note that the relatively low external quantum yield of $RuL_2L'^{2+}$ is due to the incomplete absorption of the light by the dye-coated electrode at this loading level. When the external quantum yield is corrected for the incomplete absorption of the dye, the quantum yield is 0.9. The corrected quantum yields approached unity for all the dyes except $OsL'_2(NCS)_2$, which only displayed a value of 0.12.

Table 8: External and Corrected Quantum Yields for a Representative Dye-coated Electrode

| **Complex** | **Max. external Q. Y.** | **Abs. for electrode at λ of max. Q.Y.** | **% T** | **corrected Q. Y.** |
|---|---|---|---|---|
| $OsL'_2(NCS)_2$ | 0.11 | 1.32 | 4.8 | 0.12 |
| $RuL'_2(NCS)_2$ | 0.80 | 1.13 | 7.4 | 0.86 |
| $OsL'(L'\text{-}H^+)(CN)_2^{1-}$ | 0.81 | 0.83 | 14.8 | 0.95 |
| $RuL'_2(CN)_2$ | 0.83 | 1.08 | 8.3 | 0.91 |
| $OsL_2L'^{2+}$ | 0.65 | 0.50 | 31.6 | 0.95 |
| $RuL_2L'^{2+}$ | 0.43 | 0.28 | 52 | 0.90 |
| $Os(L'\text{-}2H^+)_3^{4-}$ | 0.71 | 1.26 | 5.5 | 0.75 |
| $Ru(L'\text{-}2H^+)_3^{4-}$ | 0.67 | 1.36 | 4.4 | 0.70 |

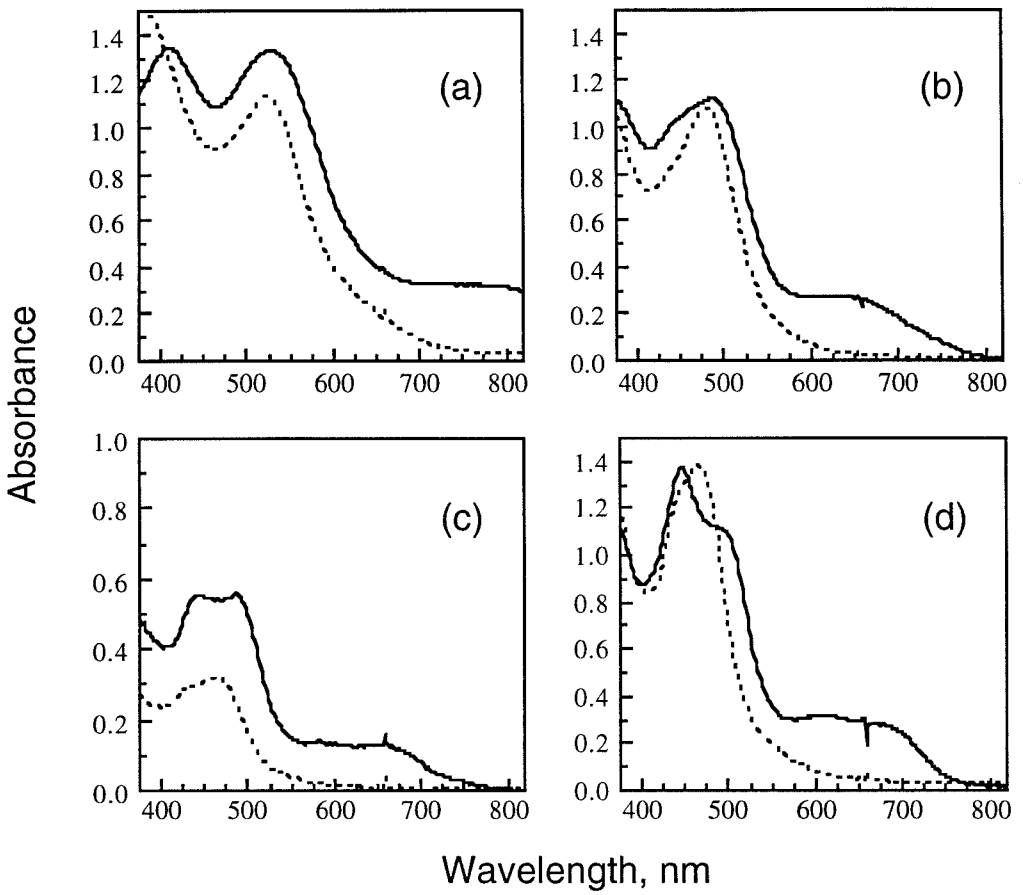


Figure 26: Absorbance spectra of representative dye-coated $TiO_2$ electrodes. (a) $ML'_2(NCS)_2$, (b) $ML'_2(CN)_2$, (c) $ML_2L'^{2+}$, (d) $M(L'\text{-}2H^+)_3^{4-}$, where M is osmium (solid line) or ruthenium (dashed line). The blank was a $TiO_2$ electrode which had been treated nominally identically but which was immersed into an ethanolic solution that contained no dye.

2. *Current-Potential Behavior of Os- and Ru-Coated $TiO_2$ Electrodes*

Figure 27 shows the J-*E* data, obtained both in the dark and under Air Mass (AM) 1.0 simulated illumination, for representative samples of the dye-coated $TiO_2$ electrodes that were studied in this work. The average short-circuit photocurrent density ($J_{sc}$) and open-circuit voltage ($V_{oc}$) values for each dye over a series of runs are reported in Table 9. Table 9 reports the fill factors for the series-resistance-corrected J-*E* curves for the representative samples shown in Figure 27-30. The data obtained with electrodes coated with Ru 535 is also included in Table 9 for comparison. Ru 535 is the commercially available $RuL'_2(NCS)_2$, from Solaronix Inc.

Table 9: Photoelectrochemical Data

| **Complex** | **N[a]** | **$V_{oc}$ ELH bulb[b] (mV)** | **$J_{sc}$ ELH bulb[b] (mA cm$^{-2}$)** | **ff[c] AM 1.0** | **$V_{oc}$ 1.0 mA cm$^{-2}$ (mV)** |
|---|---|---|---|---|---|
| $OsL'_2(NCS)_2$ | 3 | 360 ± 5 | 2.1 ± 0.3 | 0.55 | 336 ± 6 |
| $RuL'_2(NCS)_2$ | 5 | 522 ± 6 | 10.8 ± 0.5 | 0.69 | 432 ± 8 |
| Ru 535 | 5 | 620 ± 15 | 12.3 ± 0.6 | | 540 ± 16 |
| $OsL'(L'\text{-}H^+)(CN)_2^{1-}$ | 4 | 569 ± 6 | 11.6 ± 0.6 | 0.62 | 496 ± 7 |
| $RuL'_2(CN)_2$ | 3 | 581 ± 3 | 5.5 ± 0.1 | 0.63 | 524 ± 4 |
| $OsL_2L'^{2+}$ | 4 | 540 ± 10 | 7.7 ± 0.5 | 0.66 | 487 ± 9 |
| $RuL_2L'^{2+}$ | 4 | 532 ± 4 | 1.8 | 0.62 | 511 ± 7 |
| $Os(L'\text{-}2H^+)_3^{4-}$ | 3 | 514 ± 1 | 10.0 ± 0.2 | 0.69 | 448 ± 3 |
| $Ru(L'\text{-}2H^+)_3^{4-}$ | 3 | 501 ± 2 | 3.7 ± 0.1 | 0.67 | 468 ± 3 |

a. Total number of experiments, each with a different electrode.

b. The illumination was equivalent to 100 mW cm$^{-2}$, the power of the sun at AM 1.0.

b. Fill factor for a representative resistance-corrected J-*E* curve.

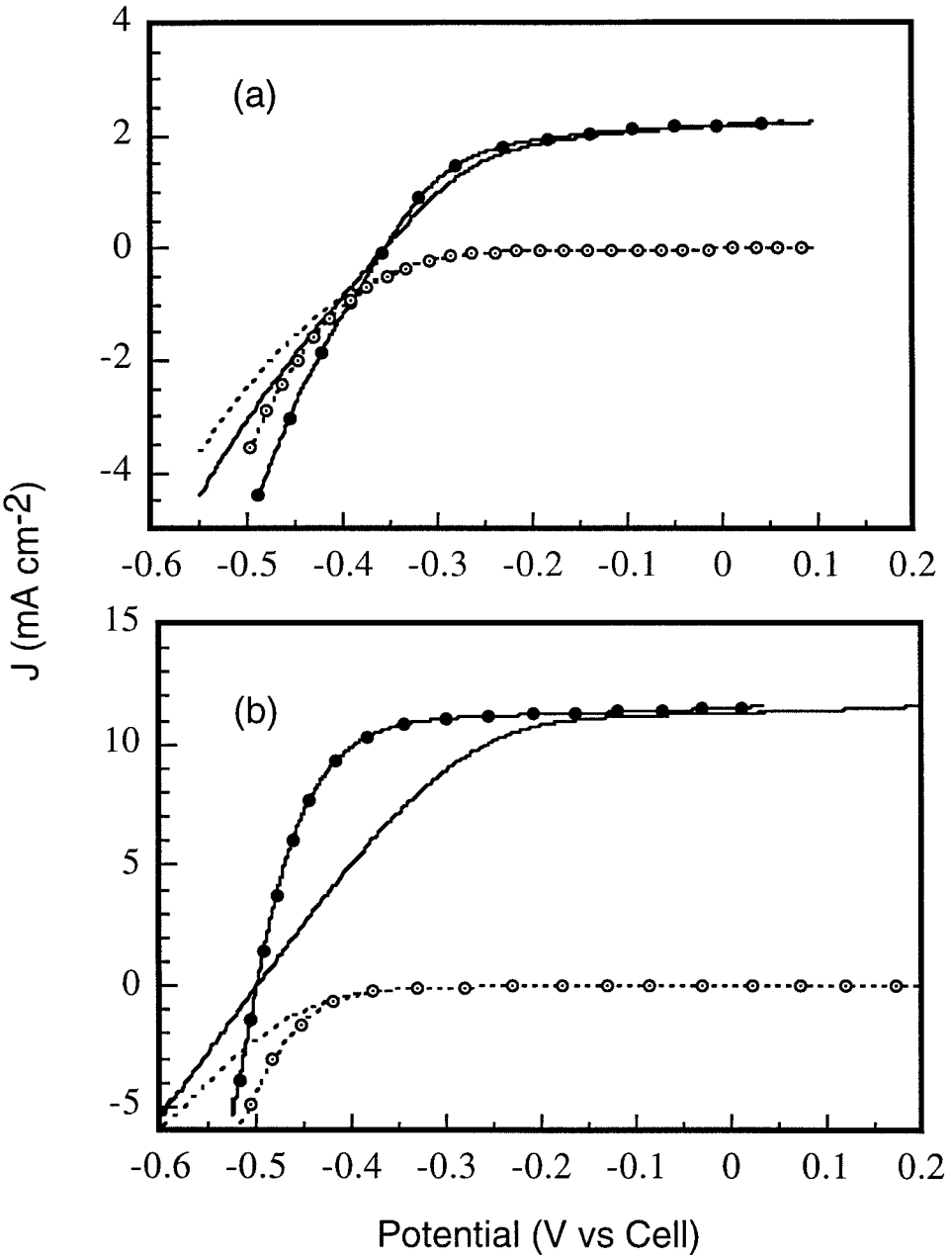


Figure 27: Current density vs potential behavior for a representative $TiO_2$ electrode sensitized with (a) $OsL'_2(NCS)_2$ and (b) $RuL'_2(NCS)_2$. The data was obtained under a light intensity equivalent to 1 Sun (solid line) and in the dark (dashed line). The lines with no symbols are raw data and the lines with symbols are corrected for cell resistance.

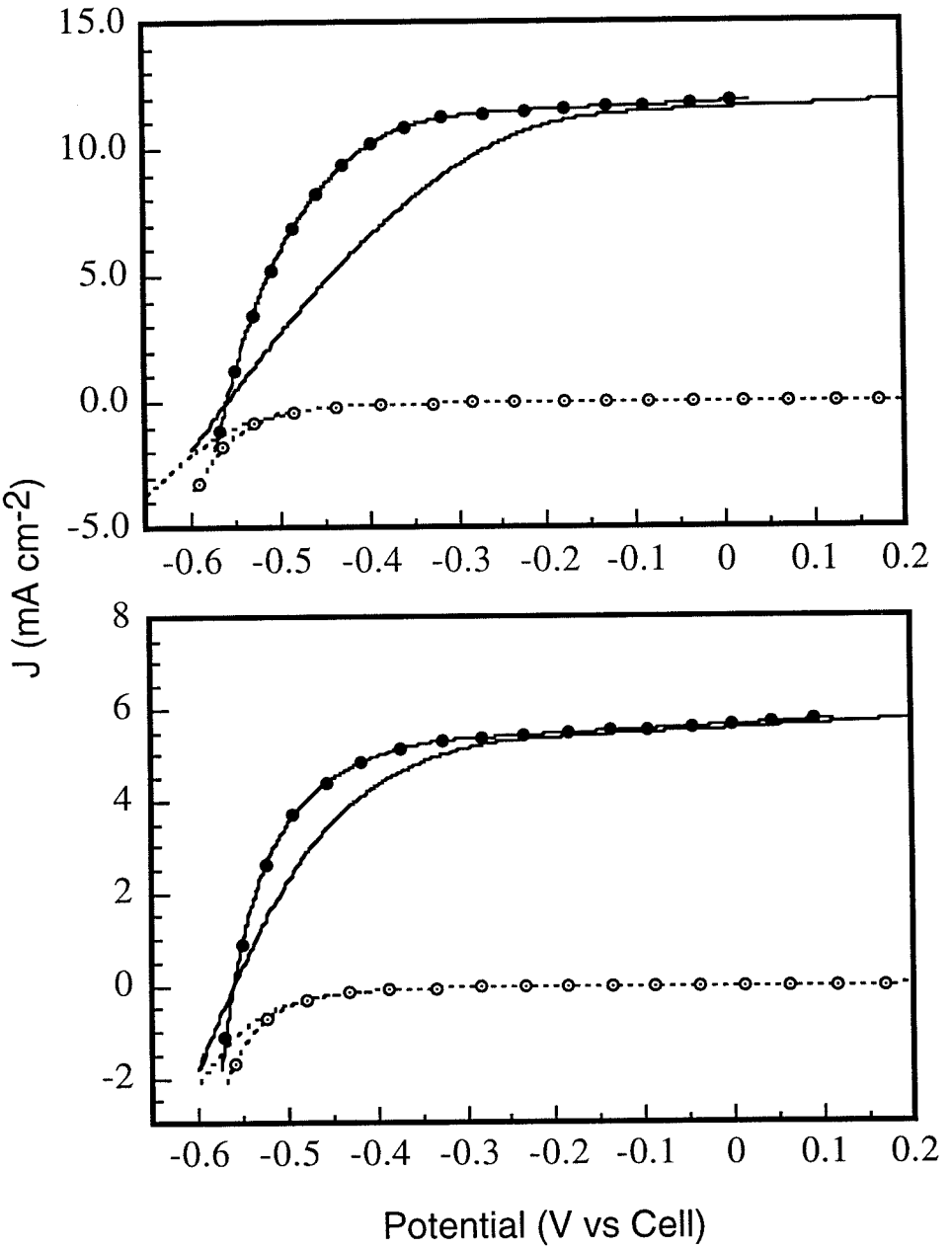


Figure 28: Current density vs potential behavior for a representative $TiO_2$ electrode sensitized with (a) $OsL'(L'\text{-}H^+)(CN)_2^{1-}$ and (b) $RuL'_2(CN)_2$. The data was obtained under a light intensity equivalent to 1 Sun (solid line) and in the dark (dashed line). The lines with no symbols are raw data and the lines with symbols are corrected for cell resistance.

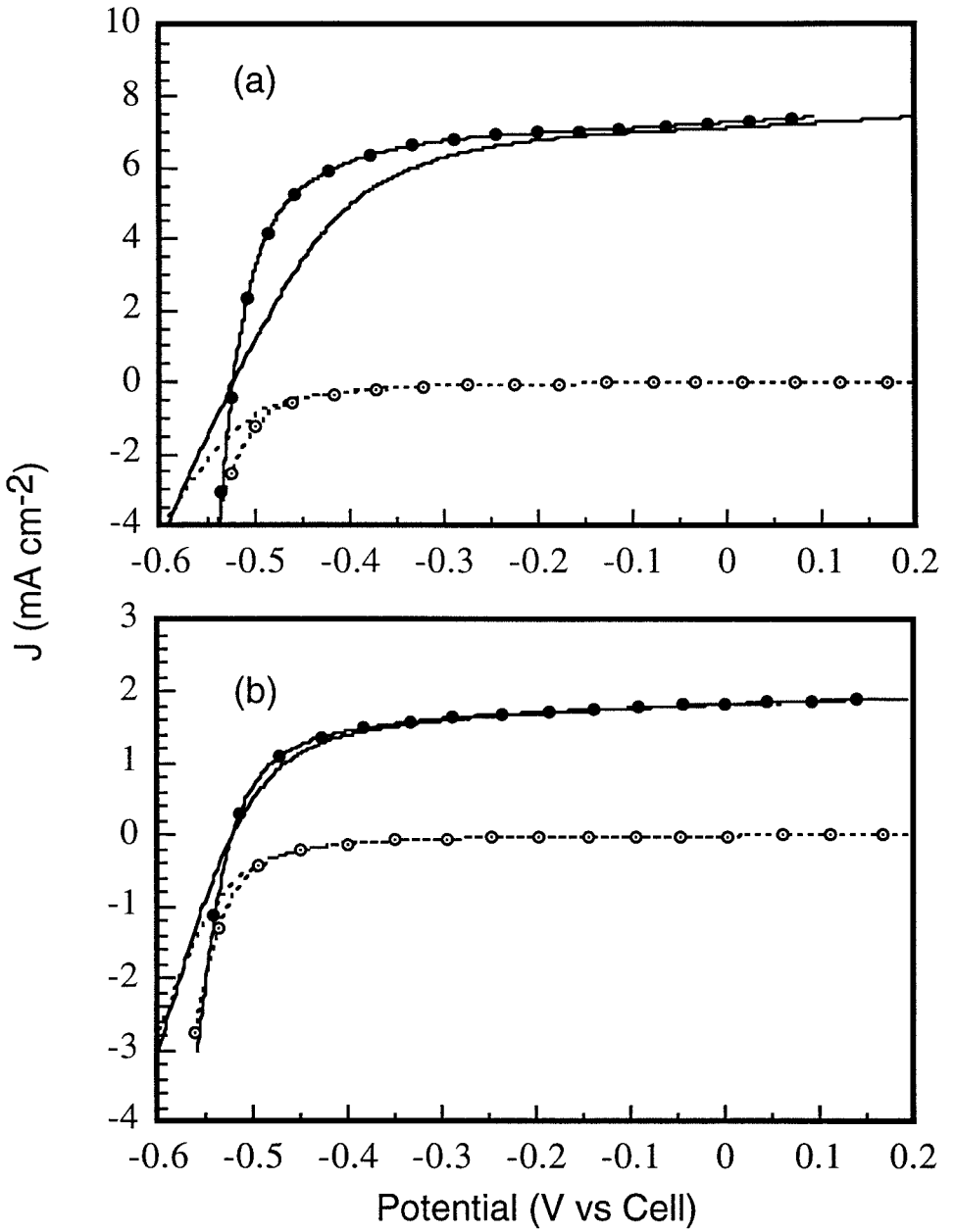


Figure 29: Current density vs potential behavior for a representative $TiO_2$ electrode sensitized with (a) $OsL_2L'^{2+}$ and (b) $RuL_2L'^{2+}$. The data was obtained under a light intensity equivalent to 1 Sun (solid line) and in the dark (dashed line). The lines with no symbols are raw data and the lines with symbols are corrected for cell resistance.

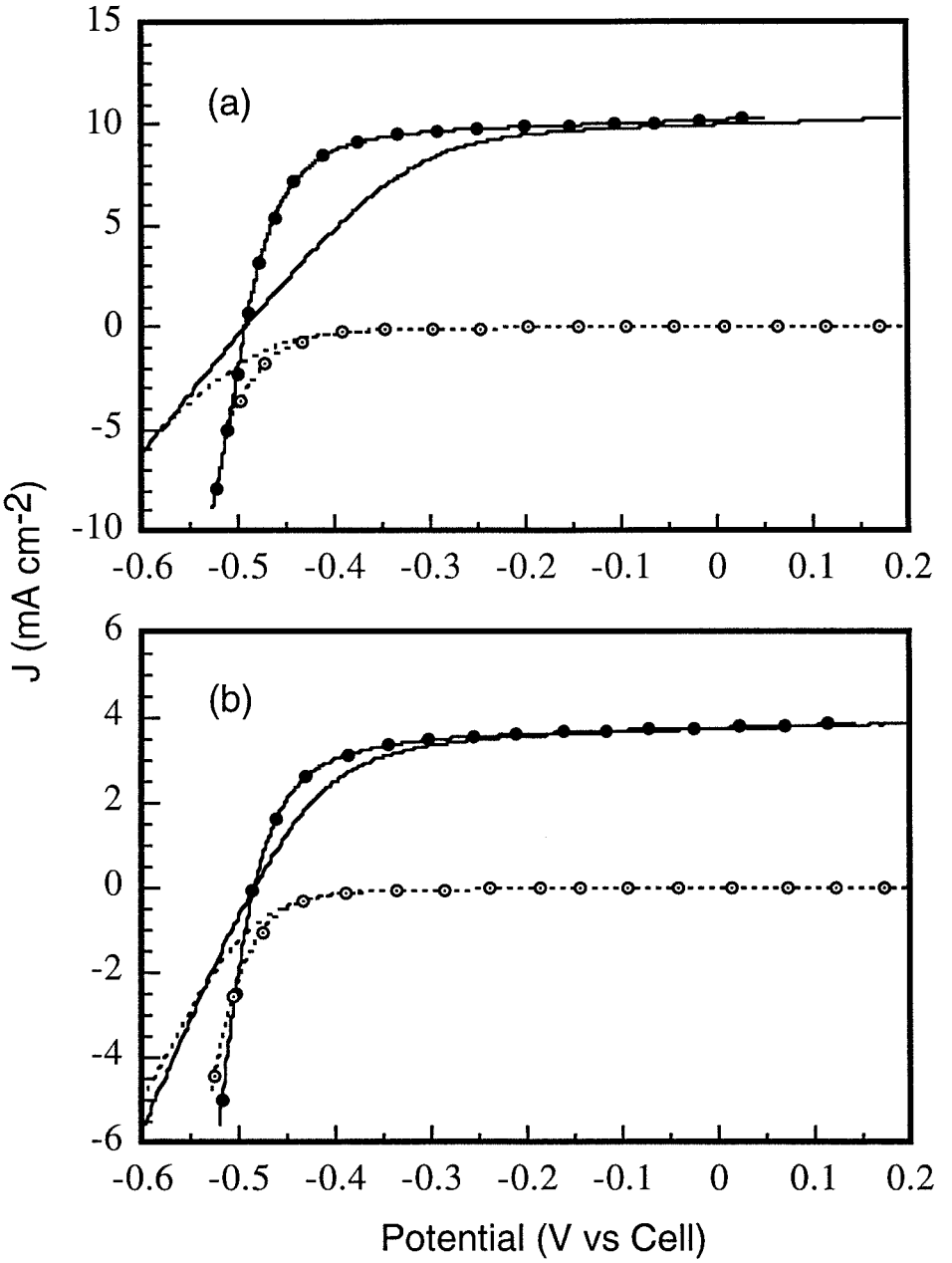


Figure 30: Current density vs potential behavior for a representative $TiO_2$ electrode sensitized with (a) $Os(L'\text{-}2H^+)_3^{4-}$ and (b) $Ru(L'\text{-}2H^+)_3^{4-}$. The data was obtained under a light intensity equivalent to 1 Sun (solid line) and in the dark (dashed line). The lines with no symbols are raw data and the lines with symbols are corrected for cell resistance.

Figure 31 shows the series-resistance-corrected J-*E* behavior for all of the dye-coated $TiO_2$ electrodes in the dark (Fig. 31a) and at a light intensity sufficient to produce $J_{sc}$ = 1 mA $cm^{-2}$ (Fig. 31b). The dark curves were different for the electrodes that had been coated with different metal complexes; similarly, at any specific potential in forward bias, the cathodic currents were different for each different electrode system. As a consequence, $V_{oc}$ was different for every type of dye-coated electrode even when nominally identical short-circuit photocurrent densities, and thus nominally identical injected carrier densities, were obtained (Table 9).

The results described above were obtained at high dye loading levels, for which the $TiO_2$ electrodes were immersed into dye solutions at least 24 h before use. When $TiO_2$ electrodes were left in the dye solution for only 15 min, the current-voltage curves for each of these types of electrodes were very similar, and so were the $V_{oc}$ values at constant $J_{sc}$ (Figure 32, Table 10). This behavior is expected for a situation in which the dark current is determined primarily by reduction of $I_2$ by electrons in the $TiO_2$, and when the rate of this process is not altered by the presence of adsorbed dye on the $TiO_2$ electrode surface. As expected, electrodes that had been immersed in the dye solution for only 15 min were much lighter in color than those immersed overnight in these dye solutions. Quantitative measurements of absorbance of the electrodes (Table 10) confirmed this observation. Also reported in Table 10 are the photoelectrochemical properties obtained under ELH-type AM 1.0 illumination for the$TiO_2$ electrodes having low dye-loading levels. The short-circuit current densities displayed by these electrodes are still high, being 1.8 to 8 times lower than those observed for electrodes having a high dye loading level.

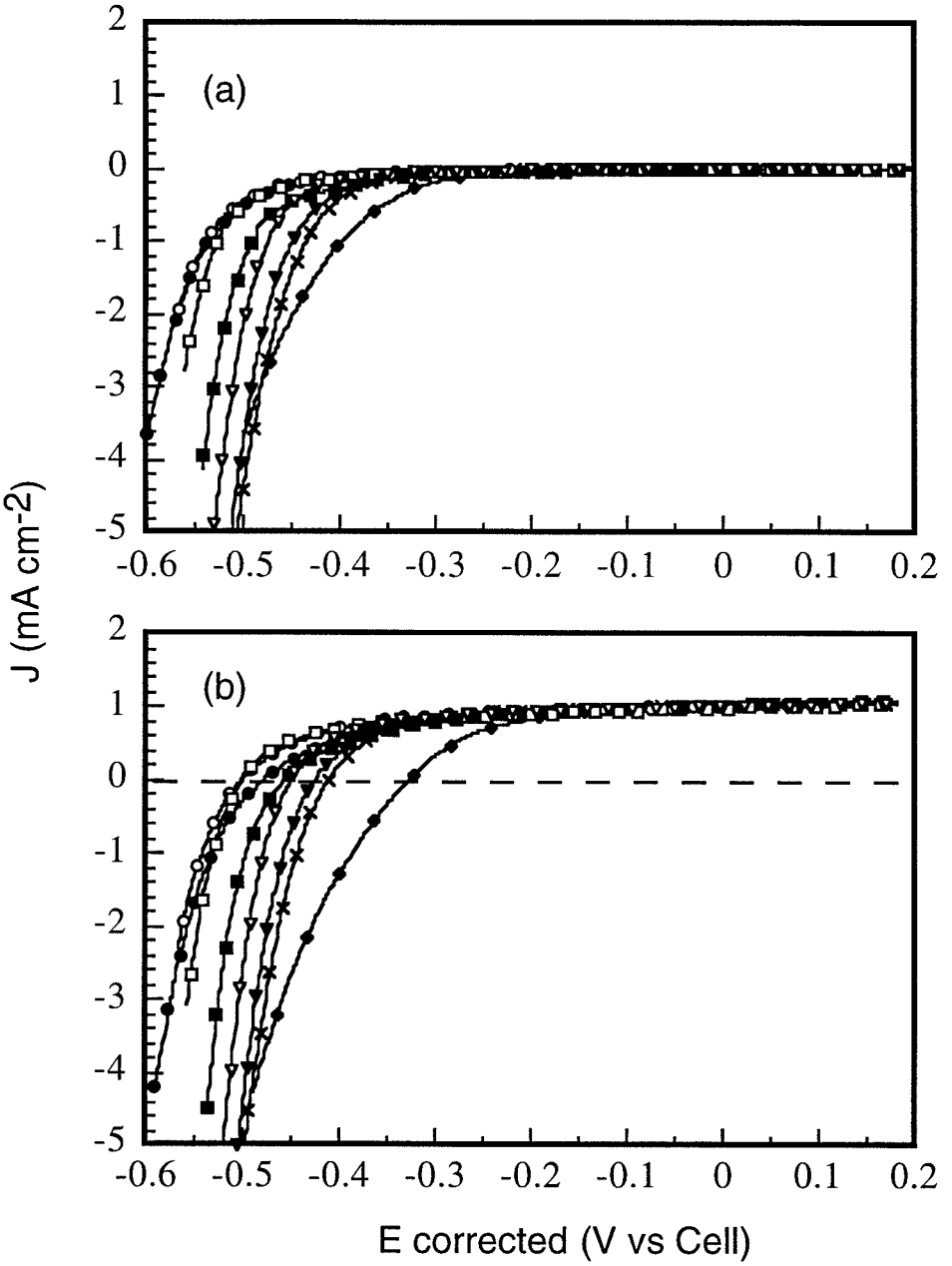


Figure 31: Corrected current density vs potential data for a representative of each of the dyes on $TiO_2$ (a) in the dark and (b) at a fixed short-circuit current density of 1 mA $cm^{-2}$. (◆) $OsL'_2(NCS)_2$, (×) $RuL'_2(NCS)_2$, (●) $OsL'(L'\text{-}H^+)(CN)_2^{1-}$, (o) $RuL'_2(CN)_2$, (■) $OsL_2L'^{2+}$, (❑) $RuL_2L'^{2+}$, (▼) $Os(L'\text{-}2H^+)_3^{4-}$ and (▽) $Ru(L'\text{-}2H^+)_3^{4-}$.

Table 10: Photoelectrochemical Data for the Electrodes with Low Dye Coverage

| **Complex** | **Abs. of electrode (at Max of spectral response)** | **$J_{sc}$ (mA $cm^{-2}$) ELH bulb[a]** | **$V_{oc}$ (mV) ELH Bulb[a]** | **ff resistance-corrected J-*E* curve[a]** | **$V_{oc}$ (mV) at constant injection of 1 mA $cm^{-2}$** |
|---|---|---|---|---|---|
| $OsL'_2(NCS)_2$ | .06 | .8 | 400 | 0.54 | 410 |
| $RuL'_2(NCS)_2$ | .07 | 2.3 | 510 | 0.64 | 470 |
| $OsL'(L'\text{-}H^+)(CN)_2^{1-}$ | .05 | 1.5 | 490 | 0.56 | 460 |
| $RuL'_2(CN)_2$ | .12 | 1.5 | 520 | 0.58 | 490 |
| $OsL_2L'^{2+}$ | .16 | 2.7 | 500 | 0.54 | 470 |
| $RuL_2L'^{2+}$ | .08 | 1 | 470 | 0.56 | 470 |
| $Os(L'\text{-}2H^+)_3^{4-}$ | .13 | 1.4 | 460 | 0.59 | 450 |
| $Ru(L'\text{-}2H^+)_3^{4-}$ | .19 | .9 | 450 | 0.62 | 460 |

a. The illumination was equivalent to 100 mW $cm^{-2}$, the power of the sun at AM 1.0.

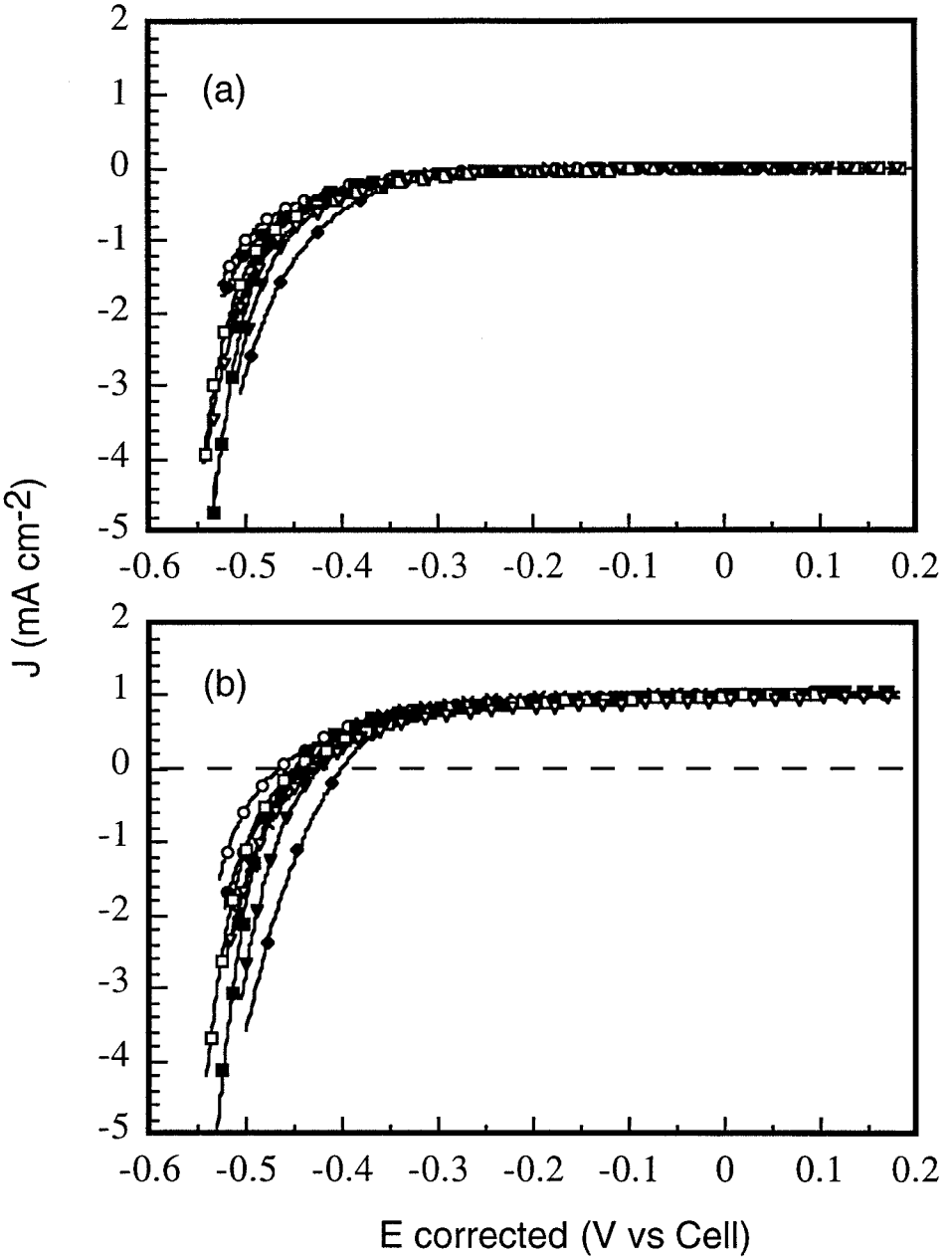


Figure 32: Corrected current density vs potential curves for $TiO_2$ electrodes having a low dye loading level (a) in the dark and (b) at a fixed short-circuit current of 1 mA $cm^{-2}$. (◆) $OsL'_2(NCS)_2$, (×) $RuL'_2(NCS)_2$, (●) $OsL'(L'\text{-}H^+)(CN)_2^{1-}$, (o) $RuL'_2(CN)_2$, (■) $OsL_2L'^{2+}$, (❑) $RuL_2L'^{2+}$, (▼) $Os(L'\text{-}2H^+)_3^{4-}$ and (▽) $Ru(L'\text{-}2H^+)_3^{4-}$.

In order to understand why the $OsL'_2(NCS)_2$-coated electrodes showed such low currents and maximum quantum yield, the photoelectrochemical properties of $OsL'_2(NCS)_2$-, $RuL'_2(NCS)_2$- and $RuL_2L'^{2+}$- coated electrodes were investigated at various $I^-$ concentrations. When the added LiI and $I_2$ concentrations were doubled, the $J_{sc}$ value at AM 1.0 illumination increased significantly in the case of $OsL'_2(NCS)_2$- coated electrodes but not in the case of $RuL'_2(NCS)_2$- and $RuL_2L'^{2+}$- coated electrodes (see Table 11 and Figure 33). To ascertain whether the effect was due to increases in $[I^-]$ or $[Li^+]$, J-*E* data were also collected in 0.5 M LiI/0.5 M $LiClO_4$/0.04 M $I_2$ (Fig. 33 a), but $J_{sc}$ did not change significantly under these conditions relative to its value in the base electrolyte. The photocurrent for $OsL'_2(NCS)_2$- coated electrodes increased from 2.2 to 5.2 mA $cm^{-2}$ upon increasing the iodide concentration five-fold to a level of 2.5 M LiI/0.04 M $I_2$, which was the maximum concentration that could be obtained in this solvent. The maximum external quantum yield also increased from 0.1 to 0.2 at this level of $I^-$. The photocurrent and the maximum external quantum yield for the $RuL'_2(NCS)_2$- coated $TiO_2$ electrodes did not increase significantly under similar conditions (Fig. 34).

Table 11: Photoelectrochemical Data for the LiI Study

| | **$J_{sc}$, ELH bulb, AM 1.0 (mA $cm^{-2}$)** | | | | **Maximum external Q.Y.** | |
|---|---|---|---|---|---|---|
| **Complex** | 0.5 M LiI 0.04 M $I_2$ | 0.5 M LiI 0.5 M $LiClO_4$ 0.04 M $I_2$ | 1.0 M LiI 0.08 M $I_2$ | 2.5 M LiI 0.04 M $I_2$ | 0.5 M LiI 0.04 M $I_2$ | 2.5 M LiI 0.04 M $I_2$ |
| $OsL'_2(NCS)_2$ | 2.2 | 2.5 | 4.0 | 5.2 | 0.11 | 0.24 |
| $RuL'_2(NCS)_2$ | 11.1 | 11.0 | 11.0 | 10.8 | 0.77 | 0.79 |
| $RuL_2L'^{2+}$ | 1.8 | 1.8 | 1.7 | | | |

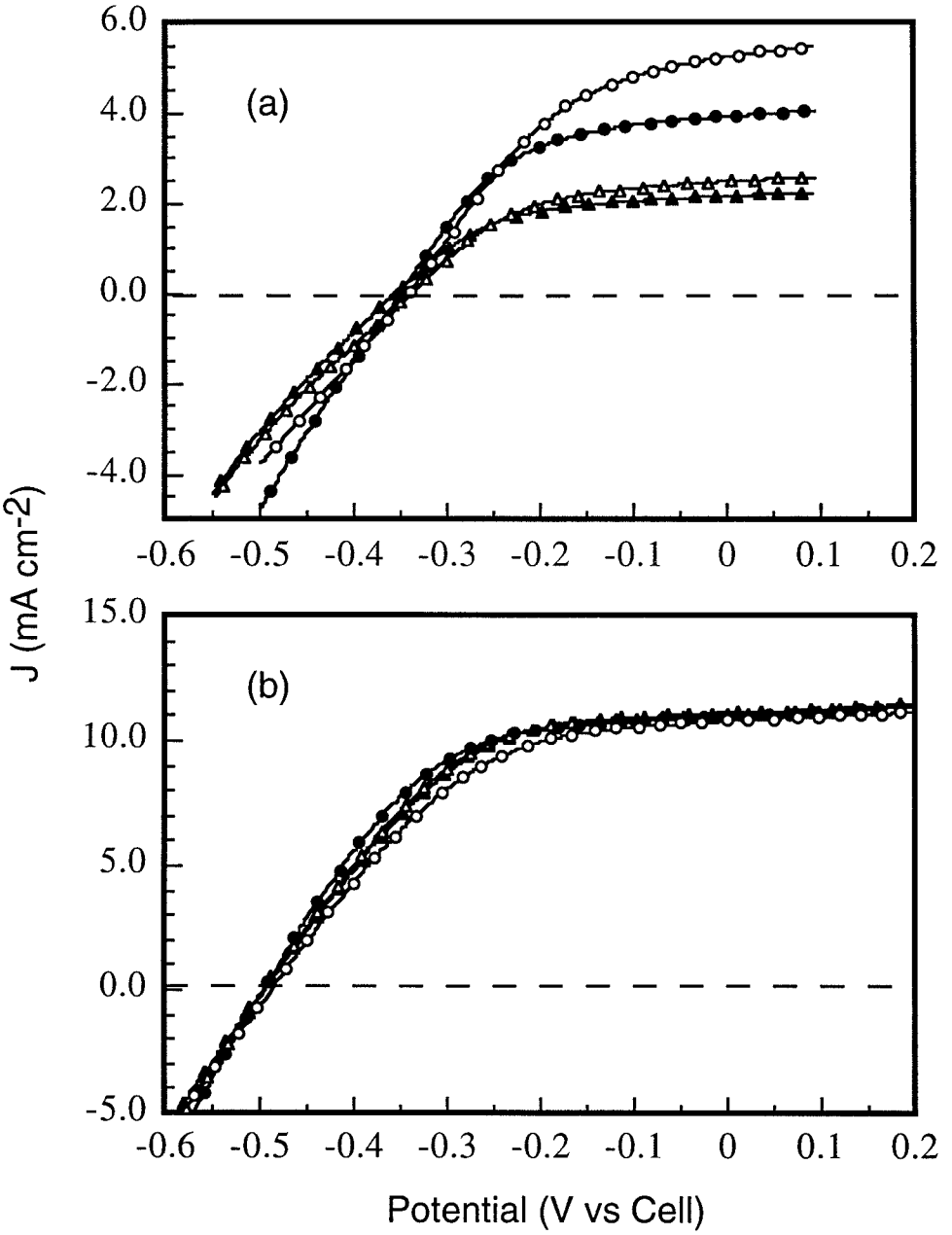


Figure 33: Current density vs potential behavior for (a) $OsL'_2(NCS)_2$ and (b) $RuL'_2(NCS)_2$ with various electrolytes. (▲) 0.5 M LiI/0.04 M $I_2$, (Δ) 0.5 M LiI/0.5 M $LiClO_4$/0.04 M $I_2$, (●) 1.0 M LiI/0.08 M $I_2$ and (○) 2.5 M LiI/0.04 M $I_2$. All electrolytes were in dry ACN and contained 0.050 M pyridine and 0.020 M pyridinium triflate.

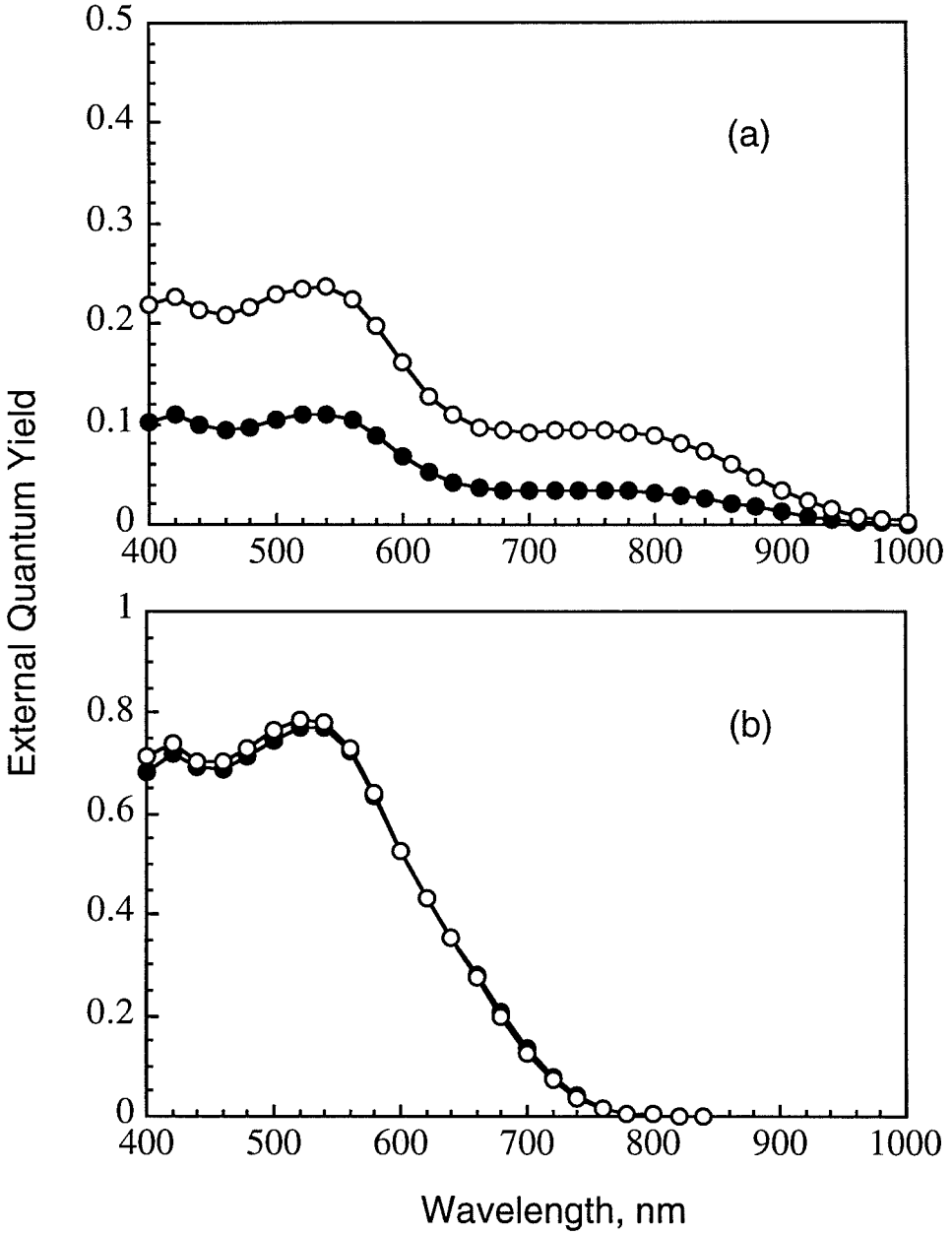


Figure 34: Spectral response data for (a) $OsL'_2(NCS)_2$ and (b) $RuL'_2(NCS)_2$ with two electrolytes. (●) 0.5 M LiI/0.04 M $I_2$ and (o) 2.5 M LiI/0.04 M $I_2$. All electrolytes were in dry ACN and contained 0.050 M pyridine and 0.020 M pyridinium triflate.

*3. Current-Potential Properties of Uncoated $TiO_2$ and Conducting Glass*

Figure 35 compares the J-*E* curves for a bare titanium dioxide electrode to that of a conducting glass electrode (F-doped $SnO_2$). Both electrodes show rectification towards anodic current flow, although the conducting glass has a much larger overpotential for reduction of $I_2$ and $I_3^-$ than does the $TiO_2$. Consequently, the contribution of the dark current from the conducting glass support can be neglected for $TiO_2$-coated conducting glass electrodes. This conclusion is in good agreement with results published by Stanley *et al.* who compared the J-*E* curves for conducting glass and $RuL'_2(NCS)_2$-coated $TiO_2$ electrodes.[101]

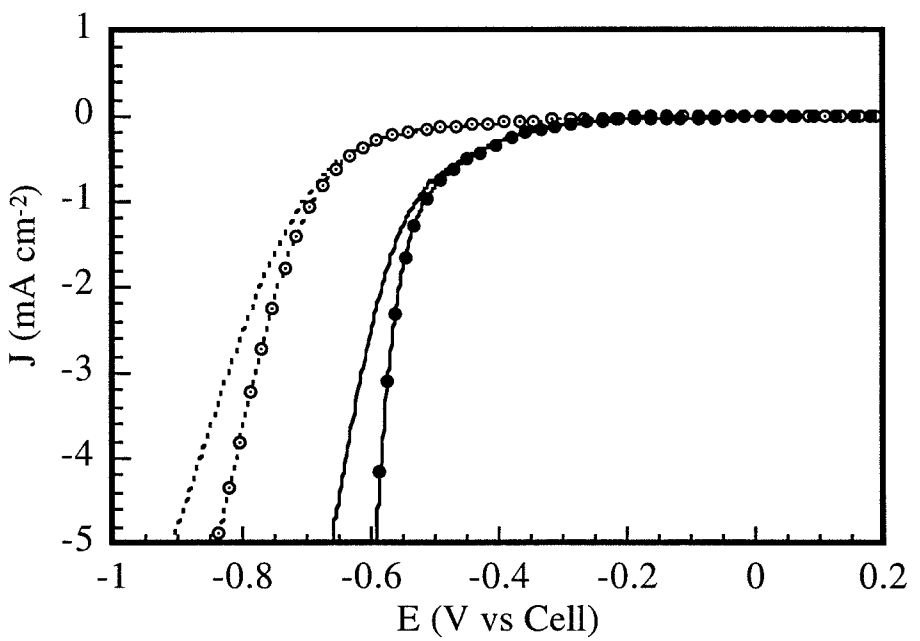


Figure 35: Current density vs potential data for an uncoated $TiO_2$ electrode (solid line) and a bare conducting glass electrode (dashed line). The lines with no symbols are raw data and the lines with circles are corrected for the cell resistance. The data was obtained in the dark.

*4. Superposition Principle*

For all these dye-coated $TiO_2$ electrodes, the superposition principle did not hold. Ideally, for a semiconductor-liquid interface, the current under illumination is obtained by simply adding the dark current with the light current (approximated as the short-circuit current under illumination), using the appropriate signs.[5] This is the superposition principle, which is based on the following: for semiconductor-liquid junctions, the majority carrier concentration is mostly unaffected by illumination while the minority carrier concentration is directly related to the photon flux.[5] Figure 36 shows the cell resistance-corrected current-voltage curves for a $RuL'_2(CN)_2$-coated $TiO_2$ electrode in the dark and under illumination. Comparison of the two gray lines in Figure 36 illustrates that the superposition principle did not hold. According to Iver Lauermann, this effect is due to a big difference in charge carrier concentration (and thus conductivity and recombination) between dark and illuminated electrodes. For $TiO_2$ nanoparticles, the majority carrier concentration is very small (no dopant atoms, large resistance) and is therefore greatly affected by light illumination.

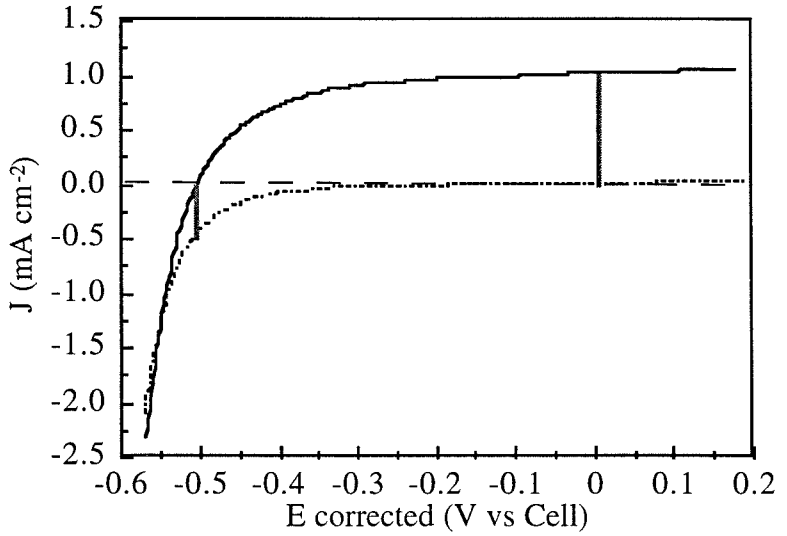


Figure 36: Corrected current density vs potential curves for a $RuL'_2(CN)_2$-coated $TiO_2$ electrode at constant short circuit current density of 1 mA cm-2 (solid line) and in the dark (dashed line).

## B. Discussion

### *1. Comments on Purification and Photoelectrochemical Properties*

We repeatedly observed during the course of this study that the photoelectrochemical properties of the cell were sensitive to the purity level of the dye used. For instance, electrodes sensitized with $Os(L'\text{-}2H^+)_3^{4-}$ purified by anion exchange chromatography yielded photocurrents that were twice as large and $V_{oc}$ values that were 100 mV larger than an electrode sensitized with unpurified $OsL'_3{}^{2+}$, even though the unpurified $OsL'_3{}^{2+}$ had satisfactory elemental analysis and $^1H$ NMR spectra. However, small impurity levels that are not detectable by those methods seem to affect the photoelectrochemical properties. Meyer and co-workers recently reported that $OsL'_2(CN)_2$ yields low external quantum yields and poor regeneration rates with iodide.[51] In our experience, any sensitizer must be purified by column chromatography to yield high

quantum yields. Meyer's paper does not report purifying their $OsL'_2(CN)_2$ by column chromatography.[1] Furthermore, when I followed the procedure for making $OsL'_2(CN)_2$ published by Meyer and co-workers,[1] I obtained a product whose $^1H$ NMR is shown in Figure 37, much different from Figure 12a. We have not identified what the trace level impurities are, but one could speculate that precursor $OsL'_2Cl_2$ or intermediate $OsL'_2(Cl)(CN)$ can act as surface traps and yield sluggish iodide regeneration rates because the chloride ligand renders the ground state potential much more positive. Though we don't know whether our $OsL'(L'\text{-}H^+)(CN)_2^{1-}$ has a slower regeneration rate or not, we can assume that it must be fast enough because we observe large external quantum yields.

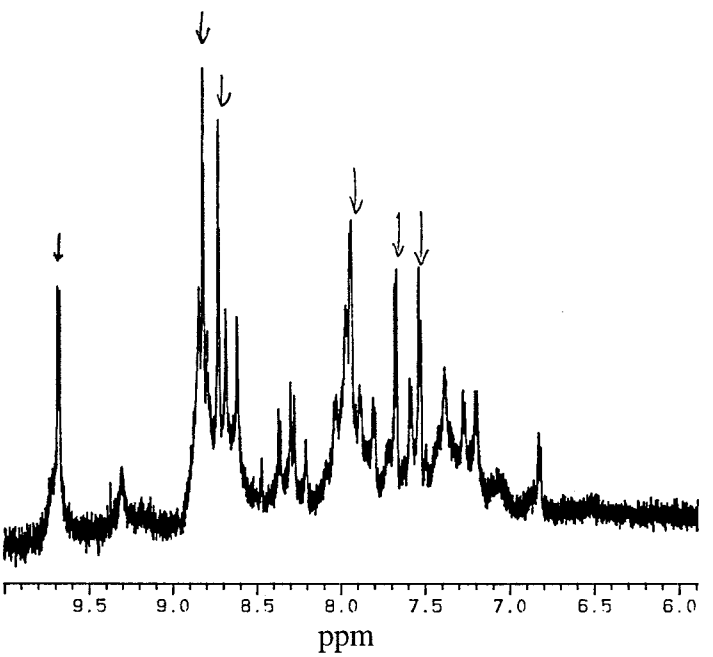


Figure 37: Aromatic region of the $^1H$ NMR in $D_2O$/NaOD for the product of the procedure for making $Os(L'\text{-}2H^+)_2(CN)_2^{4-}$ reported by Meyer and co-workers.[1]

The best purification technique identified herein is anion exchange column chromatography, which not only separates complexes based on their differing structures, but also based on their differing charges. Unfortunately, the $ML'_2(NCS)_2$ complexes could not be purified by ion-exchange column chromatography because these complexes

sorbed strongly to the column support and did not elute, even at very high electrolyte concentrations. These complexes were instead purified using size exclusion chromatography in methanol. Finally, the $NCS^-$ linkage isomers could not be separated. One must therefore keep in mind that the $ML'_2(NCS)_2$ complexes might not be as pure as the other materials, and therefore may show lower open-circuit voltages and short-circuit currents than are possible for these systems.

*2. Spectral Response Properties of Os- vs Ru-Coated $TiO_2$ Electrodes*

An interesting question raised by the systems studied herein is whether the Os complexes, which have similar excited state redox potentials to the analogous Ru complexes, can also serve as efficient photosensitizers for $TiO_2$ in contact with the $CH_3CN$-$I_3^-/I^-$ electrolyte. The spectral response data of Figures 23 and 24 and Table 8 indicate that the Os complexes are indeed effective for this application. The external quantum yields for $OsL'(L'\text{-}H^+)(CN)_2^{1-}$ are in excess of 0.8 and thus compare favorably to those of the analogous $RuL'_2(CN)_2$ system. In addition, the Os complexes show enhanced absorption to the red relative to their Ru analogs. Even the Os complex with the most positive excited state redox potential, $Os(L'\text{-}2H^+)_3^{4-}$, was found to exhibit significant quantum yields for photocurrent flow in the $TiO_2/CH_3CN$-$I_3^-/I^-$ electrolyte with 50 mM pyridine and 20 mM pyridinium triflate. The relatively small differences in maximum quantum yield between these systems were shown to be likely due to engineering-related issues such as differences in coverage of the $TiO_2$ by the complexes as opposed to fundamental issues involved in the injection of electrons into the $TiO_2$ by the excited states of the various complexes studied herein.

The only significant discrepancy in this trend was observed for the $OsL'_2(NCS)_2$ complex. Although $TiO_2$ electrodes that had been coated with this complex showed enhanced external quantum yields in the red region of the spectrum relative to those coated with the analogous Ru complex, the maximum external quantum yield for $OsL'_2(NCS)_2$ -coated $TiO_2$ was about a factor of 7 lower than that for $RuL'_2(NCS)_2$-coated electrodes.

The excited state redox potential of this system is sufficiently negative that it is expected to inject electrons efficiently into the $TiO_2$, in a fashion analogous to that of the other complexes studied herein. Also, as discussed earlier, the low quantum yield cannot be ascribed to a low absorbance of these dye-coated electrodes since as much as 95% of the incoming light is adsorbed at 520 nm.

The low steady-state maximum external quantum yield in this system can be readily explained by the fact that the $Os(III/II)L'_2(NCS)_2$ system has the most negative M(III)/M(II) redox potential of all the systems studied. Thus, this system is expected to have the slowest rate of regeneration of the M(II) species from the reaction of the M(III) complex with $I_3^-/I^-$ in the electrolyte. The slow regeneration rate allows electrons to build up in the $TiO_2$ at steady-state, and therefore allows the back reaction of these electrons with Os(III) to compete with the regeneration of Os(II) through reaction with $I^-$. Evidence to support this hypothesis has been obtained from studying the dependence of the spectral response on the concentration of $I^-$. Although the other complexes showed essentially no dependence of their quantum yields on the $I^-$ concentration, even at low light intensities, the observed photocurrent density for the $OsL'_2(NCS)_2$ increased when the concentration of $I^-$ was increased from 0.5 M to 1.0 M, keeping the redox potential of the electrolyte constant. This observation clearly implies that more rapid regeneration rates would allow the Os system to produce higher steady-state quantum yields than those obtained under the conditions used herein. This system is thus also expected to provide an efficient $TiO_2$ photosensitizer under optimized electrolyte/redox reagent conditions, although attaining such conditions will require either very high concentrations of $I^-$ in order to increase the regeneration rate sufficiently, catalysis of this reaction, or use of another redox couple with more rapid regeneration kinetics but otherwise similar properties. Finally, further purification of this dye may also improve its performance as a photosensitizer.

The quantum yields measured in the spectral response experiments were obtained at relatively low irradiance levels, and there is some concern that these values might not be

representative of the quantum yields under solar illumination intensities. A plot of $J_{sc}$ vs. light intensity for a $RuL'_2(NCS)_2$-coated $TiO_2$ electrode was linear from $J_{sc}$=0.020 mA $cm^{-2}$ to $J_{sc}$=10 mA $cm^{-2}$. Furthermore, if the spectral response is nearly independent of light intensity, the behavior of the dye-coated electrodes under solar or solar-simulated illumination can be predicted from the low-level quantum yield vs wavelength profile when convoluted with the spectral irradiance profile of the illumination source under the high light intensity conditions. The predicted $J_{sc}$ value under ELH-type illumination can be obtained by the ratio of the integrated spectral response of the dye-coated $TiO_2$ electrodes to that of a calibrated Si photodiode. As seen in Table 12, the $J_{sc}$ values predicted using this procedure are in good agreement with observations. These results also suggest that at photocurrents higher than a small threshold value, the short-circuit photocurrents are not affected by the surface electron concentration.

Table 12: Predicted Short-Circuit Photocurrents

| **Complex** | **N[a]** | **$J_{sc}$ ELH bulb[b] (mA $cm^{-2}$)** (see Table 9) | **Max. external Q.Y.** | **Predicted $J_{sc}$ ELH bulb 100 mW $cm^{-2}$ (mA $cm^{-2}$)[c]** | **Predicted $J_{sc}$ AM1.5 sun spectrum 100 mW $cm^{-2}$ (mA $cm^{-2}$)** |
|---|---|---|---|---|---|
| $OsL'_2(NCS)_2$ | 3 | 2.1 ± 0.3 | 0.11 ± 0.01 | 1.7 | 1.8 |
| $RuL'_2(NCS)_2$ | 5 | 10.8 ± 0.5 | 0.78 ± 0.03 | 10.8 | 10.4 |
| $OsL'(L'\text{-}H^+)(CN)_2^{1-}$ | 4 | 11.6 ± 0.6 | 0.82 ± 0.01 | 12.1 | 12.0 |
| $RuL'_2(CN)_2$ | 3 | 5.5 ± 0.1 | 0.80 ± 0.03 | 5.5 | 6.4 |
| $OsL_2L'^{2+}$ | 4 | 7.7 ± 0.5 | 0.67 ± 0.03 | 7.5 | 7.6 |
| $RuL_2L'^{2+}$ | 4 | 1.80 ± 0.05 | 0.45 ± 0.01 | 1.7 | 2.3 |
| $Os(L'\text{-}2H^+)_3^{4-}$ | 3 | 10.0 ± 0.2 | 0.73 ± 0.03 | 10.5 | 10.3 |
| $Ru(L'\text{-}2H^+)_3^{4-}$ | 3 | 3.7 ± 0.1 | 0.68 ± 0.03 | 3.8 | 4.7 |

a. Total number of experiments, each with a different electrode.

b. The illumination was equivalent to 100 mW $cm^{-2}$, the power of the sun at AM 1.0.

c. The predicted currents were standardized to the ELH bulb utilized using the average photocurrent for $RuL'_2(NCS)_2$.

The photocurrents expected upon exposure of these cells to the NREL Global AM 1.5 solar spectral irradiance, at a total incident light intensity of 100 mW $cm^{-2}$, can be computed in a similar fashion. Two points are of main interest from analysis of these data (Table 12). First, the variation in predicted $J_{sc}$ values arises mostly from the variation in the maximum external quantum yields; if the complexes are all normalized to the same maximum quantum yield value (Table 12), then it is clear that the Os complexes will outperform the Ru ones with respect to producing photocurrent under AM1.5 solar illumination. Secondly, even without such normalization, the $OsL'(L'\text{-}H^+)(CN)_2^{1-}$ and $Os(L'\text{-}2H^+)_3^{4-}$ systems at present provide comparable predicted $J_{sc}$ values to the $RuL'_2(NCS)_2$ complex under our conditions. The Os complexes thus seem promising

candidates for further optimization in operating photoelectrochemical cells for solar energy conversion applications based on their photocurrent and spectral response properties.

The simple model depicted in Figure 5 fails to explain why the photocurrent at short-circuit can be influenced by $[I^-]$ and not by surface electron concentration in the conduction band of $TiO_2$ for the $OsL'_2(NCS)_2$- coated electrodes. One possibility is that the back electron transfer to the dye occurs mainly from surface states and not from the conduction band electrons. In this model, the surface state electron concentration reaches a maximum constant value at a relatively small low light intensity. This model is consistent with the observation that photocurrents are non-linear at very low light intensities (Fig. 9), where the surface states may not be completely filled. Further experiments are needed to confirm this model. The available data do, however, strongly suggest that the regeneration of $Os(II)L'_2(NCS)_2$ does not compete with the back electron transfer to the dye in this system.

*3. Current Density vs Potential Behavior*

The other key property of concern is the photovoltage of the system. In our work, the performance of the devices has not been optimized through addition of surface passivating reagents, etc.; instead relatively uncomplicated, standard conditions of controlled proton activity, electrolyte concentration, etc., have been used in order to facilitate comparison between the performance of the various metal complex-coated $TiO_2$ electrodes in our studies. In a simple description of the operation of these photoelectrochemical cells, the open-circuit photovoltage should be the same for the various metal complexes, provided that the photocurrent density is constant for all electrode systems. This prediction is obtained because the dominant steady-state back reaction is thought to occur between electrons in the $TiO_2$ and $I_3^-$ (and/or between electrons in the $TiO_2$ and $I_2$) in the electrolyte. If this is the case, a constant rate of injected carriers from the light should in turn produce a constant rate of back reaction, and thus a constant photovoltage at open-circuit (where the back reaction rate exactly offsets the light-driven

forward current rate, which has been held constant experimentally), for the various systems of concern. As depicted in Table 10 and Figure 32, this behavior was indeed confirmed at low dye loadings for the various metal complexes studied in this work.

Interestingly, however, such behavior was not observed for $TiO_2$ electrodes that were coated with the higher loadings of dye that are needed to obtain the highest short-circuit photocurrent densities in an operating photoelectrochemical cell. Instead, as depicted in Table 9, the $V_{oc}$ values at high dye loadings varied by over 100 mV even when the short-circuit current densities were held constant at $J_{sc}$=1.0 mA $cm^{-2}$. As shown in Figure 31, this behavior was also seen in the dark J-*E* properties of these electrodes, where the current density for reduction of $I_3^-$ at a specific potential relative to short-circuit was observed to depend on the type of metal complex that was used to coat the $TiO_2$. In some cases, the dark currents were higher than those at an uncoated $TiO_2$ electrode, whereas in other cases, the dark reduction reaction was reduced by coating the $TiO_2$ with the metal complex.[101] Thus, in some cases adsorption of high levels of the metal complex appears to facilitate reduction of $I_3^-$ in the solution, while in other cases, such levels of dye coverage appear to inhibit $I_3^-$ reduction. At these potentials the metal complexes are all in the M(II) oxidation state, so they ought to be spectators in this reaction. However, the nature and coverage of the complex clearly play a more complicated role in determining the interfacial kinetics of the system than is produced by the simple working model for these electrode systems in the literature. Further study is clearly required in order to understand this behavior in detail. Given the relatively similar performance of the photocurrent density that is likely to be obtained from optimized systems from each of these metal complexes as described above, the variation in photovoltage is therefore likely to determine ultimately the relative utility of these various metal complexes in sensitizing $TiO_2$ for photoelectrochemical energy conversion applications.

# Chapter 5:

# Conclusions

In this thesis, a series of polypyridine complexes of osmium and ruthenium were synthesized, purified and characterized. The linkage isomerism of the $NCS^-$ complexes was assigned to contain predominantly nitrogen-bound $NCS^-$ based on our $^{15}N$ NMR study. Furthermore, the data indicate that $^{15}N$ NMR appears to be a more reliable spectroscopic tool than $^{13}C$ NMR spectroscopy for the assignment of linkage isomerism in metal complexes of the thiocyanate ligand.

Replacing the ruthenium metal center of polypyridine complexes with osmium extended the light absorption and spectral response of nanocrystalline $TiO_2$ photoelectrodes to lower wavelength values without sacrificing significant photoelectrochemical energy conversion performance. The Os complexes thus seem very promising candidates for further optimization in operating photoelectrochemical cells for solar energy conversion applications. During the course of this study, we repeatedly observed that the photoelectrochemical properties of the cell are sensitive to the purity level of the dye used.

Experiments suggested that the regeneration rate of $Os(II)L'_2(NCS)_2$ by iodide does not compete effectively with the regeneration rate of the dye by the electron in the $TiO_2$. Further experiments are required to determined whether it is the regeneration by iodide that is slower, the back reaction that is faster, or both. Answers to those questions require measuring regeneration and back electron transfer rates. In order to measure the regeneration rate by transient absorption spectroscopy, the transient spectra of excited state and the spectra of oxidized form of dye are needed. The decay kinetics of the M(III) should be measured at the isobestic point between the ground and excited state of the dye in order to eliminate any possible contributions from excited states that did not inject.

The ground-state redox potential of $Os(II/III)L'_2(NCS)_2$ (+0.42 V vs aq SCE in

methanol) may represent a lower limit for the ground-state redox potential of the dye. However, this dye was purified by chromatography on LH-20 and because it eluted slowly, the product band was very wide and could also include some $OsL'_2Cl_2$ or $OsL'_2(Cl)(NCS)$, which would lower the photocurrent, open-circuit voltage and external quantum yield. A possible way to obtain more pure $OsL'_2(NCS)_2$ is to obtain the ester version, purify it, and then transform it into the carboxylated complex. Dr. Glen Walker has started to explore this alternative.

Finally, for electrodes with very low dye coverage, $V_{oc}$ was mainly determined by the reduction of $I_2/I_3^-$, whereas a more complicated mechanism is apparently operative for electrodes having higher dye coverage. Further experiments are required to understand this phenomenon.

## References:

(1) Heimer, T. A.; Bignozzi, C. A.; Meyer, G. J. *J. Phys. Chem.* **1993**, *97*, 11987.

(2) Zweibel, K. *Harnessing Solar Power: The Photovoltaics Challenge*; Plenum Press: New York, 1990, pp 319.

(3) Kerr, R. A. *Science* **1998**, *281*, 1128.

(4) Freemantle, M. *C&EN* **1998**, *October 26*, 37.

(5) Tan, M. X.; Laibinis, P. E.; Nguyen, S. T.; Kesselman, J. M.; Stanton, C. E.; Lewis, N. S. *Prog. In Inorg. Chem.* **1994**, *41*, 21.

(6) Finklea, H. O. *Semiconductor Electrodes*; Academic Press: New York, 1988.

(7) Henry, C. H. *J. Appl. Phys.* **1980**, *51*, 4494.

(8) O'Regan, B.; Grätzel, M. *Nature (London)* **1991**, *353*, 737.

(9) Grätzel, M. *Platinum Metals Rev.* **1994**, *38*, 151.

(10) Grätzel, M. *Comments Inorg. Chem.* **1991**, *12*, 93.

(11) Grätzel, M. *Nature* **1989**, *338*, 540.

(12) Enea, O.; Moser, J.; Grätzel, M. *J. Electroanal. Chem.* **1989**, *259*, 59.

(13) O'Regan, B.; Moser, J.; Anderson, M.; Grätzel, M. *J. Phys. Chem.* **1990**, *94*, 8720.

(14) Nazeeruddin, M. K.; Liska, P.; Moser, J.; Vlachopoulos, N.; Grätzel, M. *Helv. Chim. Acta* **1990**, *73*, 1788.

(15) Grätzel, M.; Kalyanasundaram, K. *Curr. Sci.* **1994**, *66*, 706.

(16) Nazeeruddin, M. K.; Kay, A.; Rodicio, I.; Humphry-Baker, R.; Müller, E.; Liska, P.; Vlachopoulos, N.; Grätzel, M. *J. Am. Chem. Soc.* **1993**, *115*, 6382.

(17) Murakoshi, K.; Kano, G.; Sada, Y.; Yanagida, S.; Miyazaki, H.; Matsumoto, M.; Murasawa, S. *J. Electroanal. Chem.* **1995**, *396*, 27.

(18) Argazzi, R.; Bignozzi, C. A.; Heimer, T. A.; Castellano, F. N.; Meyer, G. J. *Inorg. Chem.* **1994**, *33*, 5741.

(19) Heimer, T. A.; Meyer, G. J. In *Electrochem. Soc. Proc.*; 1995; pp 189.

(20) Heimer, T. A.; Heilweil, E. J. *J. Phys. Chem. B.* **1997**, *101*, 10990.

(21) Vinodgopal, K.; Hua, X.; Dahlgren, R. L.; Lappin, A. G.; Patterson, L. K.; Kamat, P. V. *J. Phys. Chem.* **1995**, *99*, 10883.

(22) Finnie, K. S.; Barlett, J. R.; Woolfrey, J. L. *Langmuir* **1998**, *14*, 2744.

(23) Papageorgiou, N.; Maier, W. F.; Grätzel, M. *J. Electrochem. Soc.* **1997**, *144*, 876.

(24) Kalyanasundaram, K. In dcwww.epfl.ch/icp/ICP-2/solarcell_E.html: WEB, 1998.

(25) Papageorgiou, N.; Athanassov, Y.; Armand, M.; Bonhôte, P.; Pettersson, H.; Azam, A.; Grätzel, M. *J. Electrochem. Soc.* **1996**, *143*, 3099.

(26) Bonhôte, P.; Dias, A.-P.; Papageorgiou, N.; Kalyanasundaram, K.; Grätzel, M. *Inorg. Chem.* **1996**, *35*, 1168.

(27) Bach, U.; Lupo, D.; Comte, P.; Moser, J. E.; Weissörtel, F.; Salbeck, J.; Spreitzer, H.; Grätzel, M. *Nature* **1998**, *395*, 583.

(28) Cao, F.; Oskam, G.; Searson, P. C. *J. Phys. Chem.* **1995**, *99*, 17071.

(29) Savenije, T. J.; Warman, J. M.; Goossens, A. *Chem. Phys. Lett.* **1998**, *287*, 148.

(30) Moss, J.; Stipkala, J. M.; Yang, J. C.; Bignozzi, C. A.; Meyer, G. J.; Meyer, T. J.; Wen, X.; Linton, R. W. *Chem. Mater.* **1998**, *10*, 1748.

(31) Kohle, O.; Grätzel, M.; Meyer, A. F.; Meyer, T. B. *Adv. Mater.* **1997**, *9*, 904.

(32) Lindström, H.; Rensmo, H.; Södergren, S.; Solbrand, A.; Lindquist, S.-E. *J. Phys. Chem.* **1996**, *100*, 3084.

(33) Vlachopoulos, N.; Liska, P.; Augustynski, J.; Grätzel, M. *J. Am. Chem. Soc.* **1988**, *110*, 1216.

(34) Hagfeldt, A.; Grätzel, M. *Chem. Rev.* **1995**, *95*, 49.

(35) Zaban, A.; Ferrere, S.; Spraque, J.; Gregg, B. A. *J. Phys. Chem. B.* **1997**, *101*, 55.

(36) Sodergren, S.; Hagfeldt, A.; Olsson, J.; Lindquist, S.-E. *J. Phys. Chem.* **1994**, *98*, 5552.

(37) Cao, F.; Oskam, G.; Meyer, G. J.; Searson, P. C. *J. Phys. Chem.* **1996**, *100*, 17021.

(38) Schwarzburg, K.; Willig, F. *J. Phys. Chem. B.* **1997**, *101*, 2451.

(39) Zaban, A.; Meier, A.; Gregg, B. A. *J. Phys. Chem. B.* **1997**, *101*, 7985.

(40) Desilvestro, J.; Grätzel, M.; Kavan, L.; Moser, J. *J. Am. Chem. Soc.* **1985**, *107*, 2988.

(41) Fessenden, R. W.; Kamat, P. V. *J. Phys. Chem.* **1995**, *99*, 12902.

(42) Kamat, P. V.; Bedja, I.; Hotchandani, S.; Patterson, L. K. *J. Phys. Chem.* **1996**, *100*, 4900.

(43) Rehm, J. M.; McLendon, G. L.; Nagasawa, Y.; Yoshihara, K.; Moser, J.; Grätzel, M. *J. Phys. Chem.* **1996**, *100*, 9577.

(44) Cherepy, N. J.; Smestad, G. P.; Grätzel, M.; Zhang, J. *J. Phys. Chem. B* **1997**, *101*, 9342.

(45) Tachibana, Y.; Moser, J. E.; Grätzel, M.; Klug, D. R.; Durrant, J. R. *J. Phys. Chem.* **1996**, *100*, 20056.

(46) Lepore, G. P.; Langford, C. H.; Vichova, J.; Vlcek, A. J. *J. Photochem. Photobiol. A: Chem.* **1993**, *75*, 67.

(47) Hannappel, T.; Zimmermann, C.; Meissner, B.; Burfeindt, B.; Storck, W.; Willig, F. *J. Phys. Chem. B.* **1998**, *102*, 3651.

(48) Hannappel, T.; Burfeindt, B.; Storck, W.; Willig, F. *J. Phys. Chem. B.* **1997**, *101*, 6799.

(49) Ferrere, S.; Gregg, B. A. *J. Am. Chem. Soc.* **1998**, *120*, 843.

(50) Haque, S. A.; Tachibana, Y.; Klug, D. R.; Durrant, J. R. *J. Phys. Chem. B.* **1998**, *102*, 1745.

(51) Alebbi, M.; Bignozzi, C. A.; Heimer, T. A.; Hasselmann, G. M.; Meyer, G. J. *J. Phys. Chem. B* **1998**, *102*, 7577.

(52) Yan, S. G.; Lyon, A.; Lemon, B. I.; Preiskorn, J. S.; Hupp, J. T. *J. Chem. Edu.* **1997**, *74*, 657.

(53) Moser, J. E.; Bonnôte, P.; Grätzel, M. *Coord. Chem. Rev.* **1998**, *171*, 245.

(54) Boschloo, G. K.; Goossens, A. *J. Phys. Chem.* **1996**, *100*, 19489.

(55) Hagfeldt, A.; Björkstén, U.; Grätzel, M. *J. Phys. Chem.* **1996**, *100*, 8045.

(56) Schwarzburg, K.; Willig, F. *Appl. Phys. Lett.* **1991**, *58*, 2520.

(57) Willig, F.; Burgeindt, B.; Schwarzburg, K.; Hannappel, T.; Storck, W. *Proc. Indian Acad. Sci. (Chem. Sci.)* **1997**, *109*, 415.

(58) Kay, A.; Humphry-Baker, R.; Grätzel, M. *J. Phys. Chem.* **1994**, *98*, 952.

(59) Kamat, P. V. *Prog. Reaction Kinetics* **1994**, *19*, 277.

(60) Yan, S. G.; Hupp, J. T. *J. Phys. Chem.* **1996**, *100*, 6867.

(61) Skinner, D. E.; Colombo, P. J.; Cavaleri, J. J.; Bowman, R. M. *J. Phys. Chem.* **1995**, *99*, 7853.

(62) Kay, A.; Grätzel, M. *J. Phys. Chem.* **1993**, *97*, 6272.

(63) Papageorgiou, N.; Barbé, C.; Grätzel, M. *J. Phys. Chem. B.* **1998**, *102*, 4156.

(64) Kalyanasundaram, K. *Photochemistry of Polypyridine and Porphyrin Complexes*; Academic Press: San Diego, 1992, pp 626.

(65) Nazeeruddin, M. K.; Müller, E.; Humphry-Baker, R.; Vlachopoulos, N.; Grätzel, M. *J. Chem. Soc., Dalton Trans.* **1997**, 4571.

(66) Ruile, S.; Kohle, O.; Péchy, P.; Grätzel, M. *Inorg. Chim. Acta* **1997**, *261*, 129.

(67) Jing, B.; Zhang, H.; Zhang, M.; Zhuhong, L.; Shen, T. *J. Mater. Chem.* **1998**, *8*, 2055.

(68) Zakeeruddin, S. M.; Nazeeruddin, M. K.; Pechy, P.; Rotzinger, F. P.; Humphry-Baker, R.; Kalyanasundaram, K.; Grätzel, M. *Inorg. Chem.* **1997**, *36*, 5937.

(69) Kalyanasundaram, K.; Nazeeruddin, M. K. *Chem. Phys. Lett.* **1992**, *193*, 292.

(70) Nazeeruddin, M. K.; Péchy, P.; Grätzel, M. *Chem. Commun.* **1997**, *18*, 1705.

(71) Nazeeruddin, M. K.; Humphry-Baker, R.; Grätzel, M.; Murrer, B. A. *Chem. Commun.* **1998**, 719.

(72) Kohle, O.; Ruile, S.; Grätzel, M. *Inorg. Chem.* **1996**, *35*, 4779.

(73) Sugihara, H.; Singh, L. P.; Sayanama, K.; Arakawa, H.; Nazeeruddin, M. K.; Grätzel, M. *Chem. Lett.* **1998**, *10*, 1005.

(74) Amadelli, R.; Argazzi, R.; Bignozzi, C. A.; Scandola, F. *J. Am. Chem. Soc.* **1990**, *112*, 7099.

(75) Garcia, C. G.; Iha, N. Y. M.; Argazzi, R.; Bignozzi, C. A. *J. Photo. Photobio. A: Chem.* **1998**, *115*, 239.

(76) Pechy, P.; Rotzinger, F. P.; Nazeeruddin, M. K.; Kohle, O.; Zadeeruddin, S. M.; Humphry-Baker, R.; Grätzel, M. *J. Chem. Soc., Chem. Commun.* **1995**, 65.

(77) Eichberger, R.; Willig, F. *Chem. Phys.* **1990**, *141*, 159.

(78) Kober, E. M.; Caspar, J. V.; Sullivan, B. P.; Meyer, T. J. *Inorg. Chem.* **1988**, *27*, 4587.

(79) Bryant, G. M.; Fergusson, J. E.; Powell, K. J. *Austr. J. Chem.* **1971**, *24*, 257.

(80) Ethylene glycol was used as the solvent for this reaction, instead of dimethylformamide (DMF), to avoid the formation of carbonyl complexes. Such complexes can be observed in the infrared spectrum of the product, which displayed a prominent peak at 1720 $cm^{-1}$ when DMF was used as the solvent.

(81) Sprintschnik, G.; Sprintschnik, H. W.; Kirch, P. P.; Whitten, D. G. *J. Am. Chem. Soc.* **1977**, *99*, 4947.

(82) Liska, P.; Vlachopoulos, N.; Nazeeruddin, M. K.; Comte, P.; Grätzel, M. *J. Am. Chem. Soc.* **1988**, *110*, 3686.

(83) Barbé, C. J.; Arendse, F.; Comte, P.; Jirousek, M.; Lenzmann, F.; Shklover, V.; Grätzel, M. *J. Am. Ceram. Soc.* **1997**, *80*, 3157.

(84) Pomykal, K. E. Thesis, California Institute of Technology, 1997.

(85) Parks, G. A. *Chem. Rev.* **1965**, *65*, 177.

(86) Zhao, J.; Hidaka, H.; Takamura, A.; Pelizzetti, E.; Serpone, N. *Langmuir* **1993**, *9*, 1646.

(87) Kormann, C.; Bahnemann, D. W.; Hoffmann, M. R. *Environ. Sci. Technol.* **1991**, *25*, 494.

(88) Fajardo, A. M.; Lewis, N. S. *J. Phys. Chem. B* **1997**, *101*, 11136.

(89) Bard, A. J.; Faulkner, L. R. *Electrochemical Methods: Fundamentals and Applications*; Wiley: New York, 1980.

(90) Shklover, V.; Nazeeruddin, M.-K.; Zakeeruddin, S. M.; Barbé, C.; Kay, A.; Haibach, T.; Steurer, W.; Hermann, R.; Hissen, H.-U.; Grätzel, M. *Chem. Mater.* **1997**, *9*, 430.

(91) Howarth, O. W.; Richards, R. E.; Venanzi, L. M. *J. Chem. Soc.* **1964**, 3335.

(92) Pregosin, P. S.; Streit, H.; Venanzi, L. M. *Inorg. Chim. Acta* **1980**, *38*, 237.

(93) Fratiello, A.; Kubo-Anderson, V.; Adanalyan, A.; Bolanos, E. L.; Ortega, J. V.; Perrigan, R. D.; Saenz, L. *Journal of Solution Chemistry* **1995**, *24*, 1249.

(94) Levy, G. C.; Lichter, R. L. *Nitrogen-15 Nuclear Magnetic Resonance Spectroscopy*; John Wiley & Sons: 1979.

(95) Herber, R. H.; Nan, G.; Potenza, J. A.; Schugar, H. J.; Bino, A. *Inorg. Chem.* **1989**, *28*, 938.

(96) Kargol, J. A.; Crecely, R. W.; Burmeister, J. L. *Inorg. Chem.* **1979**, *18*, 2532.

(97) Shklover, V.; Haibach, T.; Bolliger, B.; Hochstrasser, M.; Erbudak, M.; Nissen, H.-U.; Zakeeruddin, S. M.; Nazeeruddin, M. K.; Grätzel, M. *J. of Sol. State Chem.* **1997**, *132*, 60.

(98) Creutz, C.; Chou, M.; Netzel, T. L.; Okumura, M.; Sutin, N. *J. Am. Chem. Soc.* **1980**, *102*, 1309.

(99) Caspar, J. V.; Kober, E. M.; Sullivan, B. P.; Meyer, T. J. *J. Am. Chem. Soc.* **1982**, *104*, 630.

(100) Harris, D. C. *Quantitative Chemical Analysis;* 2 ed.; W. H. Freeman and Co.: New York, 1987, pp 818.

(101) Stanley, A.; Matthews, D. *Aust. J. Chem.* **1995**, *48*, 1293.